Investigation on Dynamics of Drillstring Systems from Random Viewpoint

by

A Dissertation submitted to the School of Graduate Studies

in partial fulfilment of the requirements for the degree of

Doctor of Philosophy

Department of *Oil and Gas Engineering*

Faculty of Engineering and Applied Science

Memorial University of Newfoundland

May, 2023

St. John's Newfoundland and Labrador Canada

Abstract

Drillstrings are one of the critical components used for exploring and exploiting oil and gas reservoirs in the petroleum industry. As being very long and slender, the drillstring experiences various vibrations during the drilling operation, and these vibrations are random in essence.

The first part of the thesis focuses on stochastic stick-slip dynamics of the drill bit by a finite element model and a single degree of freedom drillstring model in Chapters 3 and 4, respectively. In the single degree of freedom model, the path integration (PI) method is firstly used to obtain the probability density evolution of the dynamic response. Then Monte Carlo (MC) simulation is used for validating PI results and conducting the parametric study.

The second step of my research is to study the stochastic dynamics of a vertical, multiple degrees of freedom drillstring system. The work of this part is presented in Chapter 5. The novelty of this work relies on the fact that it is the first time that the statistic linearization method is applied to a drillstring system in the bit-rock interaction to find an equivalent linear dynamic system which is then solved with the stochastic Newmark algorithm. After that, the stick-slip and bit-bounce phenomena are analyzed from random viewpoint.

The third step of my research move on to directional drilling. A static study of directional drillstring from random viewpoint is presented in Chapter 6. The finite element method (FEM) based on the soft string model is employed and built. Then

two strategies are taken to model the random component for hoisting drag calculation. The purpose of this work is to analyze the effects of the random component on hoisting drag calculation by the MC simulation method.

Acknowledgements

I would like to sincerely acknowledge the inputs and supports from many people.

First of all, I would like to express my thanks to the supervisory committee, Dr. Stephen Butt, Dr. James Yang and Dr. Geoff Rideout, for their professional supervision, critical discussions and immeasurable contributions. It is also their encouragement and support that empower me to overcome the barriers and challenges in the research.

I would like to acknowledge the financial support from Anaconda Mining Co. through Mitacs-Accelerate Graduate Internship. I would like to thank Dr. John Molgaard and Dr. Yingjian Xiao for their tutorials during the internship. I would like to express my gratitude to the faculty staff and the members of the Drilling Technology Laboratory group for their help in the experiments.

I would like to express appreciations to my friends. It is the friendship that relieves the homesickness, brings happiness and offers warm help. Especially, I would like to thank Zijian Li, Yingjian Xiao, Yubing Wen, Jiahao Zheng and Zhen Zhang, who share the same major as me. The time I spent working, studying and playing with them is precious to me.

Last but not least, I would like to express gratitude to my wife, Lei Wang, who makes it possible for me to concentrate on the doctorate program by taking care of the family. I am grateful to my parents, who always give me trust, support and patience in countless ways.

Table of Contents

List of Tables

List of Figures

Chapter 1

Introduction

Natural resources play an essential role in powering the civilization of humanity. Among them, crude oil, or petroleum, is one of the most crucial resources in the modern economy. Driven by the increasing demand for energy and the development of modern technology, the growth in drilling technology over the 20th century was enormous [1]. The rotary drilling method improves the drilling efficiency in the deep borehole drilling as the most prevalent drilling method, while Measurement While Drilling (MWD), Rotary Steerable Tools and advanced drill bits lay the foundation for directional drilling [2].

From the petroleum exploration phase to the fuel consumption phase, the oil and gas industry can be mainly classified into three parts: upstream, midstream and downstream. The upstream is responsible for exploring and producing hydrocarbons. In this business segment, after a potential reservoir is located by geophysics exploration,

a drilling rig system will be deployed to reach the target reservoir. This procedure is an essential component of exploring and exploiting hydrocarbon resources. However, it is negatively influenced by drillstring vibrations, which are considered the important cause of drillstring components' premature failure. It has been reported that drillstring vibrations can initiate fatigue cracks which are responsible for the majority of drillstring failures [3]. Furthermore, unwanted drillstring vibration may lead to bit wear and failure, deterioration of the well trajectory, stabilizer wear, decreased rate of penetration (ROP), and reduced accuracy of MWD tools. As a result, industry and academia have been making enormous research efforts to investigate the sources of unwanted vibrations and suggest corresponding strategies to suppress them. Among all the methods and technologies utilized, conducting numerical simulation with drillstring vibration models is a cost-effective way for bottom-hole assembly design and pre-drilling analysis. It has been pointed out that the study of drillstring dynamics based on vibration models is the necessary step toward developing control strategies to ensure fast and efficient drilling without premature component failures [4]. As the study of drillstring dynamics has significant application meaning, a comprehensive literature review of the drillstring dynamics will be given in Chapter 2.

This thesis focuses on the stochastic analysis of the drillstring in the drilling operation. Numerical models of drillstring are established based on the drill rig system in the upstream portion of the oil and gas industry. Therefore, an overview of a rotary drill rig system will be presented in the following 1.1 section to illustrate the

background information. Each component that is related to the drillstring numerical model will be introduced. In section 1.2, the purpose of the research will be presented.

1.1 Overview of a Rotary Drilling Rig System

A drilling rig is an integrated system that enables drilling operations in the petroleum industry. Depending on the reservoir location, a drilling rig can be established on land or at sea. Taking a land system as an example, it generally contains four major components: hoisting system, rotating equipment, circulating system and power generation system. Figure 1.1 shows the basic elements of a land drilling rig system [5]. The blowout preventer in the figure is the safety system. Normally, a drilling rig system is powered by either the internal-combustion diesel engines at the rig site or an electric power supply from existing power lines [6]. The following subsections will introduce some other vital components in the drilling rig system.

1.1.1 Hoisting System

As can be seen in Figure 1.2, a hoisting system contains derrick, crown block, travelling block, drilling line, and drawworks [7]. The derrick is a steel frame supporting the weight of the drillstring assembly. On the top of a derrick stays the crown block, which is a fixed set of pulleys. Unlike the crown block, the travelling block is a freely moving section of a block and tackle. It contains a set of pulleys or sheaves. Running from the drawworks to the first pulley on the crown block, the drilling line goes down

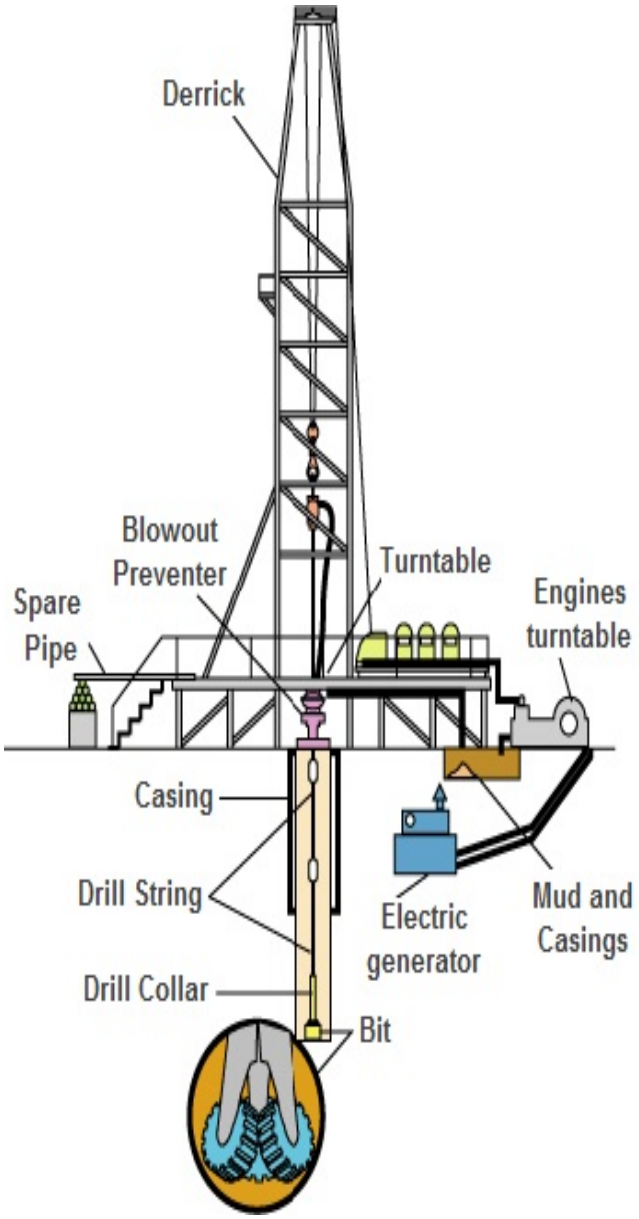

Figure 1.1: Basic Elements of a Drill Rig System [5]

to the first pulley on the travelling block, then back up to the second pulley on the crown block, etc. [8]. A similar procedure will repeat several rounds, resulting in the force on the hook being several times larger than the force provided by the drawworks. Finally, the drilling line goes over the crown block pulley and down to the deadline anchor. Working together, the crown block, drilling line and travelling block make it possible to lift or lower the drillstring and balance the hook load.

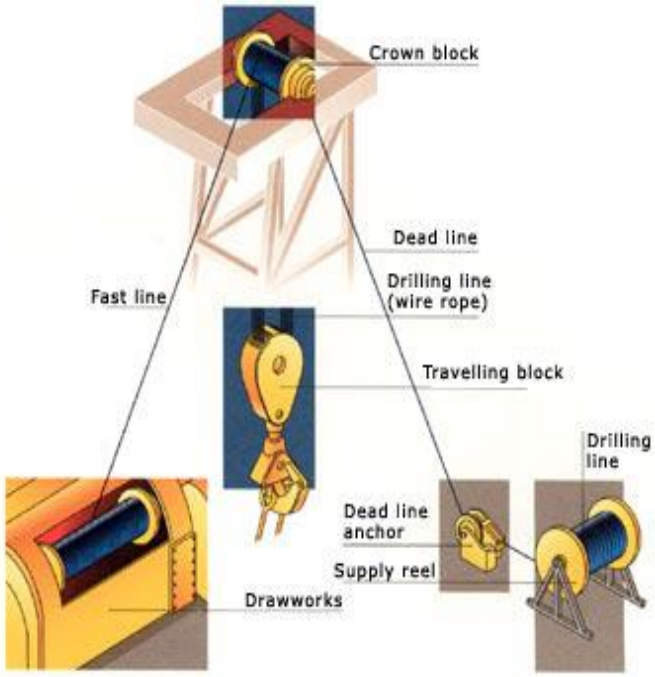

Figure 1.2: Hoisting system [7]

1.1.2 Drill Pipe and Drill Collar

The drillstring plays an important role in rotary drilling by transporting the torque from the surface to the bit, achieving directional drilling trajectory, providing the weight on the bit (WOB) and serving as a conduit for drilling fluid [2]. It is mostly made up of drill pipes. Being a tubular steel body with threaded ends, drill pipes can be connected as a section extending thousands of meters. It starts from the surface to a few hundred meters above the drill bit.

Connecting the drill pipe and the drill bit, drill collars are extra heavy steel pipes providing the necessary weight on the bit (WOB) to facilitate drilling. They are thick-walled tubes with an outside diameter larger than the normal drill pipe. Drill collars also require significant strength and rigidity to stabilize the downhole assembly, facilitate straight drilling and protect themselves from excessive fatigue or wear.

The hoisting system supports part of the drillstring weight during the drilling operation. A concept of neutral point is introduced, which marks the stress status transition from tension to compression. Usually, for safe drilling, the neutral point should be on the drill collar section by controlling the WOB; therefore, the drill pipe section is normally rotating in tension.

1.1.3 Drill Bit

Located at the end of the drillstring, drill bits are crucial components that influence ROP. They can be mainly classified into two categories: roller-cone (RC) bit and

polycrystalline diamond compact (PDC) bit. Depending on the formation property (soft or hard), different types of drill bits can be selected to enhance effective drilling performance.

Depending on the number of cones, several types of RC bits exist. Figure 1.3 shows a tricone bit [9], which is widely used in drilling. With the help of bearing, each cone of RC bits can rotate with respect to its own axis. Each cone is embedded with hardened metal inserts, which crushes the rock into cuttings when drilling. Compared with tricone bits, two-cone bits have more space for larger bearings and nozzle placements. They are suggested for soft formations to avoid the balling problem. Four-cone bits are normally selected for drilling large holes.

Unlike RC bits, PDC bits do not have moving elements since they are fixed-head bits that rotate as one piece. Figure 1.4 shows a PDC bit [10]. In drilling, the PDC bit shears the rock with the polycrystalline diamond inserts that are lined on the surface of its blades (Figure 1.4). PDC bits are generally used for drilling in soft to medium-hard formations.

A hybrid structure bit, also named roller PDC hybrid bit, was developed recently. It takes advantage of both the rock crushing strength of roller cones and the shearing mechanism of PDC bits. As can be seen in Figure 1.5, roller cones and fixed PDC cutters are combined in the hybrid bit [11]. It has been reported that such a single patented design can enhance drilling efficiency and stability [12].

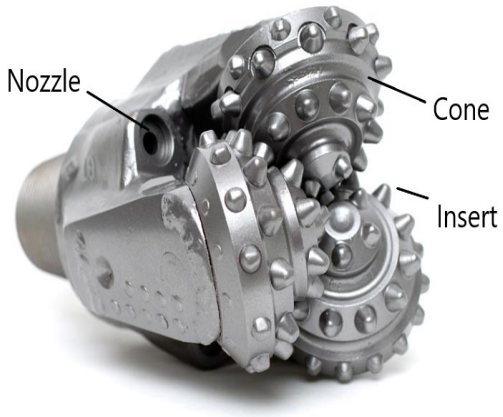

Figure 1.3: A tricone bit [9]

Figure 1.4: A PDC bit [10]

Figure 1.5: A bottom view of hybrid bit [11]

1.1.4 Drilling Fluid

In a circulating system, drilling fluid (also called drilling mud) is a critical component to aid drilling. It plays an important role in maintaining wellbore stability and keeping drilling pressure balance. In drilling, gas or water in the underground formation may exert tremendous pressure on the wellbore. Without the help of drilling fluid, the formation fluids may enter into the wellbore or even flow to the surface with unexpected high velocity, leading to a catastrophic "blow-out".

By circulating down the drillstring and ejecting from the bit nozzles, the drilling fluid also cleans the cuttings around the drill bit and carries them to the surface. In this way, the drilling fluid will prevent the accumulated debris from decreasing the rate of penetration (ROP) or even locking the drilstring in place.

The Drilling fluid can also be used to cool the drill bit and drilling assembly. Heat will be generated due to the bit-rock interaction and the friction between the drillstring and the wellbore in the drilling process. Without transferring the heat, components of the drillstring would fail more rapidly. Further, working with additive lubricants, drilling fluid can lubricate the contact surface to reduce the torque and drag. This function of drilling fluid makes a contribution to enabling drilling in the extended reach wells.

Finally, drilling fluid transmits hydraulic energy to power downhole tools, like mud motor and Rotary Steerable System (RSS), etc. Meanwhile, with the help of mud pulse telemetry, downhole Measurement While Drilling (MWD) tools can transmit information to the surface by pressure pulses. As a result, downhole real-time conditions could be presented to the rig personnel for making appropriate and effective decisions.

1.2 Research Purpose

In reality, downhole condition is highly unpredictable due to many uncertain and inconsistent factors. These uncertainties may exist in material property, borehole wall diameter, bottom hole assembly eccentricity, bit–rock interaction, drilling fluid and weight-on-hook, etc. Therefore, it is more realistic to investigate drillstring dynamics from a random/stochastic viewpoint. However, compared with drillstring deterministic dynamics analysis, research work in drillstring stochastic dynamics is slim. It is

the reason why this thesis focuses on the stochastic analysis of the drillstring.

It is well known that stick-slip is a severe format of vibration with apparent detrimental effects on the drilling system. The study of the drillstring stick-slip phenomenon has significant practical meaning. With the consideration of the randomness components in drillstring model, the dynamic characteristics of stick-slip can be evaluated more accurately, which may provide more reliable information for migrating stick-slip vibration.

Another purpose of this research work is to consider random component in calculating torque and drag. Estimating torque and drag plays a critical role in drilling complex wells, such as ultra-deep wells, extended-reach wells, directional wells, etc. Considering wellbore randomness in torque and drag calculation will allow the well planner to develop a risk assessment for a challenging well trajectory, which will benefit the exploitation of new hydrocarbon resources.

As mentioned above, there are many uncertainties in the drillstring system. However, it is meaningful and necessary to understand a complex problem gradually. That's probably why the current research works on stochastic dynamics of drillstring are focused on part of the uncertainties. The research work of this thesis consists of four parts. Each part considers different random component(s) depending on the research objective. The following four subsections will introduce them in detail.

1.2.1 Stick-slip Analysis of A Drillstring Subjected to Deterministic and Stochastic Excitations

This part of the research work is written in Chapter 3. Its objective is to investigate the stochastic response of the drill bit in the stick-slip phenomenon. The random excitation is assumed to be White noise caused by the random friction between the drill bit and the bottom of the hole. The probabilistic distribution of the responses at each discretized time instant is obtained. The two points, which represent entering and leaving the stick stage, are examined with special attention.

1.2.2 Investigation on Bit Stick-Slip Vibration with Random Friction Coefficients

This part of the research work is written in Chapter 4. As further research work from Chapter 3, it investigates stochastic stick-slip response by considering random components in both static and kinetic frictions. In the stick stage, the static friction is treated as either a deterministic value or a random variable. While in the slip stage, the random component of the kinetic friction is assumed as White noise. Then path integration (PI) method is firstly used to obtain the probability density evolution of the response. Monte Carlo (MC) simulation is used to validate the PI results and statistical analysis. In addition, parametric studies on damping, rotary speed, weight on bit, drillstring length and different combinations of pipe and collar are conducted

for both deterministic and random cases. The purpose of the research includes:

- Studying how uncertainties of the friction influence the stick-slip response.
- Analyzing how the changes of parameter influence the stick-slip response with the consideration of random friction.

The contribution of this work relies on that it is the first time differentiating the static and kinetic frictions in the model of random friction when studying the stick-slip vibration of the drillstring. Their effects on the characteristic of stick-slip, such as the period and first passage time, can be investigated. It will provide more detailed information when predicting the behavior of the drillstring stick-slip.

1.2.3 Investigation on Random Vibration of a Drillstring

This part of the research work is written in Chapter 5. In view of that the academic research in stochastic dynamics of drillstring is slim, work in Chapter 5 investigates the axial-torsional coupled vibration of a drillstring under combined deterministic and random excitations. The finite element method (FEM) is used to model the system. The random excitation at the bit-rock interaction, which is considered in the bit axial direction, is treated as Gaussian white noise. Statistic linearization will be first applied to find an equivalent linear dynamic system, which is then solved with the stochastic Newmark algorithm. The purpose of the research includes:

- Validating the Statistic linearization and stochastic Newmark algorithm by comparing the results with the Monte Carlo simulation.

- Analyzing the statistics of the responses, including the means and standard deviations of the bit axial displacement and rotational velocity.
- Analyzing stick-slip and bit-bounce phenomenon from the random viewpoint.

The contribution of this work relies on that it is the first time replacing the drillstring nonlinear bit-rock interaction model with an equivalent linear model in an axial-torsional coupled drillstring. After that, an exact analytical form of solution can be obtained by using linear system techniques. It will largely improve computational efficiency.

1.2.4 Static Study of Directional Drillstring from Random Viewpoint

This part of the research work is written in Chapter 6. Based on the literature review, work of this chapter aims to study the calculation of drillstring hoisting drag from random viewpoint. The finite element method (FEM) based on soft string model is firstly used for hoisting drag calculation of an S-shaped well. Then two strategies are taken to model the random component. The first strategy considers the randomness of the downhole friction. The second strategy considers the randomness of contact between drillstring and wellbore. Parametric studies on both strategies are conducted. Monte Carlo (MC) simulation is employed for statistical analysis. The methodology can be extended into torque or drag calculation in lowering, ream in and ream out drilling conditions. In summary, the purpose of the research includes:

- Building the finite element model of drillstring based on soft string model for hoisting drag calculation.
- Presenting two strategies to model the random component.
- Analyzing the effects of the random component on hoisting drag calculation by MC simulation method.

The contribution of this work relies on that it evaluates hoisting drag with the consideration of random components. It will improve the estimation of surface hoisting drag, making it safer to choose drilling devices, such as top drive and motor.

1.3 Research Contribution Summary

In the study of the drillstring from random viewpoint, the research work of this thesis attempts to make a contribution by considering these elements:

- Differentiate the static and kinetic frictions in the model of random friction.
- Use PI method to obtain the probability density evolution of the bit stick-slip response.
- Replace the drillstring nonlinear bit-rock interaction model with an equivalent linear model in an axial-torsional coupled drillstring.
- Suggest a novel approach for calculating random hoisting drag.

The next chapter will give a literature review of prior work related to drillstring random vibration and point out the gaps in the prior work.

Chapter 2

Literature Review

It is well known that three primary categories of vibratory motions exist in rotary oil-well downhole equipment: axial, torsional and lateral. The modes of vibration in drillstring [13] are depicted in Figure 2.1. An overview of drilling dynamics from deterministic perspective for three vibration modes and their coupling modes will be firstly given due to the fact that the deterministic dynamic models of drillstring are the foundation for stochastic analysis. As downhole vibrations are prevalent causes of drillstring failures, a brief review of drillstring fatigue failure is given in this chapter as well. Finally, stochastic drillstring models and solution techniques are surveyed and introduced.

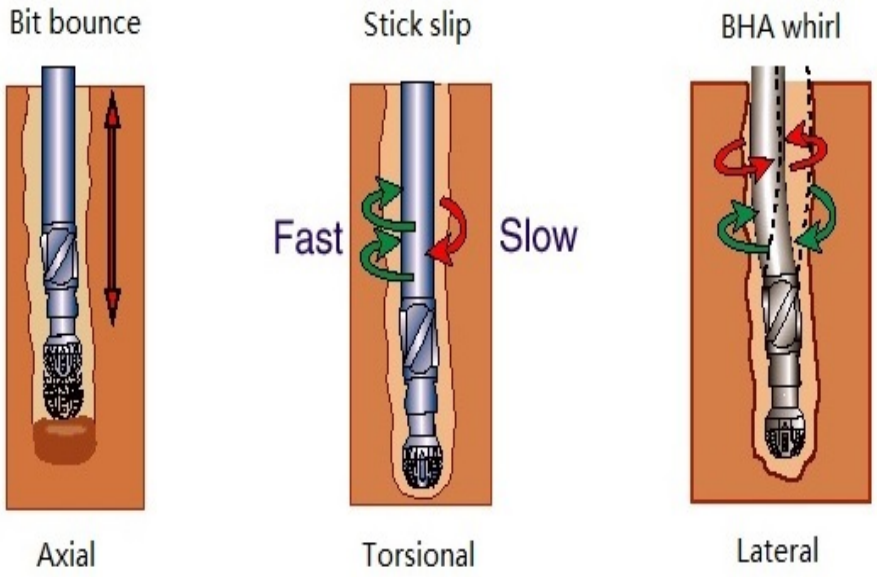

Figure 2.1: Modes of vibration in drillstring [13]

2.1 Deterministic drillstring dynamics

2.1.1 Axial vibration

Drillstring axial vibration is not difficult to be observed and detected at the surface. It is a vibration phenomenon parallel to its longitudinal axis. It has been found that the bit-formation interaction and the coupling effects from other vibration modes are the main causes of the axial vibration [14].

One of the most recognized axial vibration forms is bit-bounce, in which the bit repeatedly lifts off bottom and impacts formation. Severe bit-bounce may cause premature bit failure, damage bottom hole assembly (BHA) and decrease the rate of penetration (ROP). Spanos et al. [15] analyzed the bit-bounce phenomenon of

roll-cone bits in detail. Simulation results from their analytical model indicated that the rotary speed is associated with the axial resonant frequencies of the system. After that, many other researchers used the axial-torsional coupled model to investigate the axial bit-bounce and torsional stick-slip vibrations [16–18]. Some of the work from this perspective will be introduced in detail in the torsional vibration section.

Bit-bounce is likely to happen in near-vertical holes when drilling with RC bits due to their interaction with the formation. While in directional drilling, axial stick-slip vibration is also detected and studied by researchers. Based on a new experimental apparatus, Wang et al. [19] reported the axial stick-slip motion of drillstring while studying the toolface behavior in slide drilling. Experimental results indicated that a proper choice of rocking velocity [20] can help relieve axial stick-slip.

2.1.2 Torsional vibration

Torsional vibration is the angular vibration of the drillstring along its axis of rotation. Due to the torsional flexibility of the drillstring, downhole torsional speed may experience severe changes during drilling [21, 22]. An extreme phenomenon of drillstring torsional vibration is called stick-slip. It is a periodic switch between stick and slip phases, during which rotation of the drillstring is largely slowed down (or even stopped) and then suddenly increased when the torque on bit (TOB) overcomes the anti-torque result from the rock cutting and friction. As such, the rotary speed of the drillstring in the slip phase can be several times higher than that of the rotary table

[23].

Stick-slip vibration is harmful to drilling as it can largely decrease ROP and cause fatigue failure of the drilling tools. It has been reported that stick-slip can be destructive to the PDC bit [24]. To understand the causes and consequences of stick-slip vibration and find an effective way to migrate it, numerous researchers investigate the drillstring stick-slip vibration through numerical modelling, experimental setup and field testing.

The numerical model of drillstring in stick-slip analysis can be roughly divided into three categories: single degree of freedom (SDOF) lumped parameter model [25–28], multiple degrees of freedom (MDOF) model [16, 29–35] and distributed parameter model [36, 37].

In the SDOF lumped parameter model, the drillstring is simplified as a lumped mass-spring system with its top rotating at a constant speed [26] or driven by a rotary table [27]. Figure 2.2 presents an example of lumped mass-spring model [28]. The drill pipe is modelled by a linear torsional spring k. The drill collar and drill pipe are assumed to be rigid and modelled as the equivalent mass moment of inertia J1. Based on this model, Van de Vrande et al. [28] analyzed the stick-slip vibration of autonomous dynamic systems with dry friction. The authors used smooth functions to approximate the discontinuous friction forces. The method was validated to be accurate and reliable by simulation results.

MDOF model has the advantage of showing more drillstring details. Figure 2.3

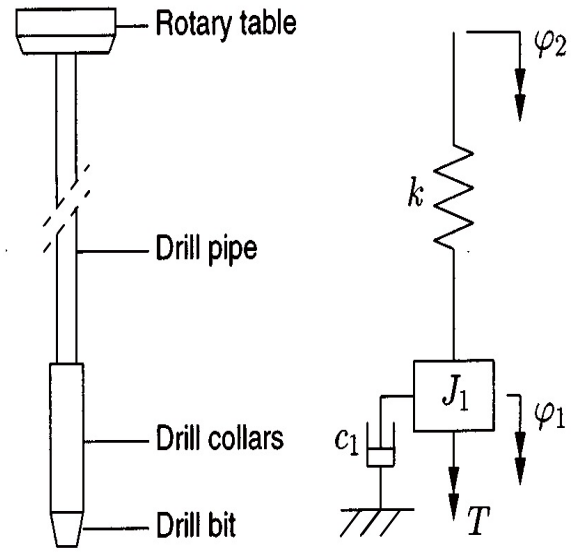

Figure 2.2: Simplified drillstring model in [28]

presents a drillstring model, which was simplified as a torsional pendulum with two degrees of freedom. Based on this model, Puebla and Alvarez-Ramirez [29] proposed an approach for suppressing stick-slip oscillations. In their work, stick-slip oscillations were analyzed using the models of Navarro-López and Suarez [38], Serrarens et al. [39] and Mihajlovic [40].

Navarro-López and Licéaga-Castro [30] developed a drillstring model considering the motion of the rotary table, drill pipes, drill collars and drill bit. The four degrees of freedom lumped pendulum model can be seen in Figure 2.4. Based on this model, a dynamical sliding-mode control was proposed to migrate drillstring stick-slip oscillations.

Figure 2.5 presented an n-dimensional lumped-parameter model of a conventional

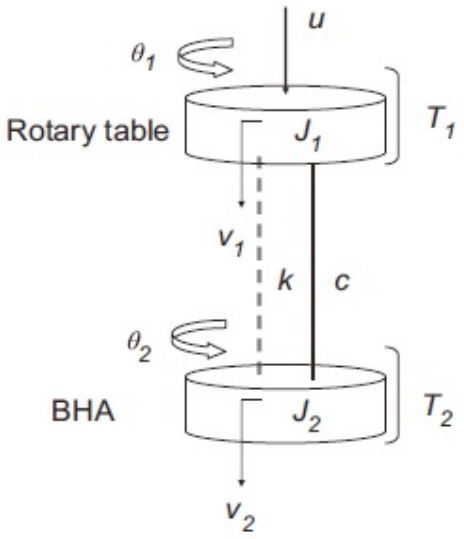

Figure 2.3: Simplified model of the drilling system in [29]

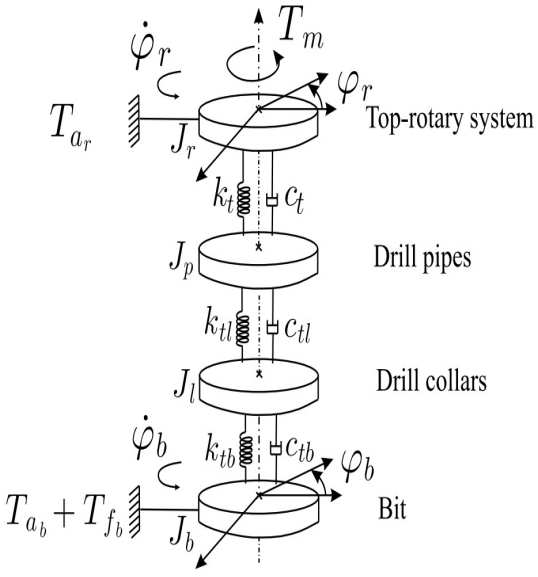

Figure 2.4: Four degrees of freedom lumped pendulum model in [30]

drillstring. Navarro-López and Cortés [31] used this model to analyze the stick-slip oscillation of the bit. In the parameter study of the WOB, the motor torque and the rotary speed, different bifurcations were identified and safe drilling parameters were suggested.

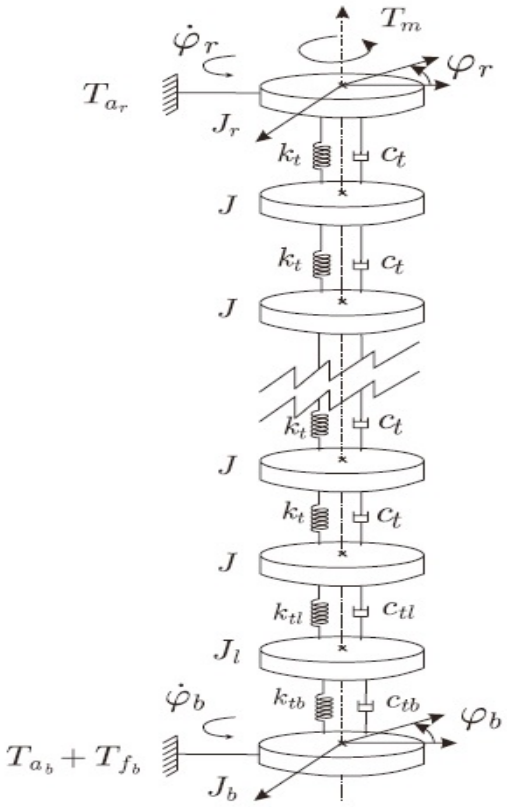

Figure 2.5: Drillstring model describing the torsional behavior in [31]

Figure 2.6 shows a discrete axial-torsional coupled model of the drillstring system. The coupling between two vibration modes was realized by modelling the TOB as a combination of friction contact and cutting processes at the bit-rock interface.

Using this model, Richard et al. [32] studied the self-excited stick-slip oscillations of drillstring with a drag bit. Simulation results indicated that the model could capture stick-slip and bit-bounce behaviors. It was reported that the delayed and coupled nature of the cutting process might initiate the self-excited vibrations and stick-slip oscillations. The model in Figure 2.6 was used or expanded by many other researchers [41, 42].

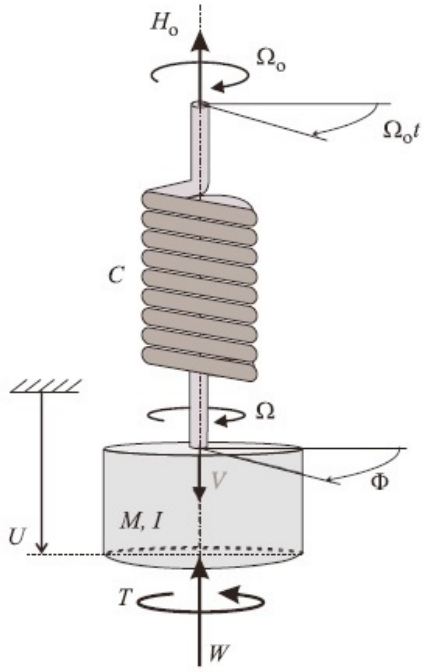

Figure 2.6: Sketch of a mechanical model of the drilling system in [32]

Yigit and Christoforou [16] formulated the equations of motion of a rotary drillstring with a lumped parameter model (Figure 2.7), which considers axial-torsional coupling. The authors suggested that rotational control along with axial control can

effectively suppress stick-slip vibrations and bit-bounce.

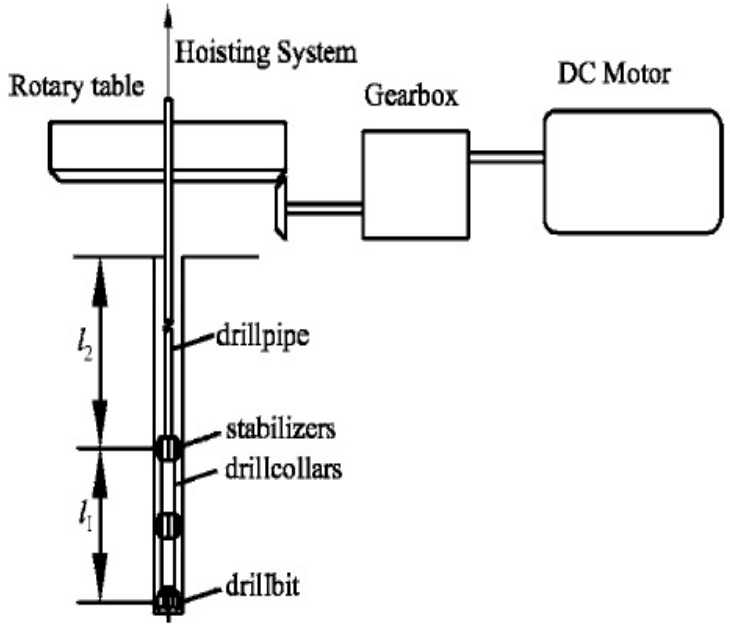

Figure 2.7: Sketch of the model in [16]

Many other researchers used the finite element method (FEM) to build drillstring dynamic models for studying stick-slip vibration. Khulief et al. [33] developed a numerical model of drillstring using the Lagrangian approach in conjunction with the finite element method (FEM). Their model considered torsional-bending inertia coupling, axial-bending geometric nonlinear coupling, gyroscopic effect and gravitational field effect. Simulation results were reported to be in excellent agreement with the observations and measurements from the field. Sampaio et al. [34] used a geometrically nonlinear model to study the drillstring axial-torsional coupling. The geometrical stiffening was realized and analyzed using a nonlinear finite element approximation,

accounting for large rotations and nonlinear strain-displacements.

Based on the lumped-segment approach, Sarker et al. [35] presented a bond graph model of drillstring to analyze the bit bounce and stick-slip vibrations. The dynamic model was axially-torsionally coupled due to bit-rock interaction. A state feedback controller, which was designed based on a linear quadratic regulator (LQR) technique, was proposed in the paper. Simulation results indicated that this controller could effectively suppress stick-slip oscillations and make it possible to drill at lower speeds. In another work of Sarker et al. [43], the authors extended their model to study the longitudinal and torsional dynamics of a horizontal drillstring.

Numerous experimental and field studies were conducted to analyze drillstring stick-slip vibrations. Based on 3500 hours of field measurements, Dufeyte and Henneuse [44] pointed out that it is possible to mitigate stick-slip vibrations by controlling rotary table velocity, WOB and mud viscosity. Research work from Chen et al. [45] indicated that roller cone bit might have the stick-slip problem in some drilling conditions. Yaveri et al. [46] analyzed the cause of the stick-slip and whirl phenomenon by conducting a case study on 16 offshore wells.

2.1.3 Lateral vibration

Lateral vibration occurs in the direction orthogonal to the wellbore centerline. In the case of lateral vibration, the center of rotation of the drillstring will diverge from the wellbore centerline. Contact between drillstring and wellbore will occur if the lateral

displacement exceeds the clearance between them [47, 48].

Lateral vibration is considered the most destructive among the three vibrations and can create large shocks. It may cause uneven drillstring and stabilizer wear, and bore-hole wall enlargement. In fact, it is one of the critical factors that induce BHA failures [49–54]. However, paradoxically, lateral vibration is difficult to detect at the surface because it barely travels beyond the neutral point [21].

Lateral vibration can be induced by many sources. The first one is mass imbalance. As explained by Vandiver et al.: "If the center of gravity of the drill collar is not initially located precisely on the centerline of the hole, then as the collar rotates, a centrifugal force acts at the center of gravity, causing the collar to bend" [54]. Mass imbalance can be caused by production and the unevenly distributed electrical components along the drillstring. It can also be generated by pre-bent or pre-buckled drillstring tools, which introduce an artificial eccentricity in drilling [54, 55]. The second is friction contact. The lateral restoring forces and tangential friction forces induced by the contact between drillstring/bit and formation were reported as the source of lateral vibration by many researchers [56–58]. Besides these, drillstring rotational speed [50] and dynamic coupling [59–62] can also generate lateral vibration.

An important subset of lateral vibrations is the BHA whirl phenomenon. Most of the BHA will operate in compression as drilling proceeds. This situation causes the BHA to be a region where buckling and whirling are likely to occur. The BHA whirl can be qualified as a forward or backward whirl depending on whether the BHA

rotates around the wellbore in the same direction as the driving rotation, as can be clearly seen in Figure 2.8. Further, forward and backward whirl can be divided into forward synchronous whirl [54], forward whirl [63], no whirl, non-synchronous backward whirl [54], synchronous ("pure") backward whirl [54, 63] and chaotic whirl [63–65]. Macpherson et.al. [66] provided a brief explanation of various whirl categories.

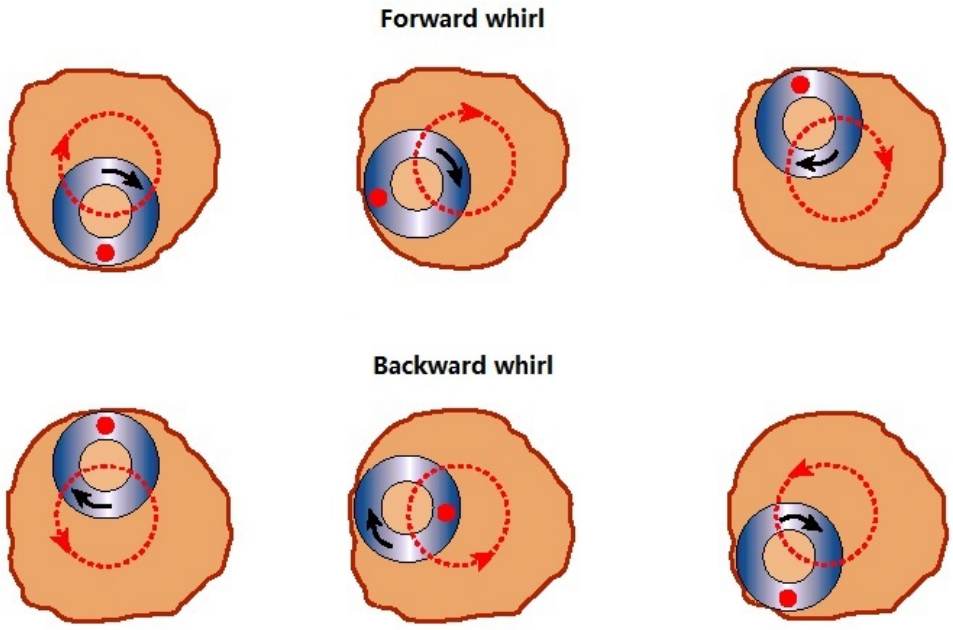

Figure 2.8: BHA whirl phenomenons in [13]

Multiple degrees of freedom finite element models were used by numerous researchers to investigate lateral vibration and whirl. Millheim et al. [67] indicated that increasing rotation speed could increase lateral vibration amplitude and the

probability of whirl could be increased by enlarging contact friction coefficient. Baird et al. [68] reported that whirl could be detected by changing the clearance between bit and wellbore. Simulation results from their paper indicated that the phenomenon of bit whirl is prominent for small hole clearances. A similar conclusion could be found in the research from Braker and Azar [69].

In 1985, Mitchell and Allen [51] pointed out that lateral vibration was responsible for BHA failures in drilling. After that, more research efforts were taken to develop new theories and models of lateral vibration and whirl.

Using a nonlinear lumped-parameter ODE, Jansen [70] built a model of drillstring between two stabilizers. Simulation results indicated that rotary speed below the lateral natural frequency of the drillstring is key to initiating forward whirl, and backward whirl is influenced by stabilizer friction contact. Later, Jansen [63] improved this work by considering the gravity and the contact between the drill collar and wellbore. Based on Jansen's work, Van der Heijden [65] improved the model by applying the Hamiltonian formulation to get analytical solutions. Van der Heijden corroborated Jansen's findings that forward whirl may change to backward whirl or chaotic whirl in some conditions.

Heisig et al. [48] reported that in some conditions, drillstring sinusoidal buckling ("snaking") could transition to whirl or backward whirl. The work of Dykstra et al. [71] suggested that BHA backward whirl can be removed by decreasing WOB and contact friction values. Theron et al. [72] pointed out that increasing friction

coefficients and contact damping will encourage whirl phenomenon. While increasing stiffness and damping of the drillstring bending mode will discourage whirl.

Gorelik and Höhn [73] reported a dependency between the whirl mode and initial conditions of drillstring. In their paper, parametric studies of hole inclination and forcing frequency were conducted. As a result, transition zones between snaking and backward whirl were presented. Popp et al. [74] analyzed backward whirl by conducting tests on an in-house backward whirl testing rig. Test results indicated that friction induced contact may lead to backward whirl.

Dunayevsky et al. [75] pointed out that axial vibration is a crucial factor in drillstring whirl, as geometric imbalance may be induced if the applied WOB is larger than the critical load for static buckling. Vandiver et al [54] reported a case study of backward whirl, which was caused by bit-bounce. Same dominant peak can be noticed in the frequency domain of the WOB and BHA bending moment. Christoforou and Yigit [56] found that backward whirl of BHA may get initiated by the parametric resonance when the frequency of axial loading at the bit is roughly twice the natural bending frequency.

Working with mass imbalance, stick-slip vibration of drillstring may also enlarge lateral vibrations [62]. Based on this phenomenon, some researchers suggested controlling lateral vibration by migrating stick-slip oscillations. Yigit and Christoforous [76] effectively eliminated the lateral vibration by adding an active controller to the rotary table. Al-Hiddabi et al. [77] took advantage of nonlinear inverse dynamic con-

trollers to modulate the rotary table speed and bit speed, respectively. The authors suggested that controlling bit speed may be more effective in migrating stick-slip oscillation and alleviating lateral vibration.

2.1.4 Directional drilling

Directional drilling is of crucial importance in the oil and gas industry due to its ability to increase drilling efficiency and maximize potential profit. For example, the number of offshore platforms has been greatly reduced by drilling long horizontal reach wells. The need for drilling deep and extended-reach wells is increasing. However, it is constrained by many factors, such as the drilling torque and drag [78], which make drilling beyond a certain measured depth impossible. Estimating torque and drag is critical in well profile planning, real-time drilling, and post-analysis [79]. Therefore, enabling an accurate prediction of torque and drag is very important.

In general, the existing torque and drag calculation methods are mainly based on two classical models: the soft-string model [80] and the stiff-string model [81]. The soft-string model developed by Johancsik et al. [80] has exerted a great influence over the petroleum industry. The basic idea of this method is based on the assumptions that the drillstring lateral stiffness can be neglected and its body is continuously contacting with the wellbore. As a result, the value of friction coefficient is crucial to the application of this method and was usually found by Coulomb's friction model [82]. Based on the soft-string model, optimal well path design was addressed [82, 83]

as well as the hydrodynamic influence on torque and drag calculation was considered [84, 85]. In recent years, Aadnoy et al. [86] developed analytical friction models for straight, build-up, drop-off, catenary profiles and side bends. In another work of Aadnoy et al. [87], new torque and drag equations for curved sections were given and a tension dominant process was presented. However, the obvious shortcoming of the soft-string model is the overestimation of torque and drag because the drillstring is in continuous contact with the wellbore.

In drilling process, especially in directional drilling, the drillstring system usually experiences overall rigid motion, 3D rotation, large wellbore deformation and severe downhole vibrations. These dynamic factors may lead to significant detrimental effects on the drilling system. Those detrimental effects include a decrease in the rate of penetration (ROP), interference with measurement while drilling (MWD) tools, and causing fatigue of the drilling components. As directional drilling has been widely used for decades and the need to drill deep and directional wells is increasing nowadays, more and more papers in the open literature study directional drilling from the dynamic viewpoint. In the existing works, some researchers took advantage of commercial software [88, 89] to study the contact between drillstring and borehole, some built models of their own using finite element models [90, 91] or multibody dynamic models [92] to study real-time torque and drag. Siamak et al. [93] employed finite element and finite segment methods to build a dynamic model for well path design. Sarker et al. [94] developed a bond graph dynamic model of a horizontal

oilwell drillsting to predict its longitudinal and torsional response. To increase ROP, an Agitator tool was simulated as a force excitation in their paper.

2.2 Drillstring fatigue

Drillstring failures are costly and time-consuming in the oil and gas industry. There are many failure modes of drillstring [3]. Among them, fatigue is the main cause for most drillstring failures according to field data [3, 95–97]. Thus, avoiding catastrophic drillstring failures caused by fatigue damage during drilling operations is of great economic significance.

The research on drillstring fatigue is based on experimental works, theoretical models analysis and case studies. There are rich literatures on experimental work of drillstring fatigue analysis [98–100]. In the experiments, full-size drill pipes were usually subjected to different excitations in the air or corrosive media. The data provided by these experimental works formed the basis for the theoretical prediction of fatigue.

Many researches about the drillstring failure analysis are based on case studies [101–105]. Among them, Wang et al. [103] systematically investigated the causes of drillstring failure encountered during drilling practice in the northeast Sichuan region (China) based on more than 130 failure cases. Fault tree analysis was conducted. It was observed that the deterioration of fatigue resistance of drillstring is related to its poor quality or manufacturing defects and unscientific design. Further, prevention

measures were proposed.

Theoretical models are developed mainly along two lines to analyze fatigue failures of drillstrings. One is based on the fracture mechanics theory, which studies the cracks propagation in drill pipe body under cyclic loads [106]. This method is developed on the assumption that micro cracks already exist in the drill pipe materials and will propagate in the drill pipe body in certain directions under cyclic loadings. The crack area constitutes a stress concentration zone and will eventually lead to drill pipe failure if the critical dimension of the crack is reached [107–109]. For example, Chi et al. [109], predicted the fatigue life of a drillstring based on the assumption that fatigue failure occurs when the initial crack in the drillstring grows to reach a limiting size.

The other method uses the cumulative fatigue damage model, which is based on the S-N curve, a failure criterion, and a damage accumulation rule [110–114]. Comparatively, the second method is more widely accepted, partly because of data support from experimental works. This method was initiated by Lubinski [110]. After that, many modifications were made to the S-N curves, boundary conditions, and cyclic stress calculation by Hansford and Lubinski [111], Wu [112, 113], Sikal et al. [114], Sathuvalli et al. [115] and other researchers. To use this method properly, a lot of factors need to be considered [116, 117]. For example, mean stress, the sequence of cyclic loading, stress concentration factor, safety factor, corrosion effect, etc.

It is recognized that the cumulative fatigue damage is of stochastic nature [118].

The randomness comes mainly from two aspects: the uncertainty of materials' fatigue resistance and the uncertainty of loading [118]. In fact, there is generally a considerable scatter in fatigue data. Even apparently identical specimens may give greatly varying fatigue data in test [119]. Therefore, it is necessary to use a statistical procedure to consider cumulative fatigue damage. To predict the rate of occurrence of stress cycles, many counting methods are available to extract and count the equivalent load cycles from a random time history. Of all the methods proposed, the rain-flow cycle counting method is regarded as the most successful and is widely used in the open literature [114, 120, 121].

Several analytical approximation techniques based on the stress autospectral density function were also developed. These methods include Rayleigh approximation method [122], peak approximation method [123], single moment method [124], the method proposed by Ortiz and Chen [125] and the formula of Wirsching and Light [126]. It is pointed out by Lutes and Sarkani [119] that, for very narrowband Gaussian processes, good agreement among all these methods can be obtained. However, for processes that are not narrowband, sometimes, significant differences can be noticed [119]. Meanwhile, it is reasonable that the probability distribution of a stress process is non-Gaussian. Thus, numerous works have been done by researchers [123, 127, 128] to approximate the non-Gaussian effect for a narrowband stress process. In the recent years, researches for predicting fatigue life under stationary broadband non-Gaussian [129] or Gaussian processes [130, 131] were published.

2.3 Stochastic drillstring dynamics

The downhole condition is highly unpredictable due to many uncertain and inconsistent factors. These uncertainties may exist in material property, system dimension, fluid-structure interaction, bit-rock interaction, etc. Therefore, it is more meaningful to investigate drillstring dynamics from random/stochastic viewpoint.

Although rich publications exist in the open literature on drillstring dynamic study, few research works are available on random vibrations of drillstring.

Bogdanoff and Goldberg [132] were regarded as the pioneer in introducing the probabilistic approach to drillstring dynamics. They modelled WOB and TOB using a zero-mean normally distributed process in the late 1950s.

With a model of a drill collar section between two stabilizers, Kotsonis and Spanos [64] analyzed the effects that a stochastic WOB would have on the overall lateral vibrations. A one-sided power spectral density was used to generate the time histories for a zero-mean random axial force. The power spectral density was characterized by two energy peaks at 3X and 6X the rotation speed. Their research indicated that the collar would undergo chaotic motion with a minor component of randomness when the collar rate of rotation reaches and exceeds the natural frequency of the collar.

The research group of Spanos and Chevallier utilized the statistical linearization method to investigate the lateral behaviors of nonlinear drilling assemblies subject to deterministic and random excitations [21, 133, 134]. In the Ph.D. thesis of Chevallier [21], the author built a drillstring finite element model based on Euler-Bernoulli beam

theory. The nonlinearity of the system due to the contact between the drillstring assembly and the formation was formulated by Hertz's contact law. The random input forces were defined by their power spectral densities, which were estimated from field data and based on the influence of the bit type on excitation mechanisms. As can be seen in Figure 2.9, the excitations induced by roller cone bits were modelled with band-limited white noise and excitations induced by PDC bits were modelled by a Kanai-Tajimi process. After synthetic time histories were generated using Auto Regressive Moving Average (ARMA) filters, Monte Carlo simulation was conducted to get the system response in the time domain. Further, the statistical linearization technique was used to find an equivalent linear dynamic system. This procedure was implemented by using the covariance matrix approach in the time domain and the spectral matrix technique in the frequency domain. However, the work of Chevallier [21] didn't consider drilling fluid in the finite element model, which influences the lateral stiffness of the drillstring.

Ritto et al. [135–140] made contributions to investigate the stochastic vibration of drillstring with uncertainties in the bit-rock interaction [135–138] and weight-on-hook [139, 140]. In one of their research works, the authors [136] developed a non-linear drillstring finite element model based on the Timoshenko beam theory. The dynamic model considered bit-rock interaction, fluid-structure interaction and impact forces. A new strategy that uses the non-parametric probabilistic approach was developed to describe the uncertainties in the bit-rock interaction. The results of the paper

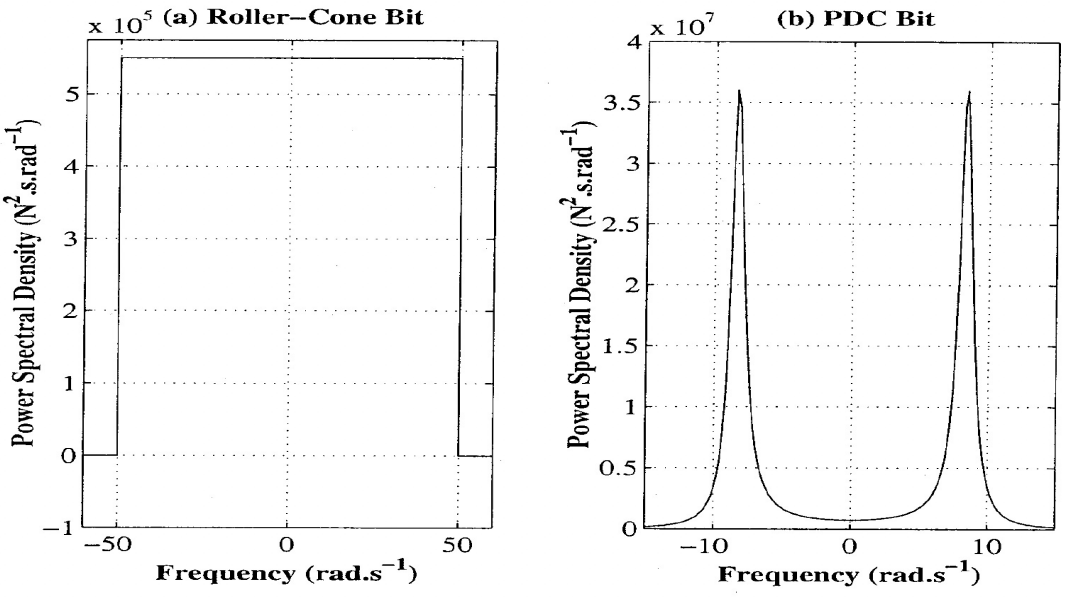

Figure 2.9: Excitation models for BHA with a tricone bit (a) and a PDC bit (b) in [21]

indicated that the uncertainties play a crucial role in the coupling among the axial, torsional and lateral responses. In their another work [140], the supporting force exerted by the hook at the top was modelled as a random variable with its probability density function constructed by means of the Maximum Entropy Principle. Results from Monte Carlo simulations indicated that the system response is sensitive to the dispersion on the weight-on-hook.

Based on a nonlinear stochastic drillstring finite element model, Ritto et al. [141] proposed a methodology for robust optimization to maximize the expected mean ROP of the drillstring. The computational model considered the uncertainties of the structure and the uncertainties of the bit-rock interaction. The nonparametric probabilistic approach was used to model these uncertainties. The proposed robust optimization problem respected the integrity limits of the system, which were represented by the ultimate stress of the material, the damage cumulated by fatigue and the stick-slip factor. Simulation results indicated that the robust analysis gives different responses between the deterministic and random optimization analysis.

Based on the bit-rock interaction law proposed by Yigit and Christoforou [16], Qiu and Yang [142] built a finite element model of drillstring with axial-torsional, lateral-torsional coupled. Gaussian white noise was added to the TOB. Dynamic behaviors of the drillstring model subject to both deterministic and random excitations were investigated. Monte Carlo simulation was employed to obtain the statistics of the stochastic response. Simulation results were analyzed in terms of the mean and

standard deviation of bit speed. Random components in drillstring axial and lateral directions were observed due to axial-torsional and lateral-torsional couplings.

Based on the Euler-Bernoulli beam theory and finite element method, Marquez [143] developed a mathematical representation of a suspended drillstring assembly subject to stationary and non-stationary excitations at the PDC bit. By using a colored noise with double-sided power spectrum (Figure 2.10) and passing it through an auto-regressive (AR) digital filter, synthesized time histories of stationary and non-stationary excitations were generated for Monte Carlo simulations. The statistical linearization technique was used to obtain an exact, analytical form of solution. Simulation results demonstrated a lower lateral displacement at the drill bit compared with the results from Chevallier [21]. Further, the author developed a stochastic model of a drillstring with RC bit for vibration assisted drilling (VAD). Synthesized time histories of a stationary process were generated by passing the band-limited white noise via a moving-average (MA) digital filter. The author analyzed the resonance effect in which the natural frequency splits into two due to the gyroscopic effects. When simulation with soft formation, it was observed that natural frequencies were separated at lower RPMs. While for compact formations, natural frequencies were separated at higher RPMs. Compared with deterministic cases, resonance effects were developed at lower RPM in Monte Carlo simulations.

With an axial-torsional coupled drillstring model discretized by means of the finite element method, Lobo et al. [144] proposed a novel stochastic model to describe the

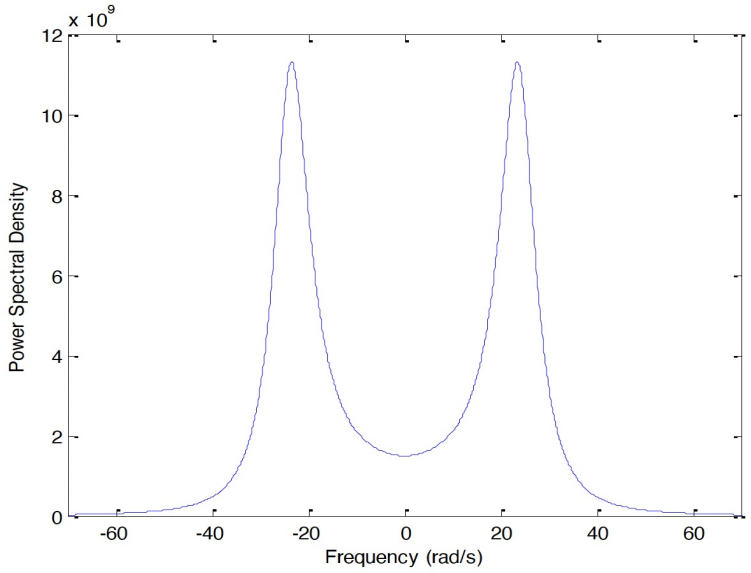

Figure 2.10: Two-sided auto-spectral density for a colored process in [143]

uncertainties on the rock strength and analyzed the effect of such uncertainties on torsional vibration severity. The cutting component of the TOB was considered a stochastic process generated by Itô stochastic differential equations. Two different stochastic processes were considered to model the rock strength. The first one was the Ornstein-Uhlenbeck process which continues to vary without considering the rotary speed of the drill bit. While the second one was a novel stochastic process which considered the bit dynamics when severe torsional vibration happens. Compared with the deterministic model, statistical analysis of the Monte Carlo simulation results indicated that the uncertainties on rock strength may lead to predictive scenarios where bit vibrations amplitude is significantly larger. However, the type of rock that is suitable for applying the novel stochastic model is obscure in the paper.

In the Ph.D. thesis, Popp [145] conducted a stochastic analysis of the BHA whirl phenomenon in drillstring with a three-degrees-of-freedom lumped parameter model. In the deterministic case, the author improved whirl models by considering gravity, asymmetry, Hertzian contact, non-Hertzian contact and BHA misalignment, respectively. In the stochastic case, lateral-torsional coupling was considered in the dynamic model. By using ARMA digital filters and target spectra from downhole TOB measurements, time-histories of excitation were synthesized. The stick-slip TOB spectrum was modelled by a modified colored noise spectrum (e.g. Kanai-Tajimi spectrum), while the consistent TOB spectrum was modelled by a modified Davenport spectrum. By implementing the Newmark-β scheme, Monte Carlo simulation was conducted to generate stochastic responses for statistic analysis. Research results indicated that backward whirl is not likely to be induced by torsional coupling in smooth drilling but could be initiated by stick-slip oscillation and friction-induced contact. The theoretical studies were supplemented by experimental tests in a rig and 2D/3D finite element analysis (FEA) models in a commercial software package. The work of Popp [145] didn't consider the fluid forces in the equations of motion when studying BHA whirl. It will lead to less consideration of WOB and TOB.

Volpi et al. [146] conducted a stochastic analysis of coupled lateral-torsional drillstring vibration based on a three-degrees-of-freedom lumped parameter model. In the stochastic model, uncertainties in the borehole wall diameter, in the bottom hole assembly eccentricity, and in the bit–rock interaction were modelled as random vari-

ables. Critical vibration phenomenons like severe torsional vibration, lateral impact, forward whirl and backward whirl were analyzed in both deterministic and stochastic cases. Probabilistic maps for three uncertain parameters were presented to analyze the impact of uncertainties on critical vibration phenomenons. Several conclusions could be drawn from statistical results. The probability of backward whirl could be enlarged by increasing either WOB or rotational speed. Randomness in the borehole diameter could reduce the chances of the backward whirl and lateral impact. Randomness in the bottom hole assembly eccentricity could largely increase the impact incidence. The uncertainties in the bit-rock interaction could greatly affect severe torsional vibration, backward whirl and impact.

Lobo et al. [147] analyzed control strategies for suppressing stick-slip vibration of drillstrings by using a torsional drillstring model with the consideration of uncertainties in the bit-rock interaction. The modelling of uncertainties was calibrated with field data to improve its reliability. The significance of the paper relies on that it calibrated stochastic excitation modelling. However, the drilling formation that is suitable for applying the calibrated stochastic excitation was not suggested by the authors.

All the works mentioned above are for vertical drilling. Some other researchers work on directional drilling from random viewpoint.

Ritto et al. [148] studied the drillstring horizontal dynamics with uncertainties on the frictional force by assuming a random frictional coefficient field. Only the

horizontal part of the drillstring was considered, which was modelled using a bar model and was discretized by means of the finite element method. As can be seen in Figure 2.11, the dynamic model was subjected to a constant force (f_{sta}) from drill pipes, a harmonic force (f_{har}) due to the mud motor driving force, friction (f_{fric}) and force from bit–rock interaction (f_{bit}). The system's performance was measured by the ratio Y between the output and input power. Results from Monte Carlo simulation indicated that the probability density functions of Y were quite different for different slenderness parameters and different uncertainty levels of the frictional coefficient. Further, stick-slip behavior in the axial direction was observed and analyzed in the paper.

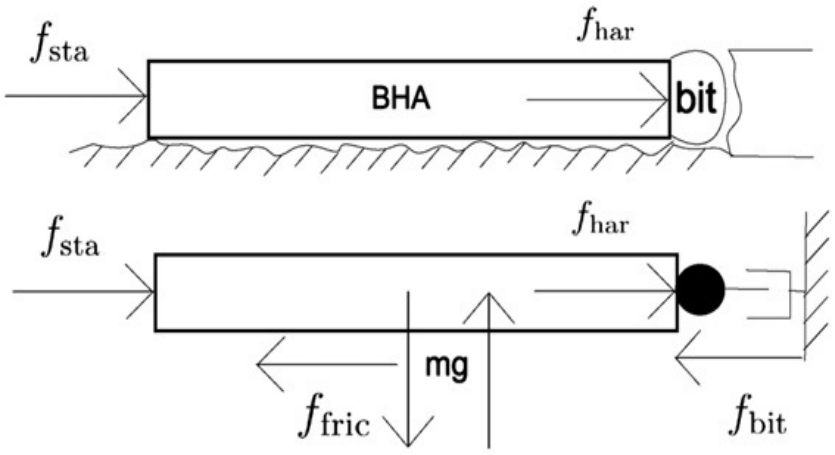

Figure 2.11: Sketch of the system analyzed in [148]

Tian et al. [149] conducted vibration characteristics analysis and experimental study of horizontal drillstring with a random friction force. The distribution of the

random friction coefficient was assumed to be Gaussian and the random variable was described by Karhunen-Loéve method. An equation was established to evaluate horizontal drilling efficiency. The analysis model of the drillstring was verified by comparing the theoretical calculation with the experimental test. The phase diagram and Poincare plot of the test point indicated a chaotic vibration response of the system. The work of Tian et al. [149] and Ritto et al. [148] only considered axial direction in their dynamic models. According to work by Aadnoy et al. [86], the rotation will decrease the axial drag compared to a non-rotating pipe.

Kremers et al. [150] proposed a model-based control strategy for directional drilling by treating the bottom hole assembly (BHA) as a linear Euler-Bernoulli beam. Parameter uncertainties and gravity-induced perturbations were considered in their work. Cunha et al. [151] analyzed the nonlinear stochastic dynamics of drillstrings in a horizontal configuration. A beam theory with the effects of rotary inertia and shear deformation was considered in their model. Parameters in the bit-rock interface law were modelled by random variables.

2.4 Summary

Compared with the research effort in deterministic drillstring dynamics, work in stochastic drillstring dynamics is relatively slim. However, the downhole condition is unpredictable in nature. Researchers have found different responses by using the deterministic and random drillstring models [141, 143] and believe that the stochas-

tic drillstring model is essential to design and evaluate control strategy for migrating stick-slip vibrations of drillstring [147]. Therefore, research in drillstring from random/stochastic viewpoint is necessary and needs strengthening.

In the majority of drillstring stochastic vibration analyses, random excitation was either generated by using a digital filter and approximated excitation spectra [21, 143, 145] or modelled by assuming critical parameters as random variables or stochastic processes [136, 140, 144, 146, 148]. MC simulation was generally used for obtaining statistic results [136, 140–142, 144–146] as a closed-form solution is challenging or impossible to derive for nonlinear stochastic drillstring systems. However, MC requires extensive computation and is often used to verify the results from other methods.

For large-scale engineering problems, combining the stochastic linearization technique and some direct schemes, such as the stochastic Newmark and stochastic difference methods, is an effective way to get an exact analytical form of solution. Following this perspective, Chevallier [21] and Marquez [143] applied the stochastic linearization technique when dealing with drillstring lateral nonlinearity. More work could be done for the drillstring in other directions. Based on this, in Chapter 5, work of this thesis will replace the nonlinear bit-rock interaction model with an equivalent linear model in an axial-torsional coupled drillstring.

Very few publications exist in the literature that modelled friction as random when dealing with the stick-slip vibration of the drillstring. To the author's best knowledge,

the works by Ritto et al. [148], Jialin et al. [149], and Cunha et al. [151] are the few papers considering friction as random. However, these works didn't differentiate the static and kinetic frictions, which were reported to exhibit randomness through experiments by Ibrahim et al. [152]. In view of this, research work of the thesis will differentiate the static and kinetic frictions in the model of random friction to analyze their influences on the stick-slip vibration of the drillstring. What's more, Path Integration (PI) method will be first applied to obtain the probability density evolution of the bit stick-slip response.

Finally, in drilling deep and extended-reach wells, the estimation of torque and drag plays an important role in well profile planning, real-time drilling, and post-analysis [79]. However, very few publication exists in the open literature dealing with torque and drag calculation from random viewpoint. To fill this gap, work of this thesis will present a novel approach for calculating random hoisting drag in Chapter 6. Based on this, the range of surface drag and torque could be estimated, allowing the well planner to develop a risk assessment for a challenging well trajectory.

Chapter 3

Stick-slip Analysis of A Drillstring Subjected to Deterministic and Stochastic Excitations

The research work of this chapter has been published: Hongyuan Qiu, Jianming Yang and Stephen Butt. Stick-slip analysis of a drillstring subjected to deterministic and stochastic excitations. *Shock and Vibration*, Volume 2016, Article ID 9168747, 7 pages.

3.1 Co-authorship Statement

Hongyuan Qiu: Dynamic Modeling, Methodology, Simulation, Data Processing, Result Analysis and Writing Manuscript. **Dr. Jianming Yang**: Supervision and

Reviewing. **Dr. Stephen Butt**: Supervision and Reviewing.

3.2 Abstract

Using a finite element model, this paper investigates the torsional vibration of a drillstring under combined deterministic and random excitations. The random excitation is caused by the random friction coefficients between the drill bit and the bottom of the hole, and assumed as white noise. Simulation shows that the responses under random excitation become random too, and the probabilistic distribution of the responses at each discretized time instant are obtained. The two points, entering and leaving the stick stage, are examined with special attention. The results indicate that the two points become random under random excitation, and the distributions are not normal even when the excitation is assumed as Gaussian white noise.

3.3 Introduction

In oil and gas industry, wells are drilled for either exploration or production purposes. The drillstring, a very long and slender structure, experiences various vibrations during drilling operations, which can have significant detrimental effects on the drilling system [153]. Those detrimental effects include decrease of rate of penetration (ROP), interference with measurement while drilling (MWD) tools, and causing fatigue of the drilling components. In general, three vibration modes exist in the

drillstring, namely axial, torsional and lateral. Among the three vibrations, torsional vibration has attracted significant research effort partially due to its severe negative effects on drilling efficiency and life of drillstring components. In the open literature, the torsional vibration /dynamics of a drillstring has been modeled in several ways [31, 33, 61]. A torsional pendulum with one or two degrees of freedom is often used [29, 41, 154] for modeling stick-slip, one special type of torsional vibration. These models are good to look at the dynamics qualitatively; however, they may not be adequate to provide more quantitative insight to the problems under investigation. Thus, some other researchers modeled the system with the Finite Element Method (FEM) [34, 155, 156]. In modeling the torsional vibration, a important factor is the excitation to the system. Some researchers accounted for the friction between the drillstring and the wellbore, others focused on the resistant torque on the bit [16, 28, 29, 31, 32, 153, 154]. Existing research has revealed that the excitation from the bit-rock interaction is especially complicated [32, 153, 154], involving both friction and cutting mechanisms. Under certain conditions, the friction mechanism may cause stick-slip motion of the bit which has particularly negative effect on the drilling system. Some researchers examined the stick-slip motion and the complicated dynamics in torsion [16, 28, 29, 31, 32, 153]. Undoubtedly, these research works are helpful to understand the complex dynamics of the drillstring in rotation; however, limitations exist. First, both field test and theoretical analysis have indicated that the friction mechanism between two surfaces is very complicated; the friction coefficient,

in reality, is related to various different factors, such as the profile of the surface, the materials and the lubrication conditions etc. The value of friction coefficient is always highly scattered. Second, the downhole condition is highly unpredictable due to the many uncertain factors in the well bore. These factors determine that the drillstring vibration and dynamics can't be well understood with deterministic theory, rather methods from random vibration and/or stochastic dynamics would be much more powerful tools. As a matter of fact, Bogdanoff and Goldberg [132] realized this point already in as early as 1950's, and proposed a probabilistic model. However, research work along this direction has progressed very little since then, probably due to the conceptual complexity of random vibration. Among the very few researchers working on random vibrations of drillstring, Chevallier [21] investigated lateral vibration with a nonlinear random model. In his work, the excitation for a tri-cone bit and a PDC bit were modeled as a Kanai Tajimi process and as band limited white noise, respectively. The nonlinearity was handled with a stochastic linearization technique. In recent years, Ritto et al. [135–138] also investigated drillstring dynamics with probabilistic models. Their focus was placed on the bit-rock interaction, and the drilling fluid effect on dynamics. In some other papers, Ritto et al. [139, 140] also studied the uncertainties in the weight-on-hook.

In general, there is a lack of work on torsional vibration of drillstrings from the random perspective. In view of this fact, this paper, which is based on the work of [157], focuses on the random torsional vibration of a drillstring. FEM is used to

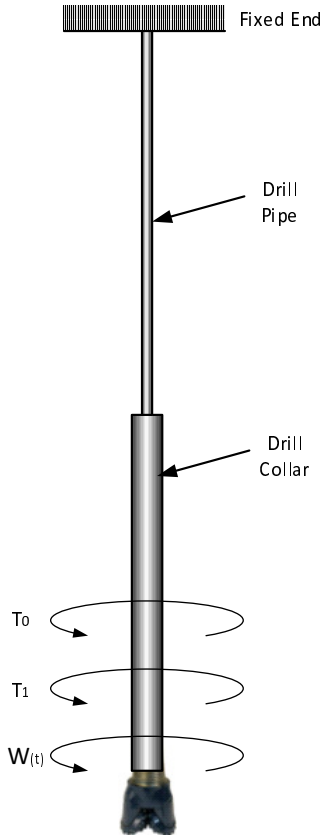

Figure 3.1: The dynamic model of the system.

build the dynamic model. The central difference method is then used to solve for the solution, and Monte Carlo (MC) simulation is carried out to obtain the statistics of the responses. The paper is organized as follows. In Section 3.4, a dynamic model is developed. Following that, the solution strategies used in both deterministic and random cases are presented in Section 3.5. Simulation results are presented and analyzed in Section 3.6. Finally, conclusions are drawn in Section 3.7.

3.4 Formulation

3.4.1 Dynamic Model

The drillstring investigated in this paper is schematically shown in Figure 3.1. For convenience of mathematical derivation, it is assumed that the top is clamped, while the ground rotates with a constant speed. This does not change the nature of problem in terms of the relative motion. The drillstring, including drill pipes and drill collars, is discretized into finite elements. If only the rotation is considered, the element stiffness matrix K_e and mass matrix M_e are given by:

$$K_e = \begin{bmatrix} \frac{GJ}{l_e} & -\frac{GJ}{l_e} \\ -\frac{GJ}{l_e} & \frac{GJ}{l_e} \end{bmatrix} \tag{3.1}$$

$$M_e = \begin{bmatrix} \frac{\rho J l_e}{3} & \frac{\rho J l_e}{6} \\ \frac{\rho J l_e}{6} & \frac{\rho J l_e}{3} \end{bmatrix} \tag{3.2}$$

where G is the shear modulus of the drillstring material, ρ is the drillstring density, J is the polar moment of inertia of drillstring cross section, and l_e is the element length.

By assembling the local stiffness and mass matrices, the global mass and stiffness matrices of the system can be obtained. After some mathematical manipulation, the governing equation of motion of the whole system can be represented by the following

form:

$$M\ddot{q}(t) + C\dot{q}(t) + Kq(t) = T \tag{3.3}$$

where $q(t)$ denotes the global rotation displacement vector; T represents the torque excitation to the system; M, C and K are the system global mass, damping and stiffness matrices, respectively; C is assumed to be a linear combination of K and M as below:

$$C = \alpha M + \beta K \tag{3.4}$$

where α and β are constants to be selected.

3.4.2 Excitation

In equation (3.3), the excitation to the system is generalized as a torque T which consists of several components explained below. The first important component of excitation is the periodic torque created by the cutting mechanism, denoted by T_0. It is straightforward to assume this excitation as a periodic function of time with a frequency of $N\omega$. For simplicity, it can be represented as a sinusoidal function as below.

$$T_0 = a + b\sin(N\omega t) \tag{3.5}$$

where a and b are constant parameters, ω is the rotary speed of the ground, and N is the number of cutters on the bit.

Another important component of the excitation is the torque T_1 created by the friction between the cutter and the bottom [31]. Depending on the two possible motion condition, the torque T_1 can be represented as:

$$T_1 \begin{cases} \leq W r_b \mu_1 & |\omega - \omega_b| = 0 \\ = W r_b \mu_2 & |\omega - \omega_b| > 0 \end{cases} \tag{3.6}$$

where W is the weight on bit, ω_b denotes the instantaneous rotary speed of the bit, r_b is a number related to the radius of the cutter, μ_1 and μ_2 represent the static and kinetic friction coefficients respectively.

Given the fact that it is almost impossible to capture the exact $\omega - \omega_b = 0$ in simulation, equation (3.6) can be recast into an alternative form as below.

$$T_1 \begin{cases} \leq W r_b \mu_1 & |\omega - \omega_b| \leq e \\ = W r_b \mu_2 & |\omega - \omega_b| > e \end{cases} \tag{3.7}$$

where e is a preset small number, the proper value of which can be determined by trial and error in simulation.

There are several different expressions for μ_1 and μ_2 available in the literature [28, 29, 31]. The kinetic friction coefficient μ_2 used in this paper is taken reference to Puebla and Alvarez-Ramirez [29] and is given as follows:

$$\mu_2 = \mu_{cb} + (\mu_1 - \mu_{cb}) \exp(-\gamma_b |\omega - \omega_b|) \tag{3.8}$$

where μ_1 and μ_{cb} are the static and Coulomb friction coefficients respectively, γ_b is a positive constant, and μ_2 is substantially smaller than μ_1 in general. The relationship between μ_1 and μ_2 in equation (3.8) is graphically shown in Figure 3.2.

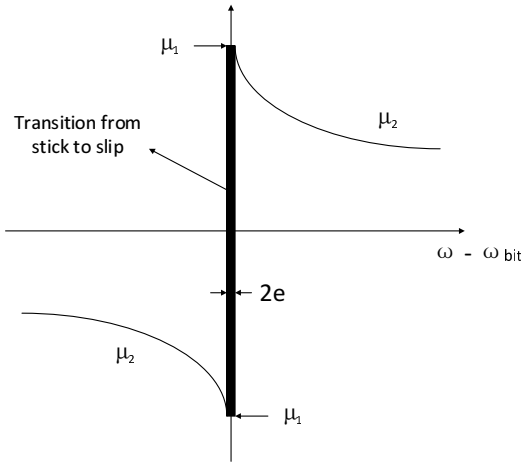

Figure 3.2: Torque created by the friction between the cutter and the bottom.

Switching between static and dynamic friction is the primary cause for stick-slip. Numerous papers have investigated stick-slip of the drilling bit from the deterministic point of view [16, 28, 29, 31, 32]. However, the deterministic representation of the excitation above is highly idealized compared to the reality. The friction, in particular, is hard to model with deterministic theory. Experiments [158, 159] in both drilling industry and other areas have indicated that friction is stochastic or random in nature. According to Kilburn's work [158], friction force can be represented by combining a deterministic component and a Gaussian form random component. As such, to account for the effect of random component in the bit rock friction, a Gaussian white noise $\xi(t)$ with a constant spectral intensity S_0 is added to the deterministic torque T_1 in this paper. The excitation T, therefore, is expressed as

$$T = T_0 + T_1 + \xi(t) \tag{3.9}$$

3.5 Solution Strategy

3.5.1 Solution of Dynamic Model

The response of equation (3.3) to the excitation is numerically solved by using the central difference method. In this method, the time is first discretized into short time steps Δt, then the acceleration and velocity vectors at time t_i can be written as [160]:

$$\dot{q}_i = \frac{1}{2\Delta t}(q_{i+1} - q_{i-1}) \tag{3.10}$$

$$\ddot{q}_i = \frac{1}{\Delta t^2}(q_{i+1} - 2q_i + q_{i-1}) \tag{3.11}$$

where subscript i indicates the time instant t_i. For the algorithm to be stable and converge, the time step Δt has to meet the following condition [161]:

$$\Delta t < \Delta t_{crit} = \frac{2}{\omega_n} \tag{3.12}$$

where Δt and ω_n represent the time step and the maximum natural frequency of the system respectively.

By substituting equation (3.10) and (3.11) into (3.3), and rearranging the terms, one has [160]:

$$q_{i+1} = \Delta t^2 N_1 T_i + N_2 q_i + N_3 q_{i-1} \tag{3.13}$$

with

$$N_1 = [M + \tfrac{1}{2}\Delta t C]^{-1} \tag{3.14}$$

$$N_2 = N_1[2M - \Delta t^2 K] \tag{3.15}$$

$$N_3 = N_1[\tfrac{1}{2}\Delta t C - M] \tag{3.16}$$

Equation (3.3) is highly nonlinear due to the presence of friction. For comparison purpose, it is solved for both deterministic and random cases. In the random case, the dynamic equation is solved to a certain time with randomly generated excitation samples, and the response statistics are obtained by Monte Carlo simulation.

The random excitation $\xi(t_i)$ in simulation is generated as below [161]:

$$\xi(t_i) = \sqrt{\frac{2\pi S_0}{\Delta t}} U_i \tag{3.17}$$

where U_i are random number series generated by the computer which is normally distributed with zero mean and unit standard deviation.

3.5.2 Strategy for probability density estimate

In order to obtain the statistics of response, the ranges of the responses, both q_i and $\dot{q}_i$, are divided into a certain numbers of small intervals.Assuming the sample size of Monte Carlo simulation is N_1 , the probabilistic density of the response falling into a specific small area in slip stage is computed by:

$$p_1 = \frac{n_1}{N_1 \delta_q \delta_{\dot{q}}} \tag{3.18}$$

In the stick case, the probabilistic density is calculated by:

$$p_2 = \frac{n_2}{N_1 \delta_q} \tag{3.19}$$

where δ_q and $\delta_{\dot{q}}$ are the interval length along the q and $\dot{q}$ directions respectively, n_1 and n_2 are the numbers of the solution falling into the slip area and the stick interval

respectively, and p_1 and p_2 are the PDF at the specific slip area and stick interval respectively.

3.6 Simulation Results

The parameters of the drillstring in the simulation are listed in Table 3.1. In the simulation, the drillstring system is divided into 30 elements, 20 elements for the drill pipes and 10 elements for the drill collars. Some other parameters used in the simulation are listed in Table 3.2

Table 3.1: Drillstring parameters.

Parameters	Drillpipe	Drillcollar
Length	$1,000\ m$	$200\ m$
Outer diameter	$0.127\ m$	$0.2286\ m$
Inner diameter	$0.095\ m$	$0.0762\ m$
Material density	$7850.0\ kg/m^3$	$7850.0\ kg/m^3$
Elastic modulus	$210\times10^9\ N/m^2$	$210\times10^9\ N/m^2$
Shear modulus	$7.6923\times10^{10}\ N/m^2$	$7.6923\times10^{10}\ N/m^2$

Table 3.2: Other parameters used in simulation.

Parameter	Value	parameter	value
a	$2 \times 10^4\ Nm$	b	$5 \times 10^3\ \ Nm$
W	$4 \times 10^5\ N$	r_b	$0.22\ m$
μ_1	0.3	e	$0.01\ rad/s$
S_0	15	α	0.03
β	0.03	Δt	0.0002
N	3	μ_{cb}	0.21
μ_{sb}	0.3		

3.6.1 Results from Deterministic Case

It has been well known that stick-slip happens when the rotary speed is lower than a threshold value [44]. This phenomenon is also observed in the simulation of this paper. Under the simulation parameters given above and a rotation speed of 10 rad/s (95 rpm), the response of the deterministic part is shown in Figure 3.3. In this figure, the time history of the relative rotation speed between the bit and the rock is given in Figure 3.3(a). It can be clearly seen the stick-slip motion exists. Two representative points, the leaving point and the entering point to the stick-slip, are marked in this figure. In the deterministic case, these points (time instants) within a motion period are uniquely determined. In Figure 3.3(b) the phase plane is shown; the stick-slip is characterized by the flat straight line. Increasing the rotary speed or decreas-

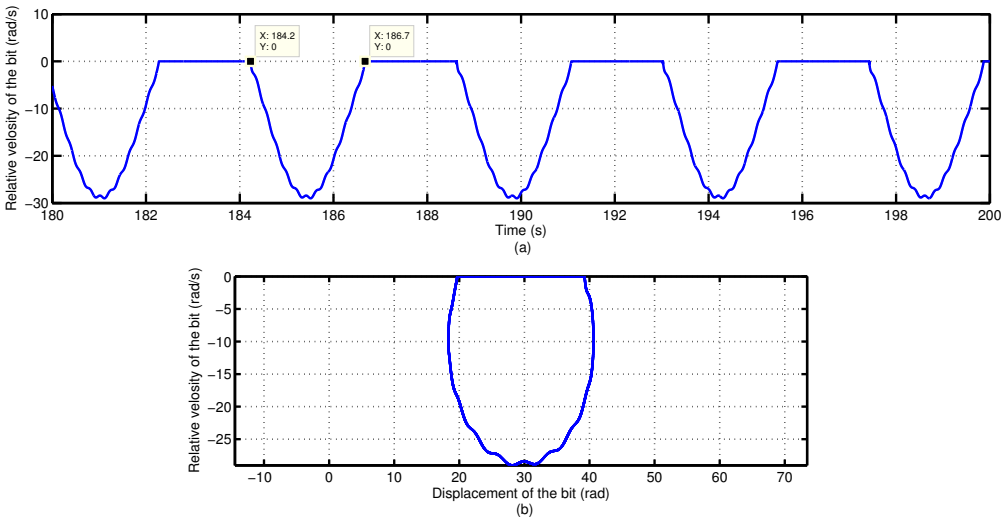

Figure 3.3: Stick-slip when the ground speed is 10 rad/s: (a) Time history; (b) Phase plane.

ing the WOB can effectively mitigate the stick-slip [16]. However, decreasing the WOB should be done cautiously because it may have negative influences on drilling efficiency. A simulation with the same parameters but a higher rotation speed of 35 rad/s (332 rpm) is also conducted, the results are shown in Figure 3.4. Clearly, stick-slip is gone. The response is analogous to a sinusoidal curve, and no horizontal line exists in the phase plane any more.

3.6.2 Results from Random Case

Due to the random component of the friction, it is expected that the response will become random as well. Correspondingly, the phase plane will become diffused around

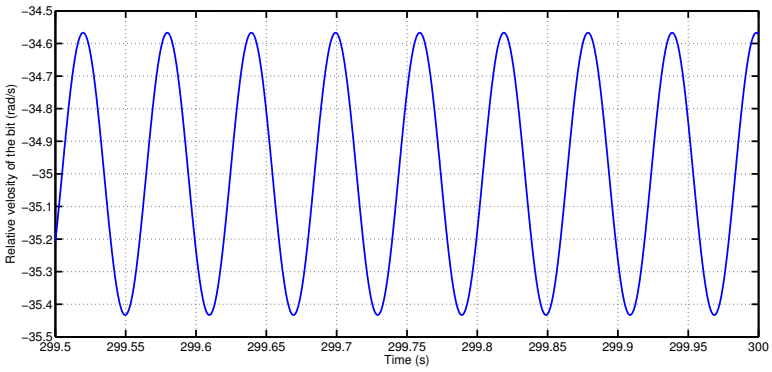

(a)

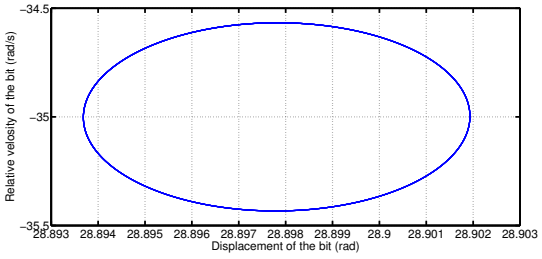

(b)

Figure 3.4: No stick-slip when the ground speed is 35 rad/s:(a) Time history; (b) Phase plane.

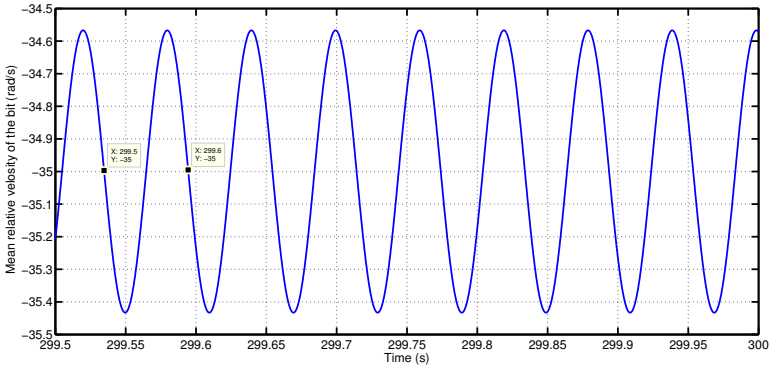

(a)

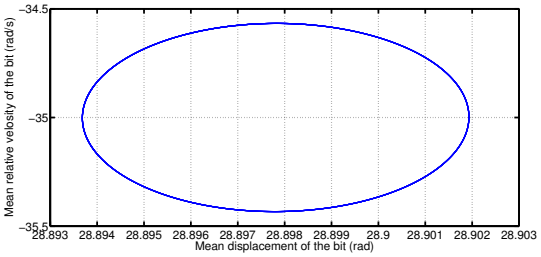

(b)

Figure 3.5: Mean responses: (a) Time history; (b) Phase plane.

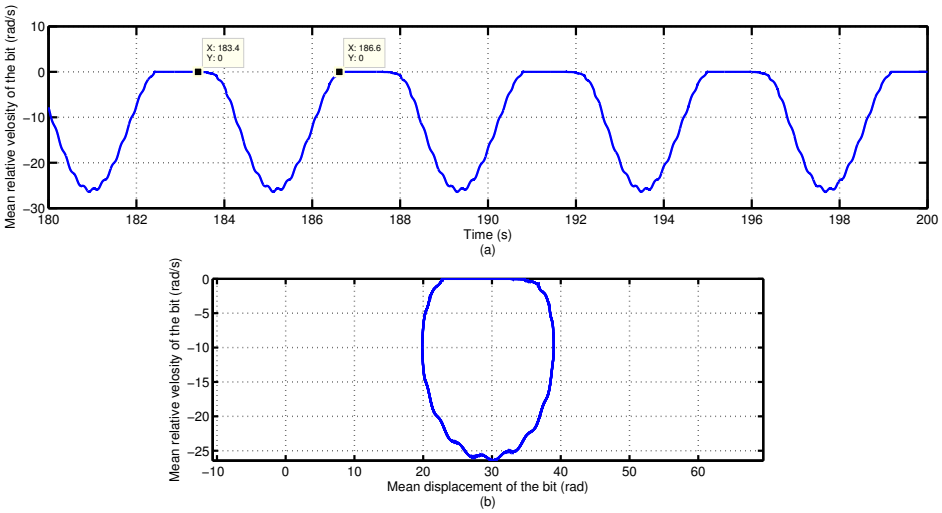

Figure 3.6: Mean responses: (a) Time history; (b) Phase plane.

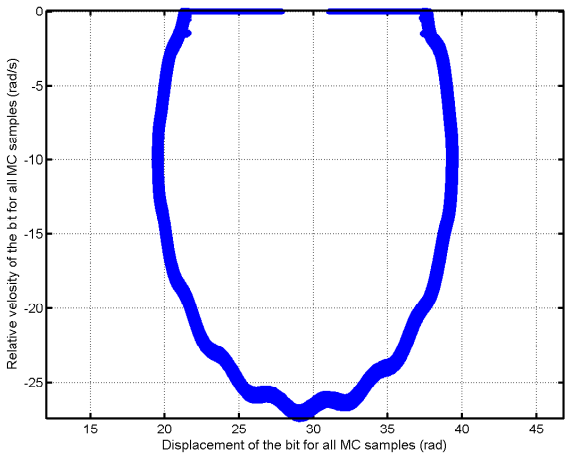

Figure 3.7: Phase plane for all MC samples between two representative points (stick-slip).

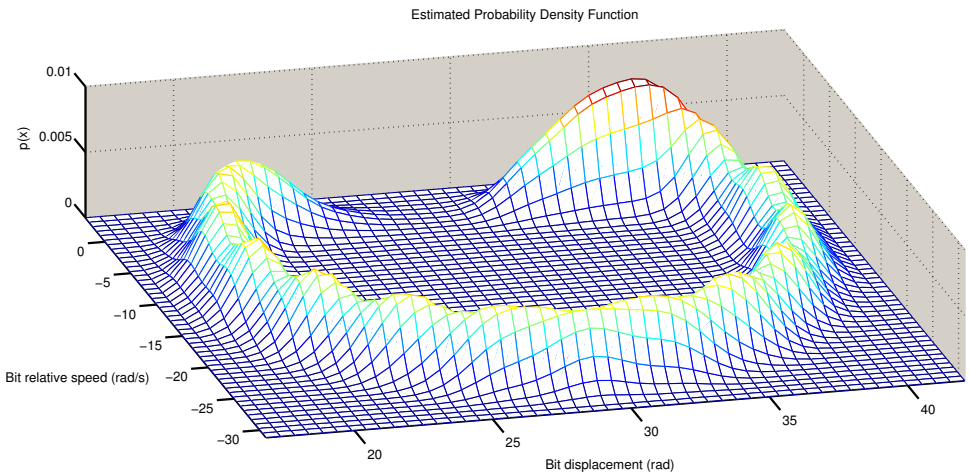

Figure 3.8: Probability density evolution in stick slip.

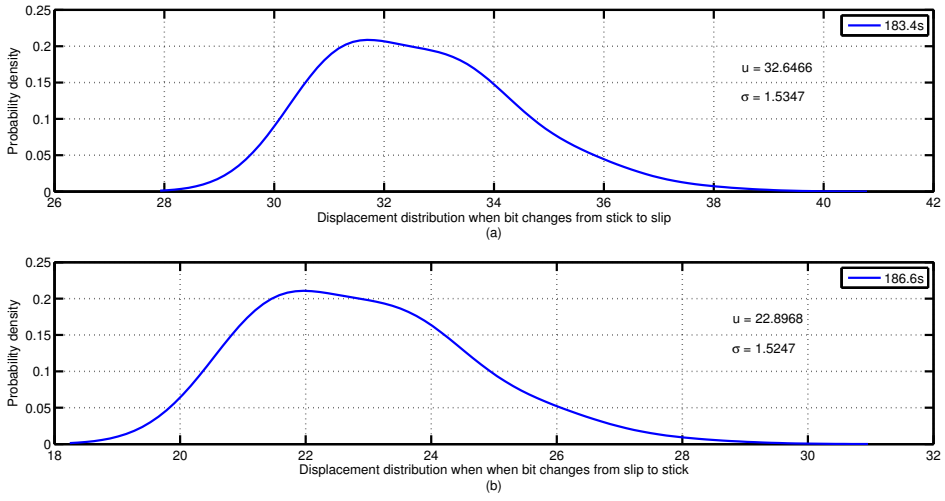

Figure 3.9: Probability density of the the switching points: (a) leaving stick; (b) leaving slip.

a single line in the deterministic case. To capture the response features of the motion in the random case, MC simulation is conducted with a sample size of 200 and a noise intensity of $S_0 = 15$.

Although field test data has long recognized the random nature of down-hole vibration, no data have been reported on the strength of the randomness in public literature. The power spectral density of $S_0 = 15$ may not be realistic in real drilling operation; however, this does not affect the significance of the study.

The first simulation case in random case in at the relatively high rotation speed at 35 rad/s which is the same as the deterministic case in Figure 3.4. Figure 3.5 gives the mean response of the case in which no stick-slip is observed. Compared with Figure 3.4, the two cases are very similar to each other. Here for saving of space, we do not give the diffused phase plane for the random case.

The stick slip case corresponding to the deterministic case in Figure 3.3, but with a random excitation component is also simulated. The mean response of this case is shown in Figure 3.6. No obvious difference exists between this figure and Figure 3.3. However, if we draw all the simulation samples together in the phase plane, the single phase plane curve in Figure 3.3 will become diffused as shown in Figure 3.7. For any time instant, the points will be scattered in a range with varying probability. Using equation 3.18 and 3.19 the probabilistic distribution density (PDD) at each time point can be obtained, as is shown in Figure 3.8. If stick-slip exists, the two representative points, entering and leaving the stick stage, have special interests;

based on which some researchers developed control algorithms in order to mitigate the stick-slip. So knowing the times of these two points are crucial for the control strategy to be successful. In the deterministic case, the time instants for these two points are deterministic. For instance, the two points in Figure 3.3 are $t = 184.2s$ and $t = 186.7s$ respectively. The statistics of these two points (marginal PDD) are shown in Figure 3.9. Clearly, both points are scattered in a range. In addition, the distribution is distorted from normal. The reason for that is the nonlinearity caused by the friction. In theory, for a nonlinear system, excitation with normal distribution may not lead to responses with normal distribution.

3.7 Conclusions

Using a finite element model, this chapter investigates the stick-slip behavior of a drillstring subject to both deterministic and random excitations. Stick-slip behaviors in both deterministic and random cases are obtained through simulation and compared. The PDF of the stick-slip response in the phase plane is also obtained. The single curve of the phase plane in the deterministic case changes to diffused in a range. Correspondingly, the two points, entering and leaving the stick stage becomes diffused too. Due to the nonlinearity caused by the friction, the PDDs of these two points are distorted from normal distribution even the excitation is assumed as Gaussian white noise.

Chapter 4

Investigation on Bit Stick-Slip Vibration with Random Friction Coefficients

The research work of this chapter has been published: Hongyuan Qiu, Jianming Yang and Stephen Butt. "Investigation on bit stick-slip vibration with random friction coefficients." *Journal of Petroleum Science and Engineering* 164 (2018): 127-139.

4.1 Co-authorship Statement

Hongyuan Qiu: Dynamic Modeling, Methodology, Simulation, Data Processing, Result Analysis and Writing Manuscript. **Dr. Jianming Yang**: Supervision and Reviewing. **Dr. Stephen Butt**: Supervision and Reviewing.

4.2 Abstract

Torsional vibration of a drillstring, bit stick-slip in particular, is investigated with a simplified single degree of freedom (DOF) model. The friction in the bit-rock interaction is modeled as random, and the motions in stick and slip stages are treated separately. In the stick stage, it is treated as in static equilibrium. By assuming a deterministic or random friction coefficient, the points leaving the stick stage are determined either as a deterministic point or scattered points in a range. In the slip stage, for random friction which is assumed as white noise, the motion becomes Markovian. Then, the probabilistic distribution of the responses with displacement and velocity is calculated with the numerical path integration (PI) technique. Also Monte Carlo (MC) simulation is conducted for verifying purposes. By considering the randomness in the excitation, the response at any time instant becomes a spreading area centred around the means. The time instants leaving and entering the stick stage also become random, and can only be represented by probability. Comparison against MC shows that results from the two methods are in good agreement. Parametric studies on damping, rotary speed, weight on bit, drillstring length and different combination of pipe and collar are conducted for both deterministic and random cases.

4.3 Introduction

Drillstrings are critical components of drilling in the oil and gas industry. The drillstring may experience three types of vibrations during drilling operation, namely axial vibration, torsional vibration and lateral vibration, or their combination. Stick-slip is a severe format of torsional vibration with apparent detrimental effects on the drilling system. It happens when the rotation of the drillstring is slowed down (or even stopped) and then suddenly increased when the torque overcomes the anti-torque from the rock cutting and friction. Under this situation, the rotary speed and torque on the bit may be several times larger than those on the surface [162], causing high cyclic stress within the drillstring and premature failure of drilling components [59]. The rate of penetration (ROP) could be drastically decreased as well by the stick-slip [17]. It is reported that stick-slip happens in as high as 50 percent of drilling time.

To control and mitigate its obvious harmful effect, numerous researchers have worked on stick-slip through modeling, simulating, lab and field test and so forth. Patil and Teoduriu [163] examined the effect of operational factors, such as rotation speed of the rotation table, drillstring stiffness, as well as weight on bit (WOB). High rotation speed can eliminate stick-slip, but may leads to whirling of the drillstring. Wu et al [23] made effort to decouple the two vibration modes and gave a schematic description of optimum zone. Viguie et al. [164] investigated the possibility to control stick-slip with passive control methods. Jansen and Steen [165] tried to mitigate the stick-slip by active damping.

It has been clear that the essential cause of stick-slip is the different friction mechanisms between the cutting bit and the rock (bit-rock interaction) in the two stages. However, friction between two objects depends on many factors, such as profile of the contact surfaces, materials and lubrication condition and so forth. It is difficult to model the friction accurately with deterministic theory. Experiments have proven that the friction between two objects be random in essence, and better represented by a random process [158]. In addition, Ibrahim et al [152] indicated that both static and kinetic friction coefficients exhibited randomness through experiments. Some other works [166, 167] found that the friction might change the qualitative character of the dynamic response. Therefore, without inclusion of the randomness in the friction, it would be less possible to fully understand the stick-slip behavior.

Although numerous publications exist in the literature dealing with stick-slip of drillstrings, very few modelled the friction as a random process. To the authors best knowledge, the works by Ritto et al [148] and Cunha et al. [151] are the few papers considering friction as random. The work by Ritto et al [148] considered friction as a random field while a random distribution of friction coefficient was employed in [151]. Both work didn't differentiate the static and kinetic frictions, which, as pointed before, is the essential factor for stick-slip.

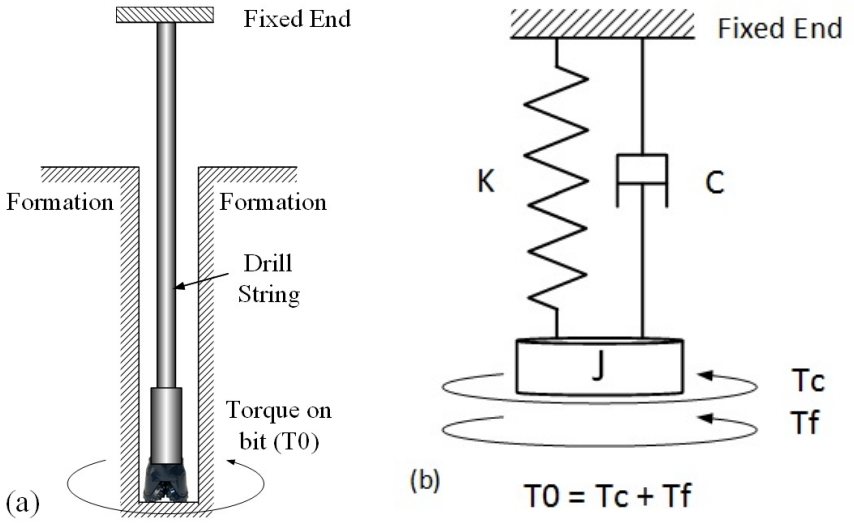

Figure 4.1: Drillstring model. (a) A drillstring; (b) Torsional vibration model

4.4 Dynamic Model

A drillstring model is schematically shown in Fig 4.1(a). If we focus on only the vibration in torsional direction, the system can be represented by a single DOF model as shown in Fig 4.1(b). For convenience, the top end of the drillstring is regarded as fixed, while the ground is considered rotating with constant rotation. This treatment does not change the vibration characteristics, but facilitates mathematic manipulation. The simple lumped mass and spring model has been used by many researchers [165, 168].

The equation of motion of the torsional vibration model can be expressed as below.

$$J\ddot{\phi}(t) + C\dot{\phi}(t) + K\phi(t) = T_o \tag{4.1}$$

where J, C and K are the equivalent inertia, viscous damping and stiffness of the

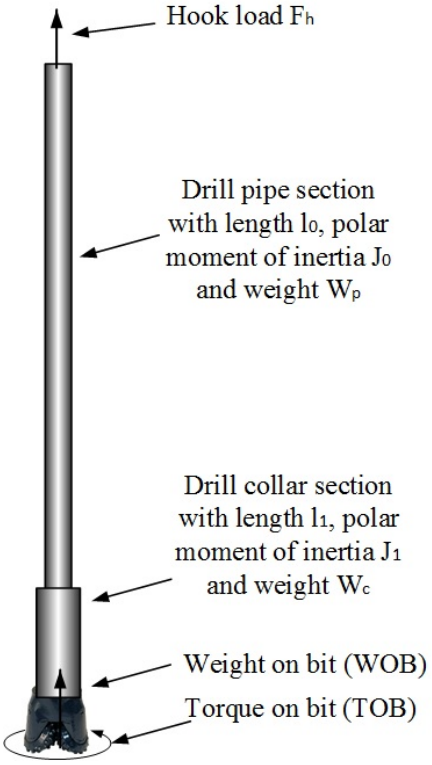

Figure 4.2: Simplified sketch of arbitrary drillstring

drillstring system respectively, $\phi(t)$ is the drill-bit torsional displacement, and T_o represents the torque on bit (TOB). For an arbitrary drillstring consisting of drill pipe and drill collar sections shown in Fig 4.2, J. K and C can be calculated as:

$$J = \rho J_0 l_0 + \rho J_1 l_1 \tag{4.2}$$

$$K = \frac{GJ_0}{l_0} * \frac{GJ_1}{l_1} / (\frac{GJ_0}{l_0} + \frac{GJ_1}{l_1}) \tag{4.3}$$

$$C = \alpha J + \beta K \tag{4.4}$$

with

$$J_0 = \frac{\pi}{32}(D_{po}^4 - D_{pi}^4) \tag{4.5}$$

$$J_1 = \frac{\pi}{32}(D_{co}^4 - D_{ci}^4) \tag{4.6}$$

where damping C is considered as Rayleigh damping, α and β are two constants to be selected, l_0 and l_1 are the length of drill pipe and drill collar respectively. ρ is the drillstring density, G is the shear modulus of the drillstring material. D is the diameter of the drill pipe or drill collar with subscripts po, pi, co and ci as pipe outer, pipe inner, collar outer and collar inner respectively. T_0 simulates the torque from the bit cutting action, which is treated differently for two distinctive mechanisms, cutting and friction. Therefore, T_0 can be divided into two parts: T_c and T_f [62] representing the component of cutting and friction respectively.

T_c , the component related to cutting action, depends on the number of cutters and the depth of cutting. There are many different representations of this component [17, 32, 62]. The general simplified expression of it can be represented by the following form.

$$T_c = \begin{cases} a & \text{if} \quad |\omega_0 - \omega_b| = 0, \\ a + b\sin(N\omega_0 t) & \text{if} \quad |\omega_0 - \omega_b| > 0. \end{cases} \tag{4.7}$$

where a and b are constant parameters which depend on the depth of cutting, rock and the geometries of the cutter [169] and formation surface elevation, N is the number of cutters on the bit, ω_b and ω_0 are the rotary speed of the bit and the

ground respectively, The two conditions, $|\omega_0 - \omega_b| = 0$ and $|\omega_0 - \omega_b| > 0$, represent the thresholds of stick and slip.

T_f, depending on stick or slip, can be represented as below [169]:

$$T_f = \begin{cases} \leq \quad Wr_b\mu_1 & \text{if } |\omega_0 - \omega_b| = 0, \\ = Wr_b\mu_2 sgn(\omega_0 - \omega_b) & \text{if } |\omega_0 - \omega_b| > 0. \end{cases} \tag{4.8}$$

where r_b is the radius of the bit, μ_1 and μ_2 are the static and kinetic friction coefficients respectively. sgn is the signum function. W is the weight on bit (WOB) as shown in Fig 4.2, which is calculated as:

$$|W| = |F_h - BF \times (W_p + W_c)| \tag{4.9}$$

where F_h is the hook load, BF is the buoyant factor, W_p is the weight of the drill pipe section and W_c is the weight of the drill collar section.

Given the fact that it is almost impossible to capture the exact $|\omega_0 - \omega_b| = 0$ with numerical methods, the two conditions for stick and slip, $|\omega_0 - \omega_b| = 0$ and $|\omega_0 - \omega_b| > 0$, are approximated by the following:

$$|\omega_0 - \omega_b| \leq e \tag{4.10}$$

$$|\omega_0 - \omega_b| > e \tag{4.11}$$

here e is a preset small tolerance approximating zero for numerical simulation, the proper value of which can be determined through trial and error.

There are several types of relations between μ_1 and μ_2 available in literature [28, 29, 31]. The two most representatives include the coulomb model [43] and the

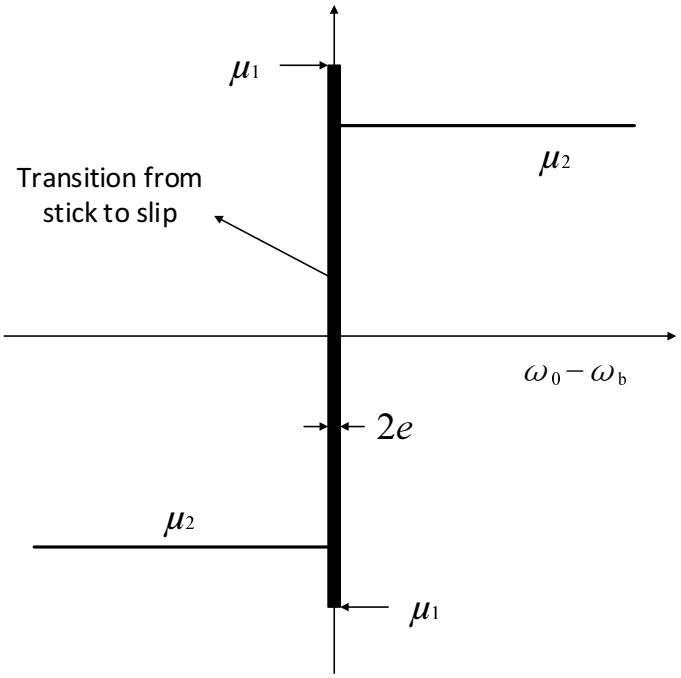

Figure 4.3: Friction Coefficients

exponential law. In the coulomb law μ_1 is greater than μ_2, but both are taken as constant. In the exponential law, μ_2 gradually decreases with the increase of the relative sliding speed. In this paper the relatively simpler coulomb law is adopted and the relationship between μ_1 and μ_2 is shown in Fig. 4.3.

By defining the following transformations,

$$x = \frac{\phi}{2\pi} \tag{4.12}$$

$$\omega_n = \sqrt{\frac{K}{J}} \tag{4.13}$$

$$\tilde{t} = \omega_n t \tag{4.14}$$

$$c = \frac{C}{J\omega_n} \tag{4.15}$$

$$\tilde{\omega} = \frac{\omega_0}{\omega_n} \tag{4.16}$$

$$\tilde{\omega}_1 = \frac{N\omega_0}{\omega_n} \tag{4.17}$$

$$f_1 = \frac{a + Wr_b\mu_1}{2\pi J\omega_n^2} \tag{4.18}$$

$$f_2 = \frac{b\sin(\tilde{\omega}_1\tilde{t})}{2\pi J\omega_n^2} + \frac{a + Wr_b\mu_2}{2\pi J\omega_n^2} \tag{4.19}$$

Eqn. (4.1) can be nondimensionalized as below.

$$\ddot{x}(t) + c\dot{x}(t) + x(t) \begin{cases} \leq f_1 & \text{if } |\omega_0 - \omega_b| \leq e \\ = f_2 & \text{if } |\omega_0 - \omega_b| > e \end{cases} \tag{4.20}$$

For simplicity, $\tilde{t}$, $\tilde{\omega}$ and $\tilde{\omega}_1$ are denoted thereafter by t, ω_0 and ω_1 respectively.

Field data indicated that drillstring vibration in general is random except for resonance cases in which some specific frequencies stand out [170]. For proper accounting of the randomness in friction, we distinguish the two different motion status, namely stick and slip, and treat them separately. In the stick stage, the bit is stuck to the ground which rotates at constant speed. Thus $\ddot{x} = 0$ and it is basically in static equilibrium. In the slip stage, the bit moves relative to the ground with different relative speed; therefore, it is a dynamic problem. These two motion status can be

represented as below:

$$c\dot{x}(t) + x(t) \leq f_1 \qquad \text{if } |\omega_0 - \omega_b| \leq e \tag{4.21}$$

$$\ddot{x}(t) + c\dot{x}(t) + x(t) = f_2 + W(t) \qquad \text{if } |\omega_0 - \omega_b| > e \tag{4.22}$$

In these equations, f_1, and f_2 are related with the static and kinetic friction, respectively. $W(t)$ is white noise representing the random component (or uncertainty) of the kinetic friction during the slip motion.

4.5 Solution Strategy

In stick stage, the bit sticks to the ground and is in static equilibrium. Once the elastic potential energy stored in the drillstring overcomes a threshold relating to the breakage of the rock, the equilibrium would be broken, and the slip stage starts. The two stages, stick and slip are treated individually as below.

4.5.1 Stick stage

The point, at which the bit leaves the stick stage and starts the slip stage, is determined as:

$$x_0 = f_1 - c\omega_0 \tag{4.23}$$

x_0 will be used as one of the initial conditions for the slip stage. Depending on μ_1, it may be a random or deterministic variable. If the static friction coefficient μ_1 is considered as random following Gaussian distribution $N(\mu, \sigma)$, then x_0 is also

Gaussian distributed. If μ_1 is taken as a constant as treated in most of the existing literature, then x_0 is a deterministic point. These two types of initial conditions for slip stage are schematically shown in Fig 4.4, with '+' representing the deterministic starting point and Gaussian like distribution representing random starting field.

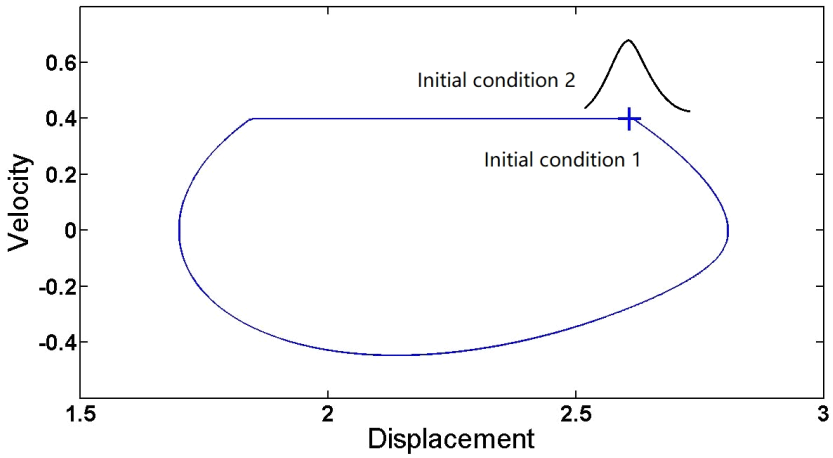

Figure 4.4: Two initial conditions for slip stage

4.5.2 Slip stage

Starting from x_0 calculated in the stick stage, the slip motion is governed by Eq. (4.22). The response of such a dynamic system under White noise is a Markov process [171]. The response probabilistic distribution function (PDF) is computed through numerical path integration in which the continuous time is first discretized into many time instant t_i. $\tau = t_i - t_{i-1}$ is the length of the small time interval. x_i and $\dot{x}_i$ represent the response displacement and velocity at t_i, respectively. As a Markovian process

the PDF of the response at time instant t_i depends only on the immediate previous time instant t_{i-1} [172]. This can be represented as:

$$p(x_i, \dot{x}_i, t_i \mid x_{i-1}, \dot{x}_{i-1}, t_{i-1}; ...; x_0, \dot{x}_0, t_0) = p(x_i, \dot{x}_i, t_i \mid x_{i-1}, \dot{x}_{i-1}, t_{i-1}) \tag{4.24}$$

Therefore, the PDF at time t_i can be calculated as the integration as below:

$$p(x_i, \dot{x}_i, t_i) = \iint_R q(x_i, \dot{x}_i, t_i \mid x_{i-1}, \dot{x}_{i-1}, t_{i-1}) \times p(x_{i-1}, \dot{x}_{i-1}, t_{i-1}) \mathrm{d}x_{i-1} \mathrm{d}\dot{x}_{i-1} \tag{4.25}$$

where $p(x_i, \dot{x}_i, t_i)$ and $q(x_i, \dot{x}_i, t_i \mid x_{i-1}, \dot{x}_{i-1}, t_{i-1})$ are the PDF at time instant t_i and the transitional PDF from time instant t_{i-1} to time instant t_i. R is the region of integration.

With a given starting instant and a known transition PDF, the long term response PDF can be calculated through a series of integration as below[173]:

$$\begin{aligned} p(x_i, \dot{x}_i, t_i) \quad = \quad & \iint_R q(x_i, \dot{x}_i, t_i \mid x_{i-1}, \dot{x}_{i-1}, t_{i-1}) \mathrm{d}x_{i-1} \mathrm{d}\dot{x}_{i-1} \\ & \iint_R q(x_{i-1}, \dot{x}_{i-1}, t_{i-1} \mid x_{i-2}, \dot{x}_{i-2}, t_{i-2}) \mathrm{d}x_{i-2} \mathrm{d}\dot{x}_{i-2} \\ & \cdots \\ & \iint_R q(x_2, \dot{x}_2, t_2 \mid x_1, \dot{x}_1, t_1) \mathrm{d}x_1 \mathrm{d}\dot{x}_1 \\ & \iint_R q(x_1, \dot{x}_1, t_1 \mid x_0, \dot{x}_0, t_0) p(x_0, \dot{x}_0, t_0) \mathrm{d}x_0 \mathrm{d}\dot{x}_0 \end{aligned} \tag{4.26}$$

If the time step τ is chosen adequately short, the transitional PDF between two adjacent time instants can be approximated as Gaussian [174–176] and be expressed

as:

$$q(x_i, \dot{x}_i, t_i \mid x_{i-1}, \dot{x}_{i-1}, t_{i-1}) \approx \frac{1}{2\pi\sigma_{x_i}\sigma_{\dot{x}_i}\sqrt{1-\rho^2}} \mathrm{e}^{\left[-\frac{z}{2(1-\rho^2)}\right]} \tag{4.27}$$

$$z = \frac{(x_i - u_{x_i})^2}{\sigma_{x_i}^2} - \frac{2\rho(x_i - u_{x_i})(\dot{x}_i - u_{\dot{x}_i})}{\sigma_{x_i}\sigma_{\dot{x}_i}} + \frac{(\dot{x}_i - u_{\dot{x}_i})^2}{\sigma_{\dot{x}_i}^2} \tag{4.28}$$

u and σ are the mean and standard deviation respectively. Depending on the subscripts, they may be for x or $\dot{x}$. ρ is the correlation coefficient calculated as:

$$\rho = \frac{\sigma_{x_i\dot{x}_i}}{\sigma_{x_i}\sigma_{\dot{x}_i}} \tag{4.29}$$

The means, which would not be zero due to the deterministic f_2, can be obtained by any numerical integration algorithm, such as the Runge-Kutta methods [171]. The standard deviations can be obtained by the following equations [119]:

$$\sigma_{x_i}^2 = \frac{G_0}{4\xi\omega_n^3}\left\{1 - \mathrm{e}^{-2\xi\omega_n t}\left[\frac{\omega_n^2}{\omega_d^2} + A - B\right]\right\} \tag{4.30}$$

$$\sigma_{\dot{x}_i}^2 = \frac{G_0}{4\xi\omega_n}\left\{1 - \mathrm{e}^{-2\xi\omega_n t}\left[\frac{\omega_n^2}{\omega_d^2} - A - B\right]\right\} \tag{4.31}$$

$$\sigma_{x\dot{x}_i} = \frac{G_0}{2\omega_d^2}\mathrm{e}^{-2\xi\omega_n t}\sin^2\omega_d t \tag{4.32}$$

$$A = \frac{\xi\omega_n}{\omega_d}\sin 2\omega_d t \tag{4.33}$$

$$B = \frac{\xi^2\omega_n^2}{\omega_d^2}\cos 2\omega_d t \tag{4.34}$$

with

$$G_0 = 2\pi S_0 \tag{4.35}$$

$$\xi = \frac{c}{2} \tag{4.36}$$

$$\omega_n = 1 \tag{4.37}$$

$$\omega_d = \omega_n\sqrt{1-\xi^2} \tag{4.38}$$

where S_0 represents the spectrum intensity of the White noise.

Theoretically, the integration in Eq. (4.26) is conducted in the whole space, or for both x and $\dot{x}$ to be $(-\infty, \infty)$. For numerical simulation, the integration can only be conducted on a limited space $x \times \dot{x} \in (x_l, x_u) \times (\dot{x}_l, \dot{x}_u)$. The subscripts l and u represent the lower and upper limits for the integration, respectively, which are determined by a rule that the majority of the probability is included in this region. In this paper, the limits are determined by $\pm 4\sigma$ around the means. After the integration space is determined, the space is first discretized into grids, and then the integration is carried out numerically within the predetermined space. To improve the accuracy of the integration, the Gauss-Legendre quadrature technique with four Gauss points is used [173].

At the intersections of the two stages (the starting and ending of the slip stage), the assumed Gaussian distributed PDF in the next discretized point may go beyond the horizontal stick line as shown in Fig. 4.5. This is called back rotation in drillstring dynamics which rarely happens in reality. In view of this fact, the PDF going beyond the stick line is dragged back and added to the corresponding points on the straight stick line. This is illustrated in Fig. 4.5(a) for a starting point and Fig. 4.5(b) for an ending point respectively. Starting from point $P1$, the distribution of PDF for the next time instant scatters around its mean point $P1'$ as shown. The probability density beyond the stick line represented by the three small points is simply dragged in parallel and added to the corresponding points on the stick line. This treatment

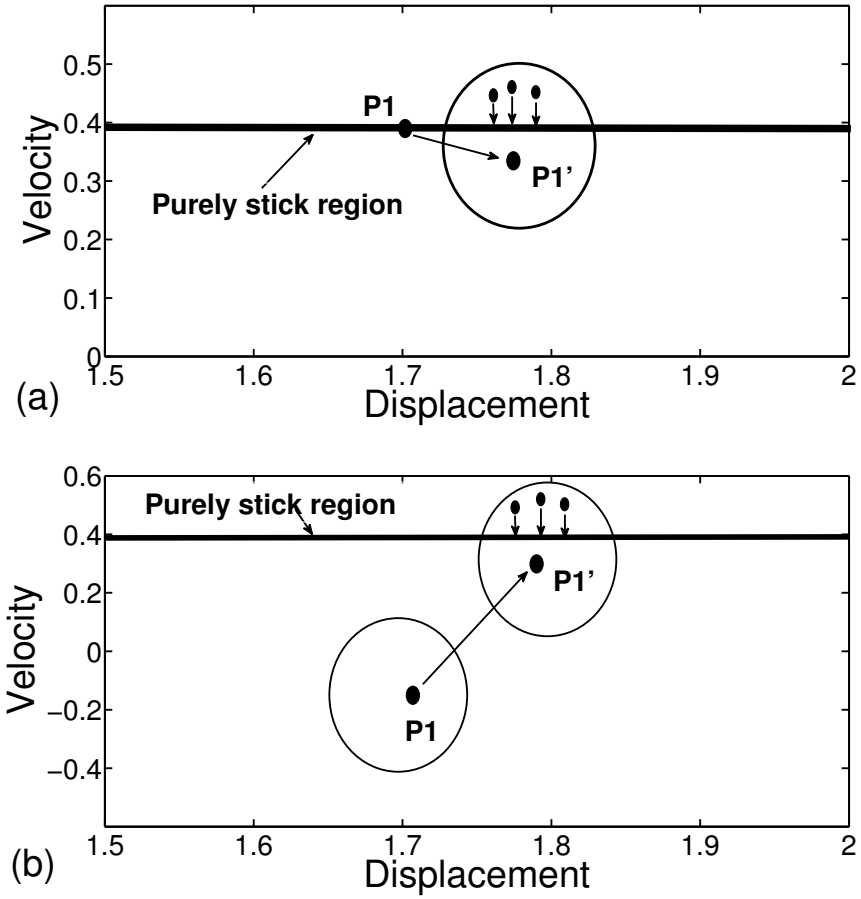

Figure 4.5: Calculation method in two cases. (a) Starting point; (b) Ending Point.

would bring in some error; however, it should be very limited given that the time step is chosen very short [171].

4.6 Simulation and Result analysis

Table 4.1: Drillstring specification

Drill pipe length l_0	850 m
Pipe outer diameter Dp_1	0.127 m
Pipe inner diameter Dp_2	0.1016 m
Drill collar length l_1	66 m
Collar outer diameter Dc_1	0.1651 m
Collar inner diameter Dc_2	0.0572 m
Hook load Fh	129 KN
Buoyant factor BF	0.83
Drillstring density ρ	7850.0 kg/m^3
Shear modulus G	7.6923×10^{10} N/m^2

Parameters of the drillstring used in the simulation of this paper are listed in Table 4.1. Other relevant parameters are given as: $J = 137.689$ kg m^2, $K_0 = 1349.2$ N m rad^{-1}, $\alpha = 0.1$, $\beta = 0.01$, $C_0 = 148.69$ N m s rad^{-1}, $W = 2\times10^5$ N, $r_b = 0.22$ m, $a = 10^4$ N m, $b = 2500$ N m, $N = 3$, $\mu_1 = 0.3$, $\mu_2 = 0.21$. The dimen-

sionless parameters obtained from Eq. (4.12) to (4.19) are given as: $f_1 = 2.7367$, $f_2 = 2.2695$ (without harmonic excitation), $f_0 = 0.2949$ (harmonic excitation amplitude), $c = 0.345$, $\omega_0 = 0.4$, $\omega_1 = 1.2$, $\xi = 0.1725$, $S_0 = 0.0002$, $e = 0.003$.

For the path integration (PI) simulation, the integration space is discretized as: $x \times \dot{x} = [1.0, 3.5] \times [-0.8, 0.8]$, and is divided into 200×120 equally sized small areas. The time in slip is divided into 14 equal time steps by $t_0, t_1, t_2, \ldots, t_{13}$ in the simulation. While in the MC, Eqs. (4.21) and (4.22) are directly solved with central difference method [177]. The sample size in taken as 10,000, and the white noise $W(t)$ in Eq. (4.22) is simulated as [161]:

$$W(t_i) = \sqrt{\frac{2\pi S_0}{\Delta t}} U_i \tag{4.39}$$

where U_i are random number series generated by the computer which is normally distributed with zero mean and unit standard deviation.

4.6.1 Simulation results

Stick-slip under deterministic load has been studied by many researchers. In this chapter, we don't intend to dig deeper into it; however, for comparison purpose the deterministic case is solved by setting the random parts in Eqs. (4.21) and (4.22) as zero. the phase plane representation of the stick-slip response under only deterministic load is shown in Fig. 4.6 in which 14 representative points are marked with "+". As expected, the phase plane is as the ones seen in many other papers with a horizontal line indicating the stick and a curve under representing the slip. Two points, points

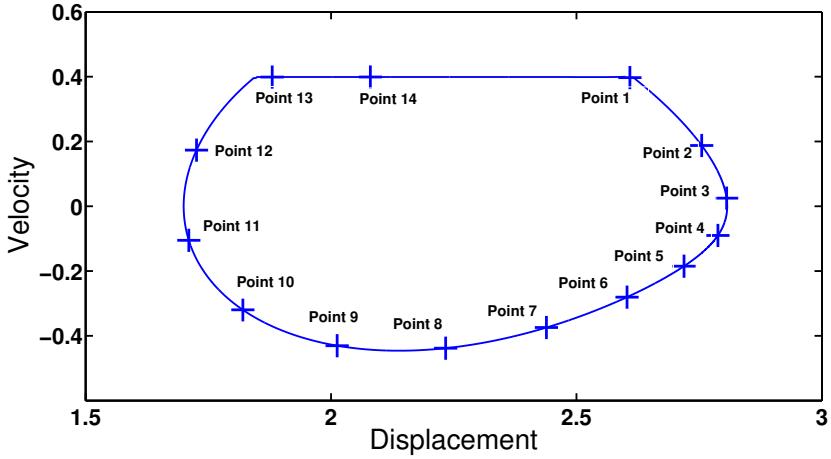

Figure 4.6: Phase plane of response under deterministic excitation with $f_1 = 2.7367$, $f_2 = 2.2695$, $f_0 = 0.2949$, $c = 0.345$, $\omega_0 = 0.4$, $\omega_1 = 1.2$

1 and 13, representing the end of and entrance to the stick stage respectively, are of special interest.

The random case is simulated with two scenarios: 1) the static friction is taken as deterministic ($\mu_1 = 0.3$), and the kinetic friction (μ_2) is treated as random and 2) both the static friction (μ_1) and kinetic friction (μ_2) are treated as random.

The simulation results for deterministic μ_1 and random μ_2 are presented in Fig.4.7. in which (a) is the results from PI and (b) is from MC. In this case, the end of the stick would be a individual point as in the deterministic case. With proceeding in the slip stage, the single point becomes a spread area due to the random kinetic friction μ_2. The spreading area is initially very small, and gradually grows into stable when approaching the entrance of the stick stage.

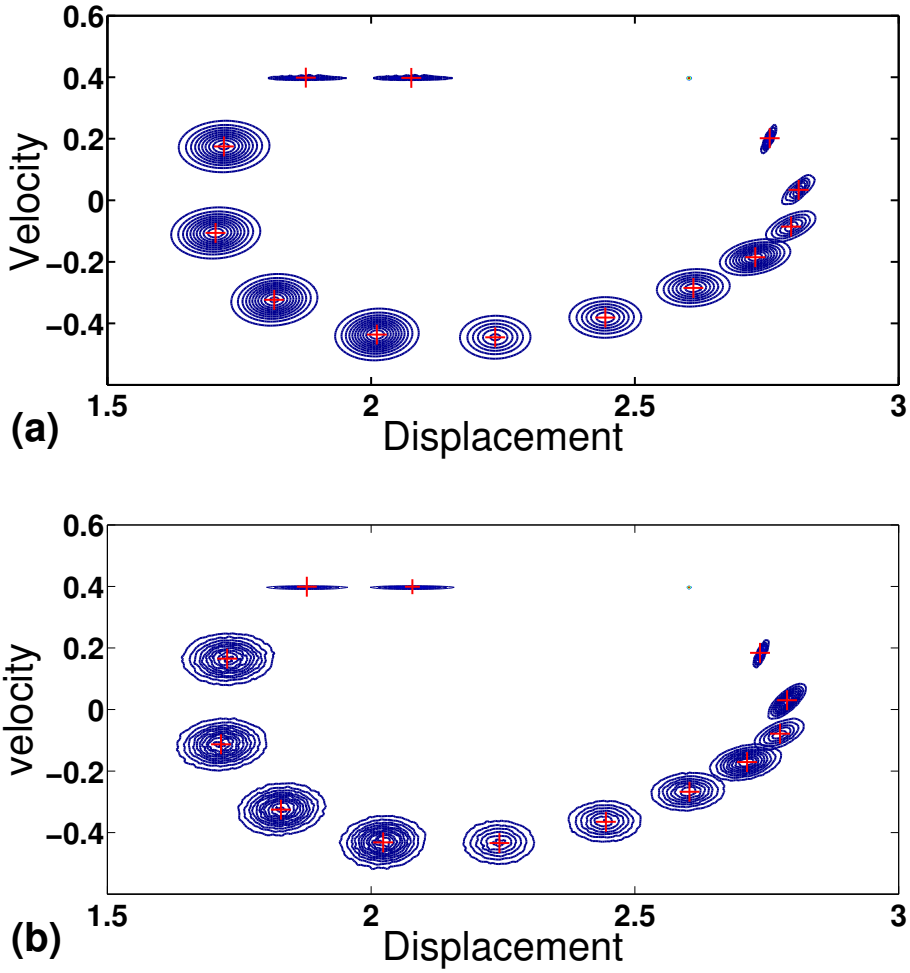

Figure 4.7: The PDF evolution with deterministic static friction ($\mu_1 = 0.3$). (a) PI simulation; (b) MC simulation.

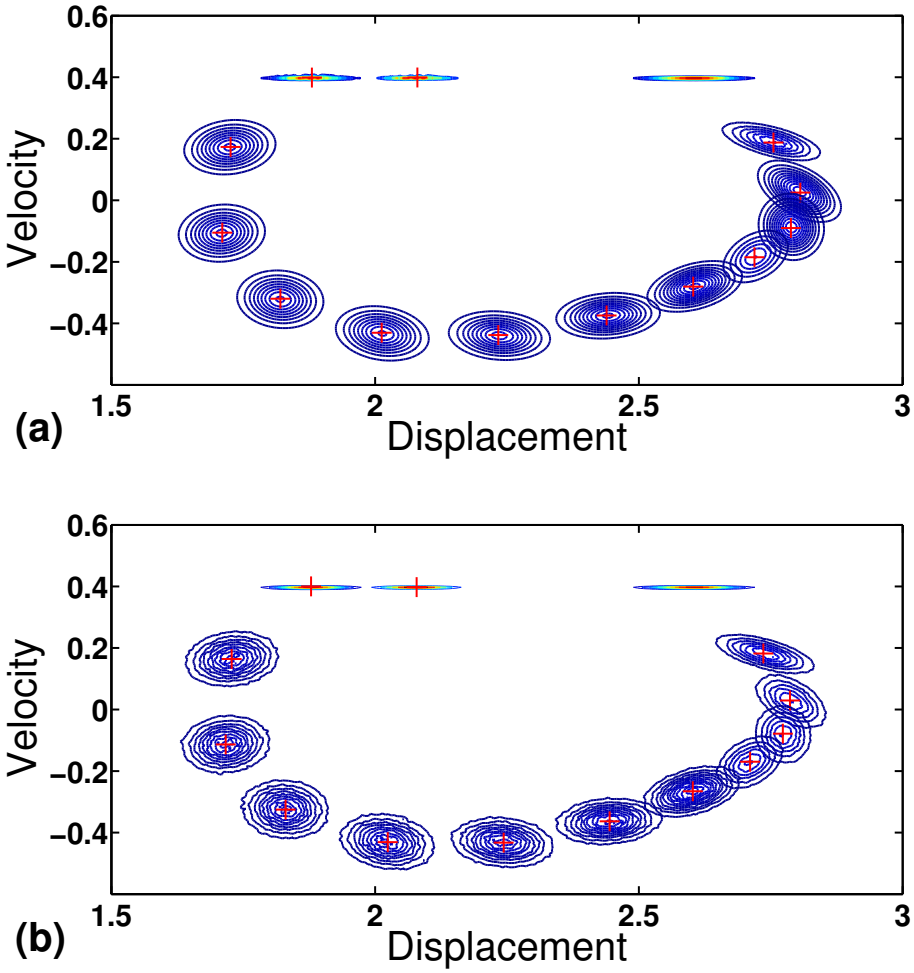

Figure 4.8: The PDF evolution with random static friction ($\mu_1 \sim N(0.3, 0.01)$). (a) PI simulation; (b) MC simulation.

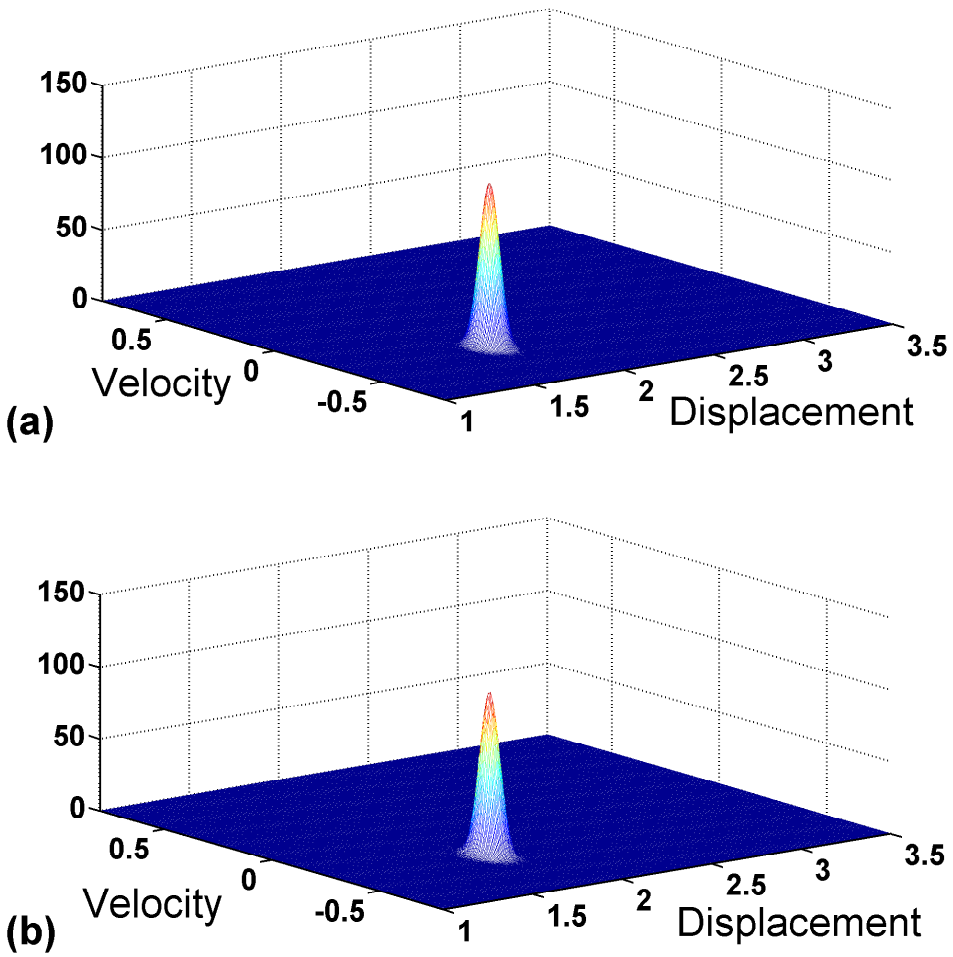

Figure 4.9: The PDF at point 10 with $\mu_1 = 0.3$. (a) PI simulation; (b) MC simulation.

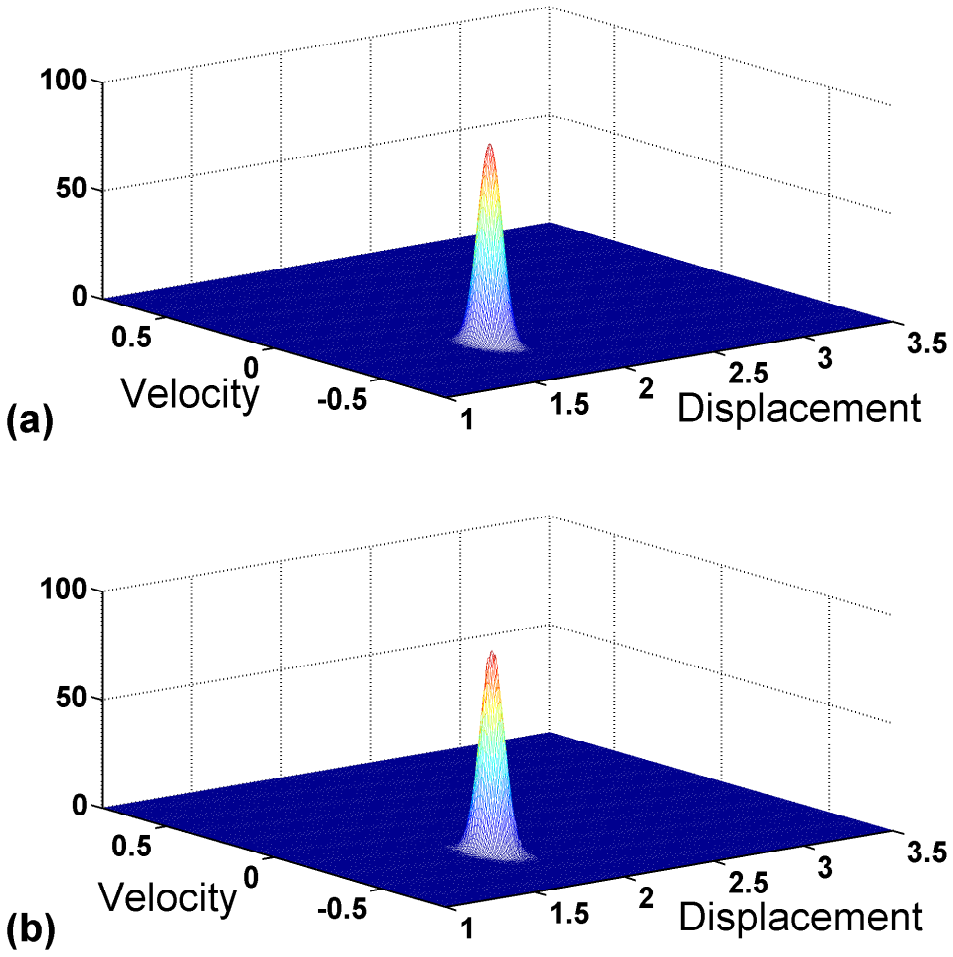

Figure 4.10: The PDF at point 10 with $\mu_1 \sim N(0.3, 0.01)$. (a) PI simulation; (b) MC simulation.

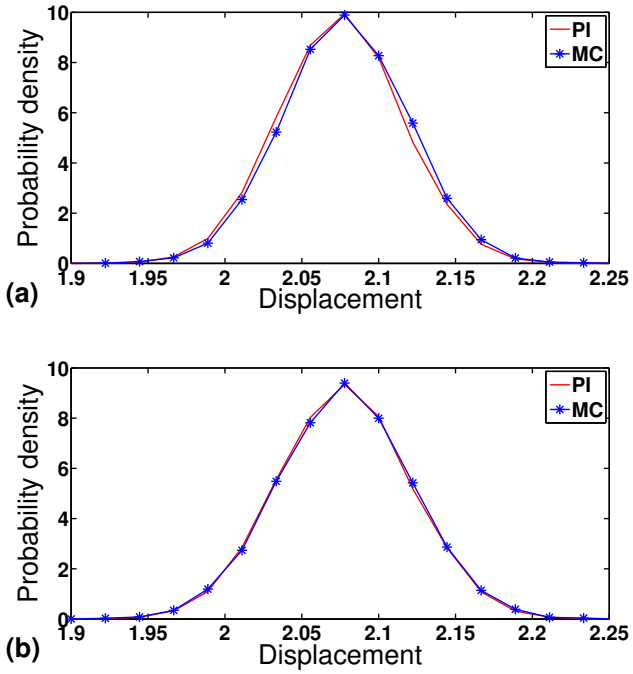

Figure 4.11: The marginal PDF of x at point 13. (a) $\mu_1 = 0.3$; (b) $\mu_1 \sim N(0.3, 0.01)$.

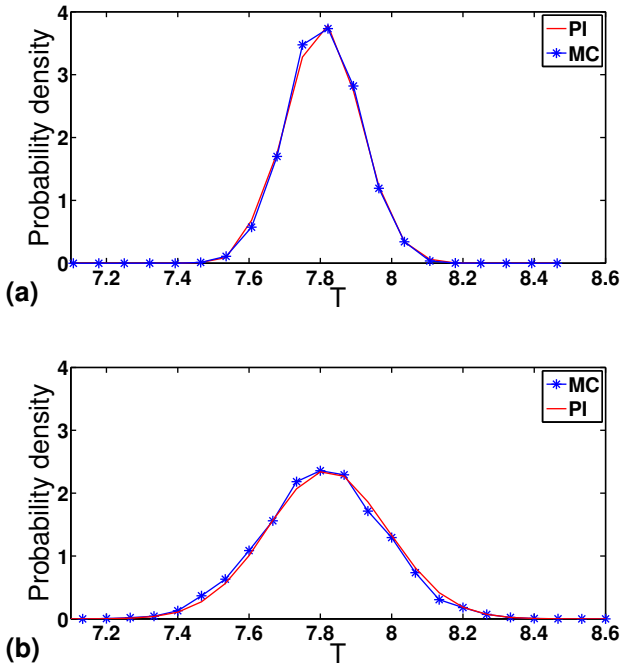

Figure 4.12: PDF of the period of the stick-slip motion. (a) $\mu_1 = 0.3$; (b) $\mu_1 \sim N(0.3, 0.01)$.

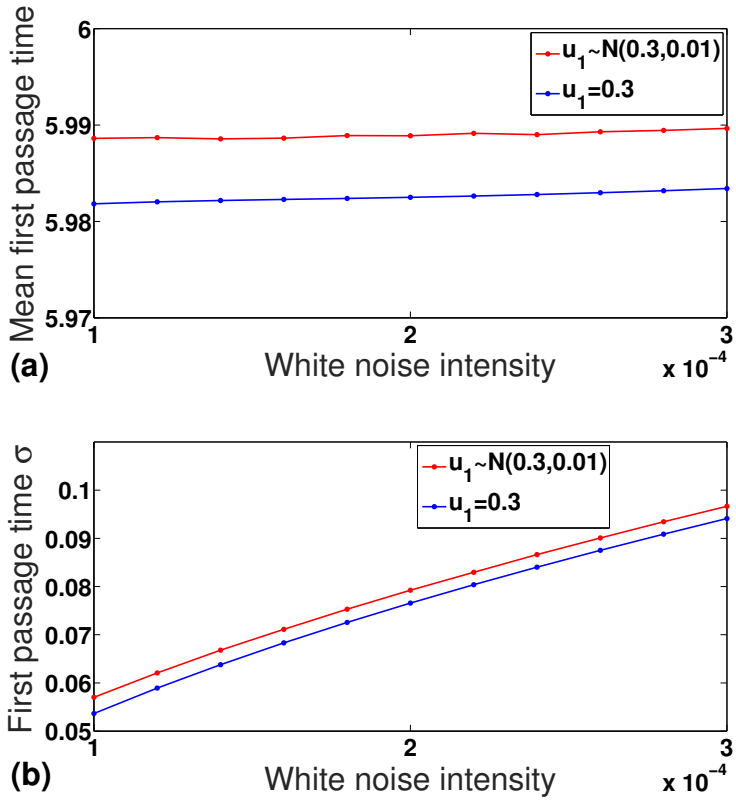

Figure 4.13: First passage time mean and standard deviation with different random intensity. (a) First passage time mean; (b) First passage time σ.

While the results for random μ_1 and μ_2 are given in Fig. 4.8, with Fig. 4.8(a) and 4.8(b) for PI and MC respectively. The difference between Fig. 4.7 and 4.8 is that the end of the stick stage (point 1 in deterministic case) becomes a horizontal line in this case. This is reasonable because random μ_2 causes the equilibrium in the stick stage be broken at different point for different value of μ_2. However, the scattered distributions approaching the entrance of the stick, such as the points 11, 12 and 13 in the deterministic case, are very similar, no obvious difference is observed. For

better understanding the probabilistic distribution of the random case, the PDF at a typical point (such as point 10) is presented in Fig. 4.9 and 4.10. Clearly, the two figures are very similar to each other.

In deterministic case, stick-slip is a periodic motion with a certain period. When the randomness in friction is considered, this certain period will become random and the point entering the stick stage will become random as well. Fig. 4.11 and Fig. 4.12 give the distribution of x and the motion period under the random case. As expected, the static friction has limited effect on the distribution of x, which matches the former observations that distributions are almost the same near the end of slip in Fig. 4.7 and Fig. 4.8. While in Fig. 4.12, a more flat distribution of motion period is obtained after using random static friction coefficient. The peak value in Fig. 4.12(b) is 2.38, almost 36.7% smaller than that in Fig. 4.12(a). It is supported by the truth that stick situation is controlled by μ_1 (Eq. (4.21)) and therefore the stick time is influenced by the random factor.

The portion of time in the slip stage is an indicator of the severity of the stick slip. This can be examined as a first passage problem with the threshold of v_0. By computing the statistics of this part of time, the fist passage time can be obtained for different random intensity, and the results are shown in Fig. 4.13. It can be seen that the mean values don't change very much while the standard deviation becomes larger as the random excitation getting stronger. The standard deviation for deterministic μ_1 is a little bit smaller than that for the random μ_1. This is reasonable given that the

randomness in μ_1 would contribute to the scattering (standard deviation) of variables.

4.6.2 Parametric study

It is well known that friction causes very complicated dynamics. Here we do not intent to make through analysis of the dynamic phenomena. Rather we simply change some of the parameters to demonstrate the changes in the responses. In the random case, MC simulation is employed to gather samples for statistical analysis.

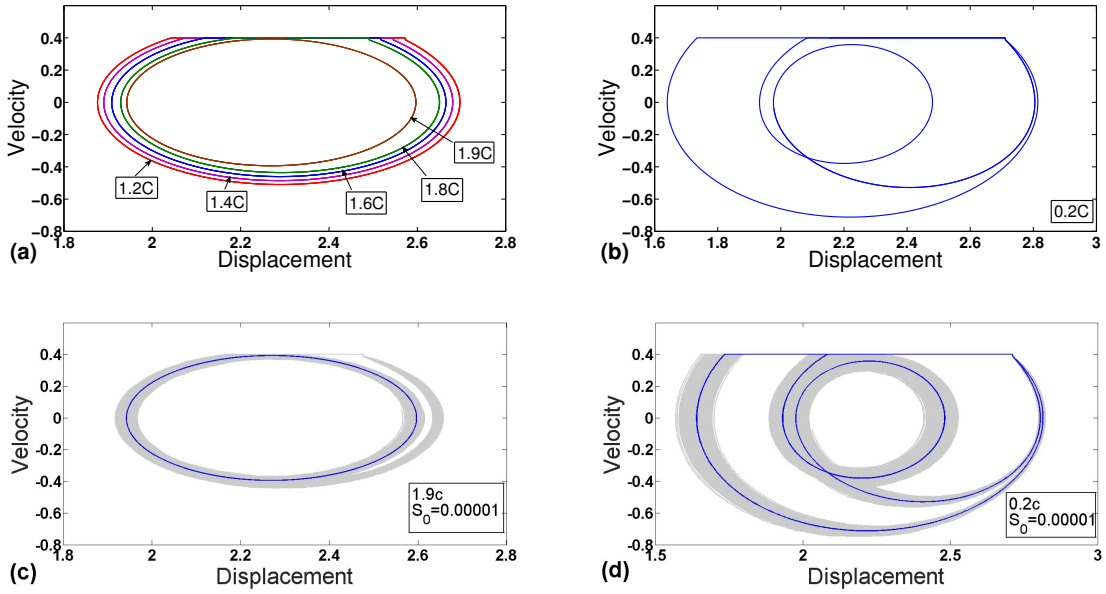

Figure 4.14: Phase plane changes due to damping with $f_1 = 2.7367$, $f_2 = 2.2695$, $f_0 = 0.2949$, $\omega_0 = 0.4$, $\omega_1 = 1.2$. (a) Limit cycle with different damping coefficient c; (b) Bifurcation; (c) Random case; (d) Bifurcation random case.

The first parameter we examine is the viscous damping coefficient c. The value

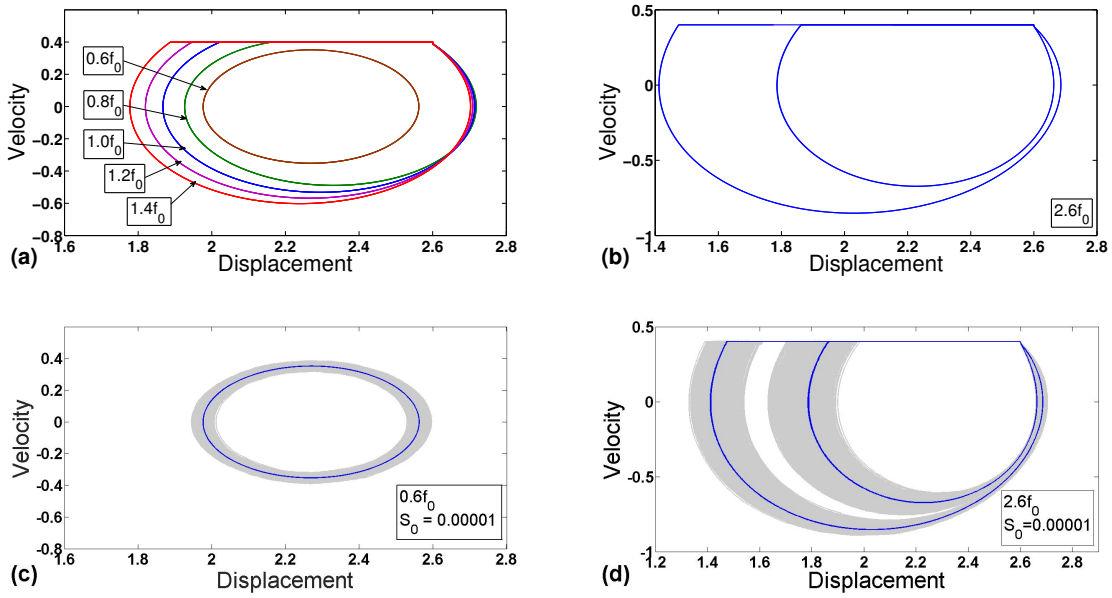

Figure 4.15: Phase plane changes due to harmonic excitation amplitude f_0 with f_1 = 2.7367, f_2 = 2.2695, c = 0.345, ω_0 = 0.4, ω_1 = 1.2. (a) Limit cycle enlarged as f_0 increasing; (b) Bifurcation; (c) Random case; (d) Bifurcation random case.

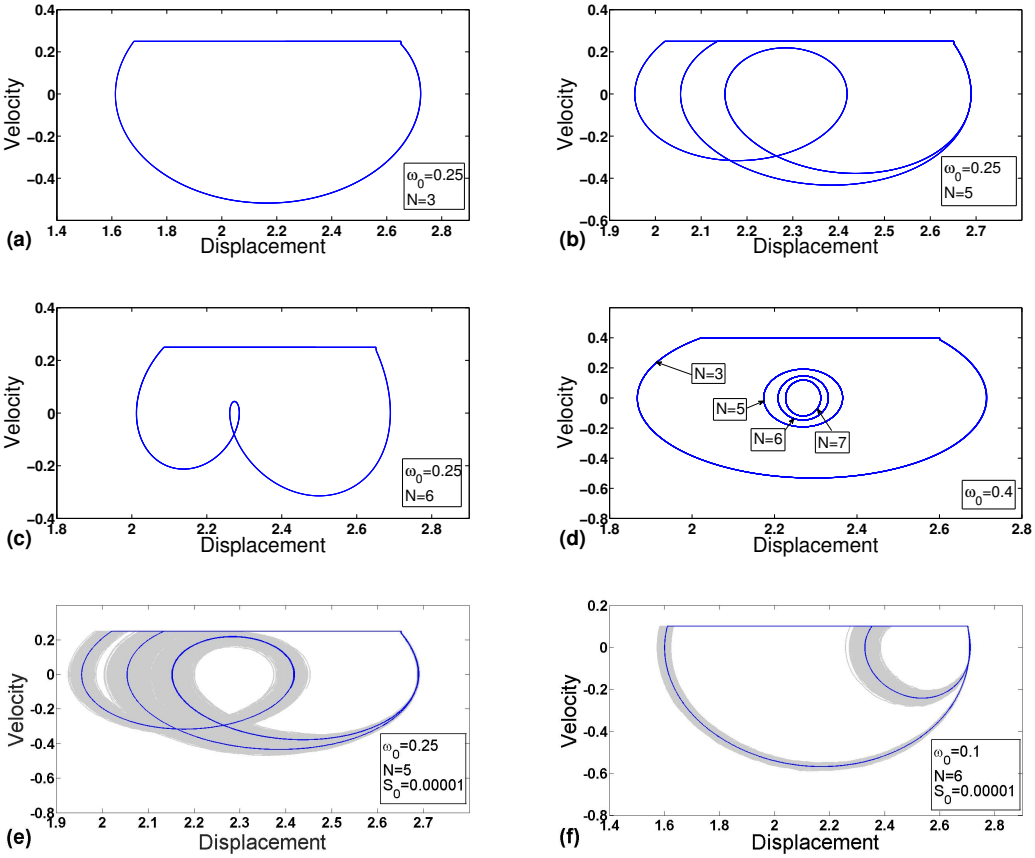

Figure 4.16: Phase plane changes due to harmonic excitation frequency with $f_1 = 2.7367$, $f_2 = 2.2695$, $f_0 = 0.2949$, $c = 0.345$. (a) Single period motion; (b) Bifurcation; (c) Single period motion; (d) Stick vanish as N increasing; (e) Random case; (f) Random case.

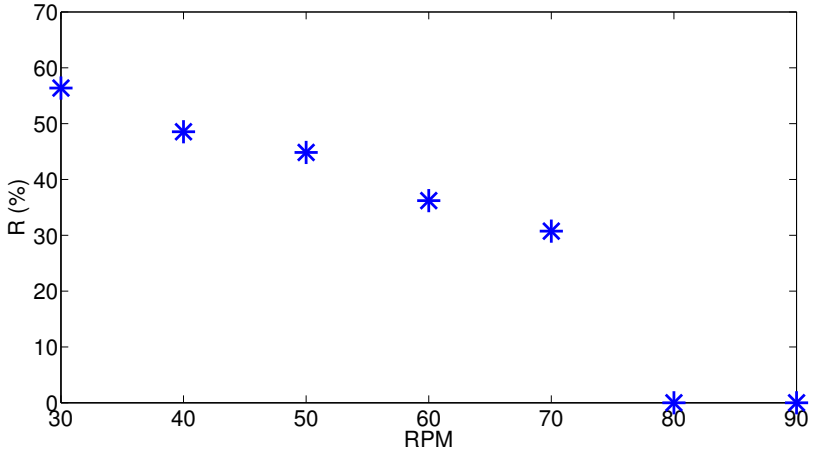

Figure 4.17: Ratio of stick time to total drilling time for different rotary speed at surface in deterministic condition. Pipe length 850 m, collar length 66 m, WOB 200 KN.

$c = 0.345$ used in the simulation of previous section is taken as the base. We gradually change its value and present the results in Fig. 4.14. First, the damping is increased from $1.2c$ to $1.9c$ with only deterministic excitation, and the results are shown in Fig. 4.14(a). It can be seen that with the increase of damping, the stick stage becomes smaller and smaller, but no essential change in the response. To a certain point, $1.9c$ in this case, the stick disappears completely, and the bit motion becomes general one periodic oscillation. If decreasing the damping gradually to $0.2c$, it is found that the stick-slip remains but the form of the phase plane changes to the one shown in Fig. 4.14(b). Obviously the nature of response has changed and this is called bifurcation in dynamics. The cases corresponding to $1.9c$ and $0.2c$ with random excitation are given in Fig. 4.14(c) and 4.14(d). As seen in Fig. 4.14(c), some responses

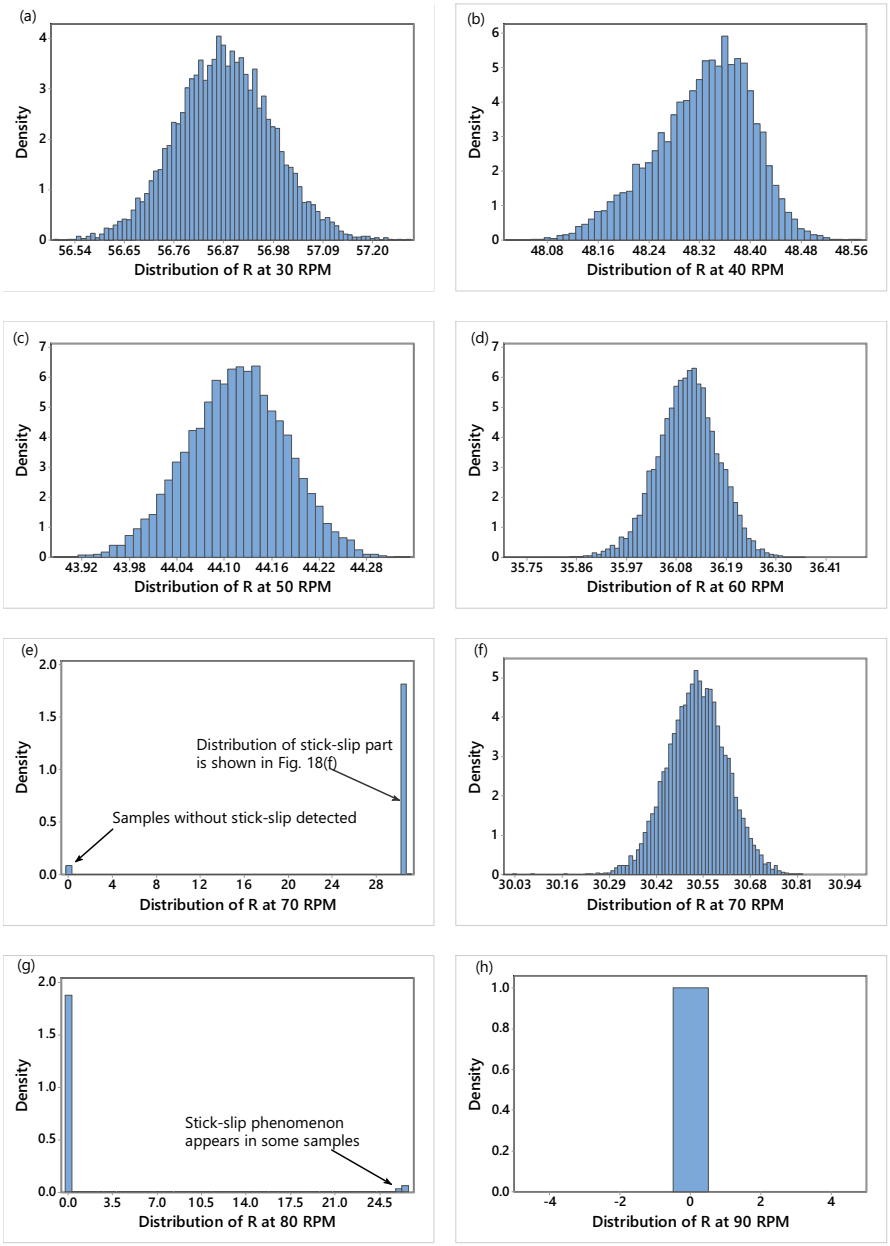

Figure 4.18: Distribution of R for different rotary speed at surface under random friction: (a) 30 RPM; (b) 40 RPM; (c) 50 RPM; (d) 60 RPM; (e) 70 RPM; (f) Partial enlargement of result at 70 RPM; (g) 80 RPM; (h) 90 RPM.

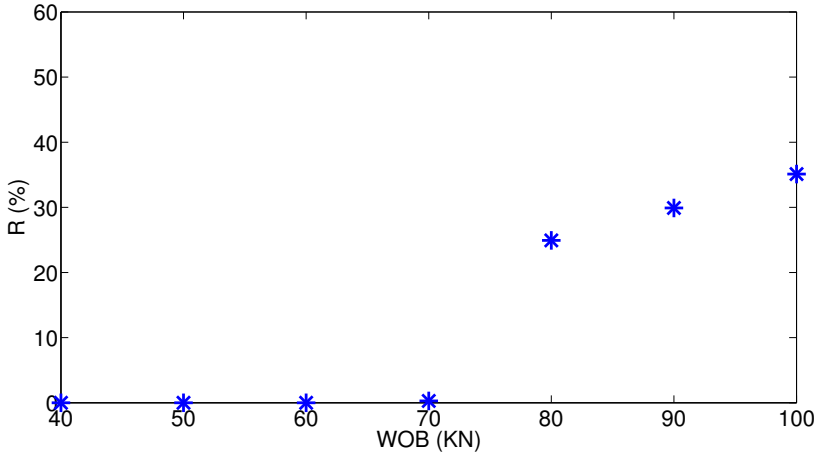

Figure 4.19: Ratio of stick time to total drilling time for different WOB in deterministic condition. Pipe length 850 m, collar length 66 m, rotary speed 30 RPM

still see the stick stage appeared even though in deterministic case the motion is completely slip.

The second parameter we studied is the amplitude of the harmonic excitation, and the results are showed in Fig. 4.15. In Fig. 4.15(a), we consider only the deterministic excitation by gradually changing the excitation amplitude from $0.6f_0$ to $1.4f_0$. At $0.6f_0$, no stick appears. With the increase of the excitation amplitude, stick appears and the size of the limit cycle is increased as well. If the amplitude is further increased to $2.6f_0$, a two-periods motion is detected as shown in Fig. 4.15(b). The random cases corresponding to $0.6f_0$ and $2.6f_0$ are given in Fig. 4.15(c) and 4.15(d) respectively. It is noted that the random excitation does not change the basic form of the response, simply scattering the single line to an area.

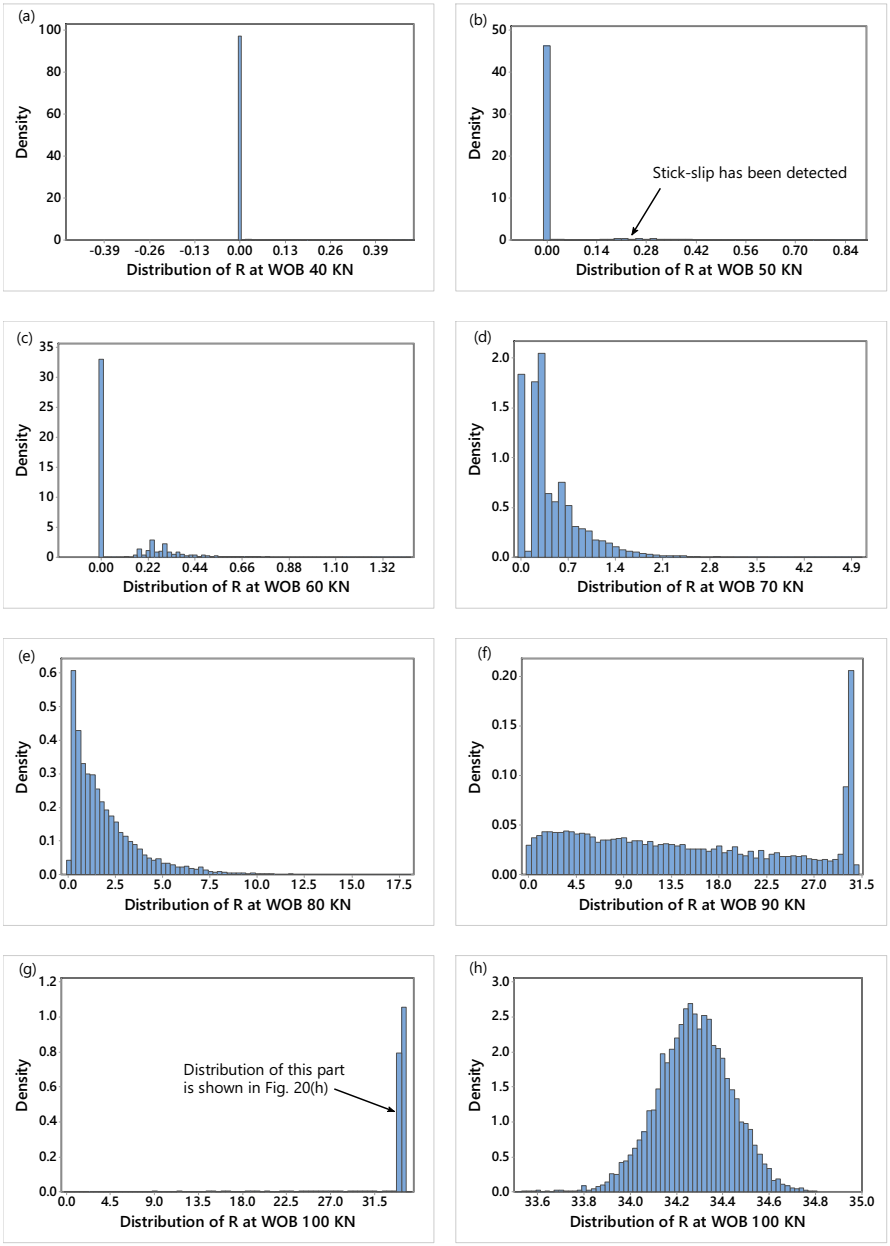

Figure 4.20: Distribution of R at different WOB at random friction: (a) WOB 40 KN; (b) WOB 50 KN; (c) WOB 60 KN; (d) WOB 70 KN; (e) WOB 80 KN; (f) WOB 90 KN; (g) WOB 100 KN; (h) Partial enlargement of result from WOB 100 KN.

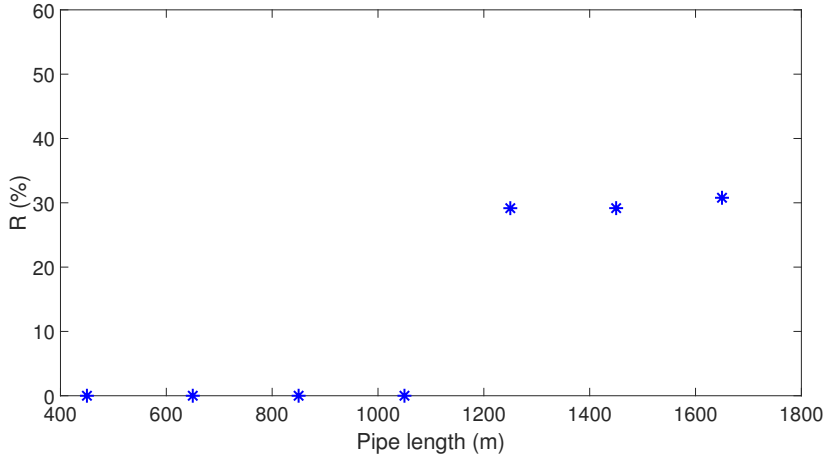

Figure 4.21: Ratio of stick time to total drilling time for different pipe length in deterministic condition. collar length 66 m, WOB 200 KN, rotary speed 77 RPM

The third parameter studied is the harmonic excitation frequency. According to Eq. (4.7), the excitation frequency is determined by the rotation velocity ω_0 and the cutter number N. We examine several combinations of ω_0 and N and the results are depicted in Fig. 4.16. First, for the most common three cutter bit ($N = 3$) with $\omega_0 = 0.25$ under only deterministic excitation, a regular stick-slip motion is observed in Fig. 4.16(a). Keeping all other parameters unchanged, but increasing the cutter number N to 5 and 6, the motion is still stick-slip, but the forms are changed to Fig. 4.16(b) and 4.16(c) respectively. If we keep $\omega_0 = 0.4$, but change N from 3 to 7, the responses are shown in Fig. 4.16(d). We can see that the stick is gone with higher number of cutters. However, it is hard to draw general conclusion due to the fact that innumerous combinations are possible. Two cases with random excitations

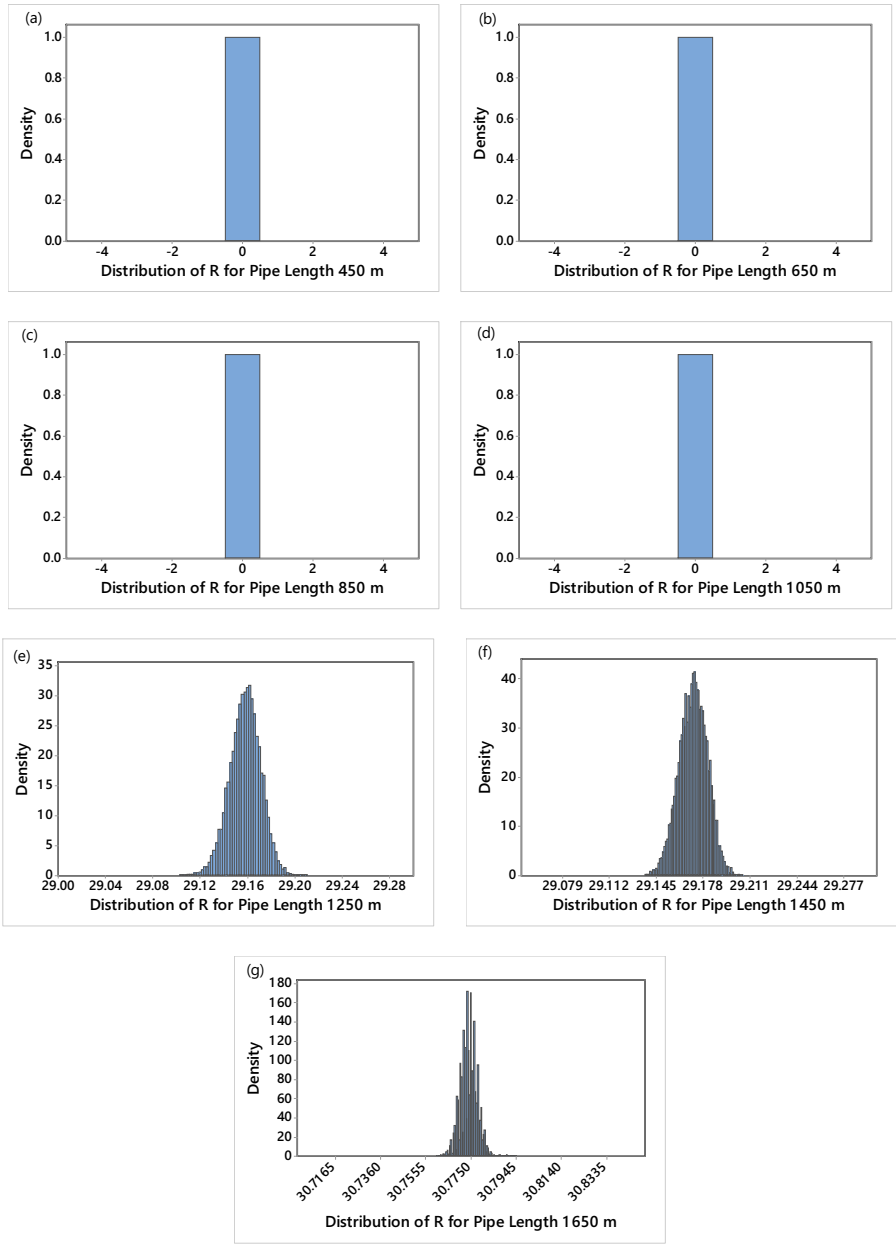

Figure 4.22: Distribution of R at different drill pipe length at random friction: (a) Case 1; (b) Case 2; (c) Case 3; (d) Case 4; (e) Case 5; (f) Case 6; (g) Case 7.

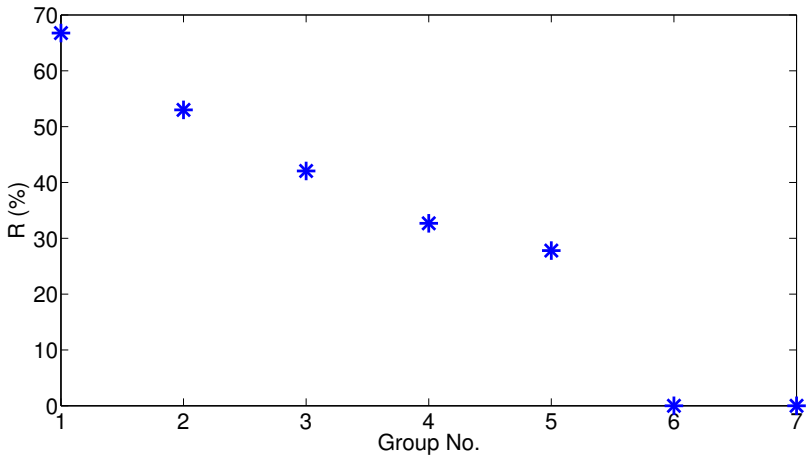

Figure 4.23: Ratio of stick time to total drilling time for different combination of drill pipe and drill collar in deterministic condition. WOB 100 KN, rotary speed 35 RPM, pipe length 850 m, collar length 66 m

are also shown in Fig. 4.16(e) and 4.16(f). The scattering effect of the randomness in excitation is seen clearly.

The portion of time staying in stick is a important indicator of the severity of stick-slip. We define a parameter R in this paper to evaluate this parameter as:

$$R = \frac{stick\ duration}{motion\ period} \times 100\% \tag{4.40}$$

First we change the rotary speed at surface, keeping other parameters in the simulation unchanged. If only deterministic excitation considered, R would be certain, and the results are given in Fig. 4.17. As can be seen with increasing of the the rotary speed, the time staying on stick (R value) decreases gradually. This is in agreement with common sense. Under the simulation case, the stick disappears (R becomes

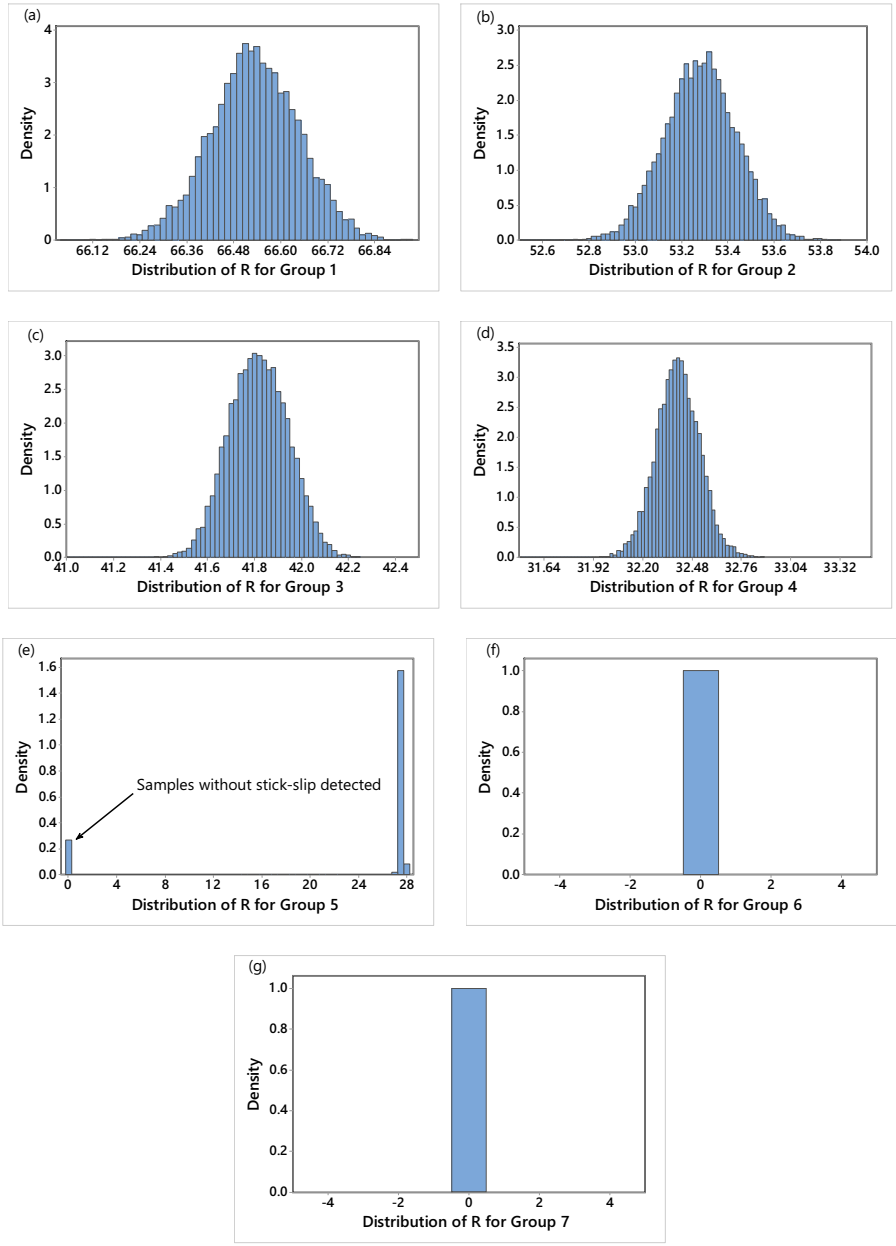

Figure 4.24: Distribution of R for different combination of drill pipe and drill collar at random friction: (a) Group 1; (b) Group 2; (c) Group 3; (d) Group 4; (e) Group 5; (f) Group 6; (g) Group 7.

zero) at 80 RPM. In the random case, R would be random and its distributions from 30 RPM to 90 RPM are shown in Fig. 4.18. From Fig. 4.18(a) to 4.18(d) the dominant motion is stick slip. The distribution of R is sometimes off normal, for example Fig. 4.18(b). This is reasonable given that the friction is a strong nonlinear factor. At 70 RPM, motions with no stick slip appear as shown in Fig. 4.18(e). A closer look at the stick slip part (the right part of the distribution) as given in Fig. 4.18(f) reveals that the distribution of this part is still close to normal. However, with further increase of RPM, more motions move to the non-stick-slip. At 90 RPM, stick slip almost completely disappears as in Fig. 4.18(h).

Then, we examine the effect of weight on bit (WOB) on the value of R. In the simulation the rotary speed is taken as 30 RPM, and WOB is changed from 40 to 100 (kN) with other parameters unchanged. The case with only deterministic excitation is given in Fig. 4.19. As can be seen, R gradually increases with the increase of WOB. With random excitation considered, at low WOB, such as 40 (kN), no stick slip happens (Fig.4.20(a)). With the increase of WOB, more motions move to stick slip as shown from Fig.4.20(b) through 4.20(f). To the point of 100 (kN), almost all motions are in stick slip as shown in Fig.4.20(g) and 4.20(h).

Length and diameter of drill pipe and drill collar have significant effect on the dynamics of drillstrings through affecting the stiffness and mass. We examine the dynamics by setting the drillpipe length as 450 m, 650 m, 850 m, 1050 m, 1250 m, 1450 m and 1650 m, and the results are presented in Fig. 4.21 and 4.22. In Fig. 4.21,

only deterministic excitation is considered. We can see that for the length under 1000 m no stick slip is observed. Also, the value of R increases with the increase of drill pipe length. The results with inclusion of random excitation are given in Fig. 4.22. Similar conclusion can be drawn with Fig. 4.21, but with extra information of probability.

Table 4.2: Specification for different pipe and collar group

Item	Group 1	Group 2	Group 3	Group 4	Group 5	Group 6	Group 7
Drill pipe outer diameter D_0 (m)	0.1010	0.1143	0.1270	0.1270	0.1270	0.1397	0.1397
Drill pipe inner diameter d_0 (m)	0.0848	0.1005	0.1120	0.1016	0.095	0.095	0.095
Drill collar outer diameter D_1 (m)	0.1207	0.1524	0.1651	0.1651	0.1651	0.1842	0.2286
Drill pipe inner diameter d_1 (m)	0.0508	0.0572	0.0572	0.0572	0.0572	0.0714	0.0762
Drillstring stiffness K (Nm/rad)	456.08	603.98	903.42	1342.71	1558.10	2606.43	2637.55
Drillstring inertia J (kg m^2)	44.75	71.87	104.58	137.86	154.31	253.38	333.34

For the effect of drillpipe and drillcollar diameter, seven combinations are considered based on real pipe (6 types) and collar (5 types) which are given in Table 4.2. The stiffness K and mass J for each case are given in this table as well. The simulation results are schematically plotted in Fig. 4.23 and 4.24 for deterministic and random case respectively.

4.7 Conclusion Remarks

This chapter investigates the stick-slip motion with a SDOF drillstring model subjected to combined deterministic and random excitations. The static friction in stick

and kinetic friction in slip are treated separately in this chapter, but both include randomness. Therefore, the dynamic response becomes random as well. Path integration and Monte Carlo simulation are used to obtain the probabilistic response. Simulation indicates that results from PI and MC agree very well with each other. In the last, parameter study is carried out through MC for the main drillstring parameters. The conclusions can be drawn as follows:

- Randomness in friction has a significant effect on torsional stick-slip vibration of a drillstring system. To account for the random effect, a stochastic dynamic model is developed and the response in probability is obtained.

- Static friction coefficient μ_1 has more obvious influence on stick. More specifically, random μ_1 mainly affects the response at the end of stick, while its effect on the starting of stick is very limited. Also it has an obvious effect on the period of the stick-slip.

- Kinetic friction coefficient μ_2 has more apparent effect on slip. The randomness of μ_2 causes the response in slip stage scattering in an area. The stronger the randomness, the larger the scattered area.

- Factors which lead to stick-slip include decreasing RPM, increasing WOB, enlarging the pipe length and employing weaker combination of pipe and collar. Simulation indicates that although the system doesn't have stick-slip problem in deterministic case, it may be still in stick-slip in random case.

Chapter 5

Investigation on Random Vibration of a Drillstring

The research work of this chapter has been published: Hongyuan Qiu, Jianming Yang, Stephen Butt, Jinghan Zhong. "Investigation on random vibration of a drillstring." *Journal of Sound and Vibration* 406 (2017): 74-88 [178].

5.1 Co-authorship Statement

Hongyuan Qiu: Dynamic Modeling, Methodology, Simulation, Data Processing, Result Analysis and Writing Manuscript. **Dr. Jianming Yang**: Supervision and Reviewing. **Dr. Stephen Butt**: Supervision and Reviewing. **Jinghan Zhong**: Data Support.

5.2 Abstract

This paper investigates the axial-torsional coupled vibration of a drillstring under combined deterministic and random excitations. Finite element method (FEM) is used to model the system. The random excitation at the bit-rock interaction, which is considered in the bit axial direction, is treated as Gaussian white noise. Statistic linearization is first applied to find a equivalent linear dynamic system which is then solved with stochastic Newmark algorithm. The statistics of the responses, including the means and standard deviations of the bit axial displacement and rotational velocity are obtained and analyzed.

5.3 Introduction

Drillstrings are slender structures used to dig into the rock in search of oil and gas. Failures of drillstrings are time and money consuming; therefore, the dynamics of drillstrings must be investigated and carefully controlled.

In the recent decades, the drillstring dynamic models can be mainly divided into three categories: finte element method (FEM) model [33, 34, 136], lumped parameter method model [16, 60] and continuous parameter method model [22, 170, 179].

During drilling process, the drilling system usually experiences three types of vibrations, namely axial vibration, torsional vibration and lateral vibration. Each individual vibration mode is of great academic interest; however, coupled vibration

study has more practical significance. Typically, a drillstring vibrates in three major coupled modes: lateral-torsional, axial-lateral and axial-torsional. Bit-rock interaction is regarded as a major cause of axial-torsional coupling. To represent the bit-rock interaction, some researchers [180] used friction-based models; some others considered both cutting and friction [41, 153, 154, 181].

Downhole condition is highly unpredictable due to many uncertain and inconsistent factors. These uncertainties may exist in material property, system dimension, fluid-structure interaction, bit-rock interaction, etc. Therefore, it is more meaningful to investigate drillstring dynamics from random/stochastic viewpoint. In fact, Bogdanoff and Goldberg [132] realized this point already in as early as 1950's, and proposed a probabilistic model of drillstring dynamics. However, research along this direction thereafter has progressed slowly, probably due to the inherent complexity of random vibration. Among the very few researchers working on random vibration of drillstring, Chevallier [21] investigated the lateral vibration with a nonlinear random model. In his work, the excitations for a tri-cone bit and a PDC bit were modeled as a Kanai Tajimi and band limited white noise precess, respectively. The nonlinearity in the contact between drillstring and formation was handled with a stochastic linearization technique. In recent years, Ritto [135–138] made great contribution in drillstring dynamics with probabilistic models. Their focus was placed on the bit-rock interaction, and the drilling fluid effect on dynamics. In some other papers, Ritto [139, 140] also studied the uncertainties in the weight-on-hook. Qiu et al. [169]

studied stick-slip vibration with random excitation on the bit in torsional direction.

5.4 Dynamic Model

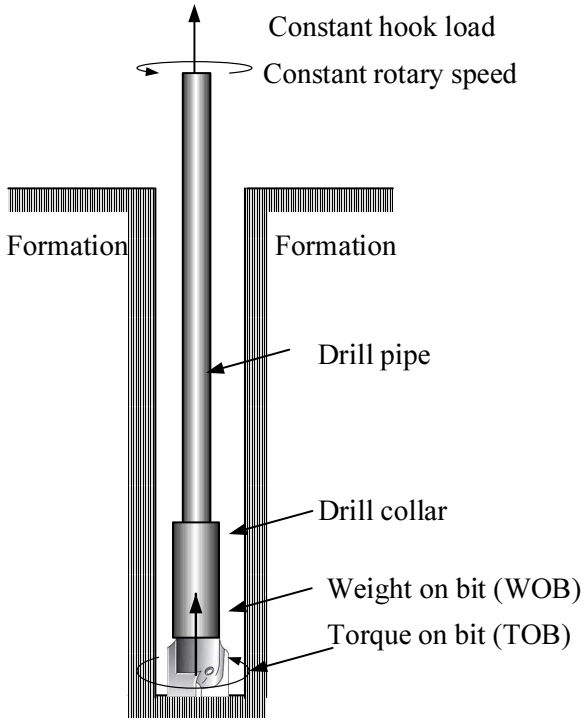

Figure 5.1: Schematic representation of a drillstring

The drillstring investigated is schematically shown in Fig. 5.1. It is a fixed-free model with the top rotating at a constant speed and under constant hook load. It is composed of drill pipe, drill collar and drill bit. At the bottom, the drill bit is subjected to a combination of weight on the bit (WOB) and torque on the bit (TOB). The body of the drillstring is subjected to the buoyant weight and drilling

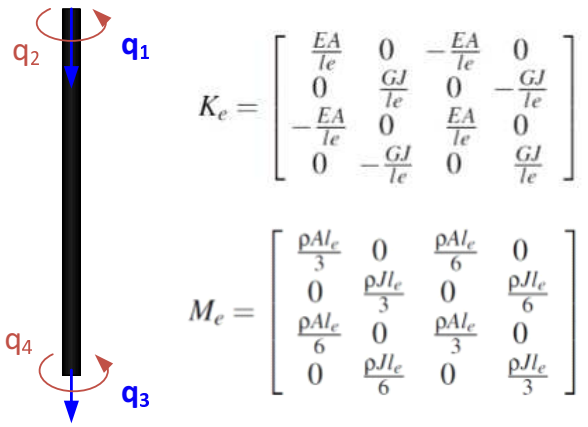

Figure 5.2: Finite element and its stiffness and mass matrices

fluid axial force.

The drillstring is discretized into finite elements considering axial and torsional degrees of freedom at each node, as shown in Fig. 5.2. The local stiffness and mass matrices of the finite element, which are given in the figure, can be found in any finite element textbook. In the matrices, E is the Young's modulus of drillstring material, G is the shear modulus, ρ is drillstring density, J is the polar moment of inertia of drillstring cross section, A is the cross section area and l_e is the element length. J, A and l_e have different values for pipe and collar. By assembling the local stiffness and mass matrices of each element, the global mass and stiffness matrices of the system can be obtained, and the equation of motion is expressed in the general form as below:

$$\mathbf{M}\ddot{\mathbf{q}}(t) + \mathbf{C}\dot{\mathbf{q}}(t) + \mathbf{K}\mathbf{q}(t) = \mathbf{F}(\mathbf{q}) \tag{5.1}$$

where $\mathbf{q}(t)$ denotes the general coordinate vector, $\mathbf{F}(\mathbf{q})$ represents the deterministic excitation vector, including weight on the bit W_B, torque on the bit T_B, buoyant

weight f_b, drilling fluid axial force f_d and constant hook load f_0, $\mathbf{M}$, $\mathbf{C}$ and $\mathbf{K}$ are the system's global mass, damping and stiffness matrices, respectively, $\mathbf{C}$ is assumed to be a linear combination of $\mathbf{K}$ and $\mathbf{M}$ as below:

$$\mathbf{C} = \alpha\mathbf{M} + \beta\mathbf{K} \tag{5.2}$$

where α and β are constants to be selected.

The buoyant weight on each node of the element is given as:

$$f_b = \frac{1}{2}\rho g A l_e (1 - \frac{\rho_1}{\rho}) \tag{5.3}$$

where ρ_1 is the density of the drilling fluid and g is the gravitational acceleration. The drilling fluid axial force on each node of the finite element, according to [136], is given as:

$$f_d = \frac{1}{2}M_f l_e g - \frac{1}{2}A_i \rho_1 l_e g - \frac{1}{4}C_f \rho_1 l_e D_o U_o^2 \tag{5.4}$$

where M_f is the fluid mass per unit length, A_i is the inner cross section area of the beam element, C_f is the fluid viscous damping coefficient, D_o is the outside diameter of the element and U_o is the outside dilling fluid velocity.

Hook load f_0 is on the top of the drillstring, which is given as:

$$f_0 = F_h W_d \tag{5.5}$$

where F_h is the hook load factor, W_d is total drillstring buoyant weight, which can be calculated as:

$$W_d = \rho g (A_p l_p + A_c l_c)(1 - \frac{\rho_1}{\rho}) \tag{5.6}$$

where A_p and A_c are cross section area of drillpipe and drillcollar, l_p and l_c are length of drillpipe and drillcollar section.

According to [41, 181], the W_B and T_B account for the sum of a cutting term acting on the cutting faces of an equivalent cutter and a friction term at the all wear flats/rock interfaces:

$$W_B = W_f + W_c \tag{5.7}$$

$$T_B = T_f + T_c \tag{5.8}$$

W_f and T_f are represented as:

$$W_f = \begin{cases} 0 & \text{if } x_{b_n} \leq 0 \\ k_c n x_{b_n} & \text{if } x_{b_n} < d_* \quad with \quad d_* = \dfrac{R_b \sigma l}{k_c} \\ R_b \sigma n l & \text{if } x_{b_n} \geq d_* \end{cases} \tag{5.9}$$

$$T_f = r\frac{R_b}{2} u W_f \tag{5.10}$$

where k_c is the rock linear contact stiffness, n is the blade number of an ideal drag bit, x_{b_n} is related to the bit axial displacement and represents the drag bit instantaneous depth of cut at time t_n, d_* marks a critical depth of cut beyond which the increase of depth of cut will have no influence on the contact forces [181], R_b is the bit radius, σ is the rock contact stress, l is the wear flat length for the bit, r is a parameter typically in the range from 1 to 4/3 [32], u is the friction coefficient, which is modeled with distiction between static and kinetic frictions, is represented as [29]:

$$u = u_k + (u_s - u_k)\exp(-\gamma_b |\omega_b|) \tag{5.11}$$

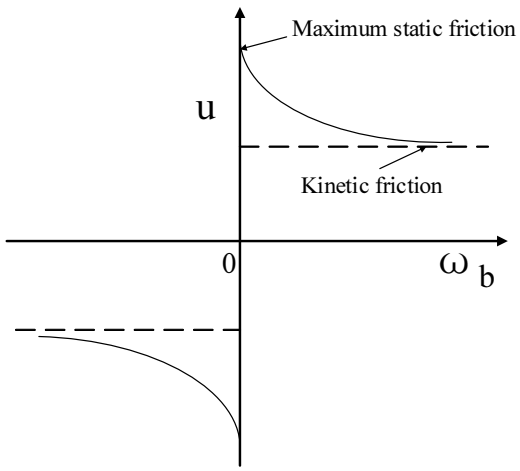

Figure 5.3: Sketch of velocity weakening function

where u_s and u_k are the static and kinetic friction coefficients respectively, γ_b is a positive constant, ω_b is the rotary speed of drill bit. u is graphically shown in Fig. 5.3.

Being independent of the bit cutter arrangement and the bit shape, the cutting components W_c and T_c are written as [181]:

$$W_c = \begin{cases} 0 & \text{if} \quad x_{b_n} \leq 0 \\ \zeta \varepsilon R_b n x_{b_n} & \text{if} \quad x_{b_n} > 0 \end{cases} \tag{5.12}$$

$$T_c = \begin{cases} 0 & \text{if} \quad x_{b_n} \leq 0 \\ \varepsilon \frac{R_b^2}{2} n x_{b_n} & \text{if} \quad x_{b_n} > 0 \end{cases} \tag{5.13}$$

where ζ is the ratio of the vertical to horizontal force for a sharp cutter, ε is the intrinsic specific energy required to remove a unit volume of rock.

It is worth of noting that Eq.(5.9) to Eq.(5.13) are not exactly the same as those given in [181]. In [181], the W_B and T_B are renewed at each angle of $\frac{2\pi}{n}$. While in this paper, the W_B and T_B are renewed at each time step. The contact between the rock

and bit will be lost only when the displacement of the bit is negative. In addition, backwards rotation of the bit is not considered.

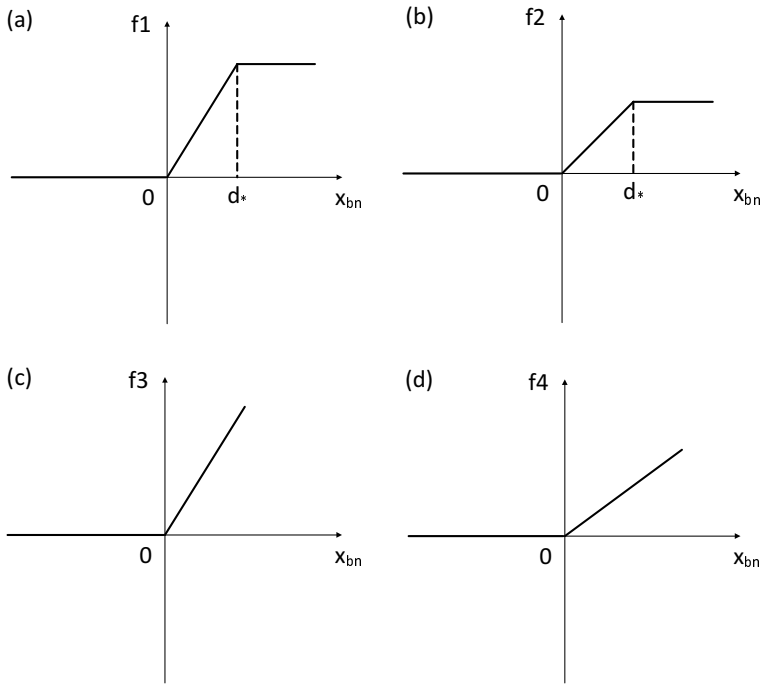

Figure 5.4: Nonlinearity in the bit rock interaction. (a) Nonlinearity in W_f; (b) Nonlinearity in T_f; (c) Nonlinearity in W_c; (d) Nonlinearity in T_c.

To incorporate random excitation into the system, Gaussian white noise is added to the right hand side of Eq. (5.1). It is added at the end of the drillstring finite element in the axial direction. Then, the equation of motion becomes:

$$\mathbf{M}\ddot{\mathbf{Q}}(t) + \mathbf{C}\dot{\mathbf{Q}}(t) + \mathbf{K}\mathbf{Q}(t) = \mathbf{F}(\mathbf{Q}) + \mathbf{B}\mathbf{W}(t) \tag{5.14}$$

where $\mathbf{Q}(t)$ is the random general coordinate vector, $\mathbf{W}(t)$ represents an array of

Gaussian white noise and **B** is a matrix representing the intensity of the white noise (For detail, please see Appendix. A or [178]).

5.5 Solution Strategy

Eq.5.14 is solved with both stochastic Newmark [182] and Monte Carlo simulation (MC), so that they can verify each other. In the MC simulation, Eq.5.14 is numerically solved by using deterministic Newmark integration scheme and the sample size is taken as 2000.

5.5.1 Statistical Linearization

Eq. 5.14 is nonlinear due to W_B and T_B. If we draw pictures of W_B and T_B versus the depth of cut x_{b_n}, the nonlinearities in the bit-rock interaction will be clearly noticed as depicted in Fig. 5.4. For simplification, f_1 represents W_f, f_2 is T_f, f_3 stands for W_c and f_4 is T_c. To use the stochastic Newmark scheme, we first apply the statistical linearization (SL) technique to transform Eq.5.14 into a equivalent linear set. In addition, SL is applied to each time step for accuracy consideration. For each time step, an equivalency of f_i, which is represented by f_i^e, can be represented in the following linear form:

$$f_i^e = k_i^e x_i + f_i^0 \tag{5.15}$$

where the subscript i is from 1 to 4, and the superscript e denotes the equivalent. f_i^0 is a constant. The difference between the equivalent linear force f_i^e and the original

nonlinear f_i is defined as δ_i:

$$\delta_i = f_i - f_i^e = f_i(x_i) - k_i^e x_i - f_i^0 \tag{5.16}$$

To find optimum k_i^e and f_i^0 that make δ_i minimum in probabilistic sense, the expected value of δ_i^2 is minimized by solving the following two equations:

$$\frac{\partial}{\partial k_i^e} E(\delta_i^2) = 0 \tag{5.17}$$

$$\frac{\partial}{\partial f_i^0} E(\delta_i^2) = 0 \tag{5.18}$$

where $E(\cdot)$ is the operation of ensemble average. This leads to:

$$k_i^e = \frac{E(x_i f_i(x_i))}{\sigma_i^2} \tag{5.19}$$

$$f_i^0 = E(f_i(x_i))) - k_i^e E(x_i) \tag{5.20}$$

If x_i is a Gaussian process, Eq. (5.19) can be simplified as below:

$$k_i^e = E(\frac{df_i(x_i)}{dx_i}) \tag{5.21}$$

After some mathematical manipulation the following equations for k_i^e and f_i^0 can be obtained:

$$k_1^e = \frac{k_c n}{2}(erf(y_2) - erf(y_1)) \tag{5.22}$$

$$f_1^0 = \frac{k_c n\sigma}{\sqrt{2\pi}}(e^{-y_1^2} - e^{-y_2^2}) + \frac{R\sigma nl}{2}(1 - erf(y_2)) \tag{5.23}$$

$$k_2^e = \frac{rR_b u}{2}k_1^e \tag{5.24}$$

$$f_2^0 = \frac{rR_b u}{2}f_1^0 \tag{5.25}$$

$$k_3^e = \frac{\xi\varepsilon R_b n}{2}(1 - erf(y_1)) \tag{5.26}$$

$$f_3^0 = \frac{\xi\varepsilon R_b n\sigma}{\sqrt{2\pi}}e^{-y_1^2} \tag{5.27}$$

$$k_4^e = \frac{\varepsilon R_b^2 n}{4}(1 - erf(y_1)) \tag{5.28}$$

$$f_4^0 = \frac{\varepsilon R_b^2 n\sigma}{2\sqrt{2\pi}}e^{-y_1^2} \tag{5.29}$$

where $erf(\cdot)$ is the error function, and y_1 and y_2 are calculated as follows:

$$y_1 = -\frac{\mu}{\sqrt{2}\sigma} \tag{5.30}$$

$$y_2 = \frac{d_* - \mu}{\sqrt{2}\sigma} \tag{5.31}$$

where μ and σ are the mean and standard deviation of bit axial displacement respectively. The derivation of Eq. (5.22) to (5.31) is presented in Appendix. B.

It can be seen that k_i^e and f_i^0 depend on μ and σ, which, in turn, depend on k_i^e and f_i^0. Ideally, iteration is needed generally to get the converged k_i^e and f_i^0 at each step. However, the computation would become drastically intensive if the iteration is conducted. A remedy to this issue is to calculate k_i^e and f_i^0 using the mean and the

variance of the previous time step. Given the fact that the time step is very small and both the mean and variance change pretty smoothly, the error caused by this approximation is limited. For the friction coefficient u, we calculated a mean value $E(u)$ at every simulation step using mean and variance of bit rotary speed.

5.5.2 Stochastic Newmark scheme

After the stochastic linearization, Eq. 5.14 becomes:

$$\mathbf{M}\ddot{\mathbf{Q}}(t) + \mathbf{C}\dot{\mathbf{Q}}(t) + \mathbf{K_{eq}}\mathbf{Q}(t) = \mathbf{F} + \mathbf{B}\mathbf{W}(t) \tag{5.32}$$

where $\mathbf{K_{eq}}$ is the equivalent stiffness matrix, $\mathbf{F}$ is the deterministic excitation vector. $\mathbf{K_{eq}}$ and $\mathbf{F}$ should be updated at each simulation time step. By using the stochastic Newmark scheme introduced by Bernard and Fleury [182] and setting the parameters $\gamma = \frac{1}{2}$ and $\delta = \frac{1}{2}$, we obtain the following equations:

$$\begin{aligned}(\mathbf{C} + \frac{\Delta t}{2}\mathbf{K_{eq}})\mathbf{Q}_{n+1} + \mathbf{M}\dot{\mathbf{Q}}_{n+1} = \ & (\mathbf{C} - \frac{\Delta t}{2}\mathbf{K_{eq}})\mathbf{Q}_n + \mathbf{M}\dot{\mathbf{Q}}_n \\ & + \frac{\Delta t}{2}(\mathbf{F}_n + \mathbf{F}_{n+1}) + \sqrt{\Delta t}\mathbf{B}\mathbf{N}_{n+1}\end{aligned} \tag{5.33}$$

$$\mathbf{M}\mathbf{Q}_{n+1} - \mathbf{M}\frac{\Delta t}{2}\dot{\mathbf{Q}}_{n+1} = \ \mathbf{M}\mathbf{Q}_n + \mathbf{M}\tfrac{\Delta t}{2}\dot{\mathbf{Q}}_n + \mathbf{B}\tfrac{\Delta t\sqrt{\Delta t}}{12}\mathbf{P}_{n+1} \tag{5.34}$$

where Δt is the length of time step, $\mathbf{N}_n$ and $\mathbf{P}_n$ are independent Gaussian random sequences with zero mean and variance of unity. The subscripts n and n+1 indicate the corresponding value of parameters at time instant t_n and t_{n+1}. The computation

can be achieved step by step starting from a deterministic initial condition $[\mathbf{q}_0 \;\; \dot{\mathbf{q}}_0]^T$. Eq. 5.33 and 5.34 can be rearranged in a more concise form:

$$\mathbf{Y}_{n+1} = \mathbf{A}_1\mathbf{Y}_n + \mathbf{A}_2\mathbf{H}_n + \mathbf{A}_3\mathbf{W}_n \tag{5.35}$$

The matrices in Eq. 5.35 are defined as below:

$$\mathbf{Y}_n = \begin{bmatrix}\mathbf{Q}_n & \dot{\mathbf{Q}}_n\end{bmatrix}^T \tag{5.36}$$

$$\mathbf{H}_n = [\mathbf{F}_n \;\; \mathbf{F}_{n+1}]^T \tag{5.37}$$

$$\mathbf{A}_1 = \begin{bmatrix}\mathbf{C}+\frac{\Delta t}{2}\mathbf{K_{eq}} & \mathbf{M} \\ \mathbf{M} & -\mathbf{M}\frac{\Delta t}{2}\end{bmatrix}^{-1}\begin{bmatrix}\mathbf{C}-\frac{\Delta t}{2}\mathbf{K_{eq}} & \mathbf{M} \\ \mathbf{M} & \mathbf{M}\frac{\Delta t}{2}\end{bmatrix} \tag{5.38}$$

$$\mathbf{A}_2 = \begin{bmatrix}\mathbf{C}+\frac{\Delta t}{2}\mathbf{K_{eq}} & \mathbf{M} \\ \mathbf{M} & -\mathbf{M}\frac{\Delta t}{2}\end{bmatrix}^{-1}\begin{bmatrix}\frac{\Delta t}{2}\mathbf{I} & \frac{\Delta t}{2}\mathbf{I} \\ 0 & 0\end{bmatrix} \tag{5.39}$$

$$\mathbf{A}_3 = \begin{bmatrix}\mathbf{C}+\frac{\Delta t}{2}\mathbf{K_{eq}} & \mathbf{M} \\ \mathbf{M} & -\mathbf{M}\frac{\Delta t}{2}\end{bmatrix}^{-1}\begin{bmatrix}\sqrt{\Delta t}\mathbf{B} & 0 \\ 0 & \mathbf{B}\frac{\Delta t\sqrt{\Delta t}}{\sqrt{12}}\end{bmatrix} \tag{5.40}$$

$$\mathbf{W}_n = [\mathbf{N}_{n+1} \;\; \mathbf{P}_{n+1}]^T \tag{5.41}$$

5.5.3 Solution for Statistics

Multiplying Eq. 5.35 with its transpose and taking the ensemble average, the following recursive equation can be arrived (Appendix. C):

$$\mathbf{R}_{n+1} = \mathbf{A}_1\mathbf{R}_n\mathbf{A}_1^T + \mathbf{A}_2\mathbf{H}_n\mathbf{H}_n^T\mathbf{A}_2^T + \mathbf{A}_3\mathbf{I}\mathbf{A}_3^T + \mathbf{A}_1E(\mathbf{Y}_n)\mathbf{H}_n^T\mathbf{A}_2^T + \mathbf{A}_2\mathbf{H}_nE(\mathbf{Y}_n^T)\mathbf{A}_1^T \tag{5.42}$$

where $\mathbf{R}_n$ is the correlation matrix, which is expressed as:

$$\mathbf{R}_n = E(\begin{bmatrix} \mathbf{Q}_n\mathbf{Q}_n^T & \mathbf{Q}_n\dot{\mathbf{Q}}_n^T \\ \dot{\mathbf{Q}}_n\mathbf{Q}_n^T & \dot{\mathbf{Q}}_n\dot{\mathbf{Q}}_n^T \end{bmatrix}) \tag{5.43}$$

The ensemble average $E(\mathbf{Y}_n)$ is obtained by taking the ensemble average of Eq. 5.35. As the means of $\mathbf{N}_n$ and $\mathbf{P}_n$ are equal to zero, $E(\mathbf{Y}_n)$ is given as:

$$E(\mathbf{Y}_{n+1}) = \mathbf{A}_1 E(\mathbf{Y}_n) + \mathbf{A}_2\mathbf{H}_n \tag{5.44}$$

5.5.4 Initial Condition

The initial conditions could be either stochastic or deterministic. For the sake of simplicity, deterministic initial condition is used in this paper. By neglecting the terms related to the acceleration and velocity on the left hand side of Eq. 5.1, deterministic initial displacement can be obtained by solving the equation below:

$$\mathbf{K}\mathbf{q}_0 = \mathbf{F}(\mathbf{q}_0) \tag{5.45}$$

For the initial velocity, the axial velocity is set zero and the torsional velocity is set equal to the constant rotary speed at the top. It is proven that the initial conditions do not affect the final stationary response [119].

5.6 Simulation and Result analysis

5.6.1 Parameters in Simulation

The drillstring model is made up of drillpipe and drillcollar sections. the parameters of the drillstring used in the simulation are given in the following. The length of drillpipe is 1000 m and is evenly divided into 20 finite elements. Drillpipe outer diameter is 0.127 m, inner diameter is 0.095 m. Drillcollar is 200 m long with outer diameter 0.2286 m and inner diameter 0.0762 m. It is evenly divided into 10 finite elements. The values of the other parameters used in the simulation are listed as below: $\rho = 7850.0$ kg m^{-3}, $E = 210\times10^9$ N m^{-2}, $G = 7.6923\times10^{10}$ N m^{-2}, $r = 1.3$, $R_b = 0.22$ m, $l = 5$ mm, $\zeta = 0.8$, $k_c = 37.5$ MN m^{-1}, $\varepsilon = 45$ MPa, $\sigma = 45$ MPa, $\rho_1 = 1310$ Kg m^{-3}, $C_f = 0.0125$, $U_0 = 1.5$ m s^{-1}, $u_s = 0.30$, $u_k = 0.21$, $\gamma_b = 1$, $n = 3$, $\alpha = 0.1$, $\beta = 0.1$, $\Delta t = 0.0002$ s.

5.6.2 Results Analysis

Based on the above parameters, simulation is first conducted for three hook load factors, $F_h = 0.807, 0.983$ and 0.768, representing a medium, heavy and light hook load. It is noted that only the statistics of the axial displacement and torsional velocity are presented in the following for the sake of space-saving given that they are related to bit bounce and stick slip.

In case study 1, the hook load factor F_h is taken as 0.807. Using Eq. 5.5 and 5.6,

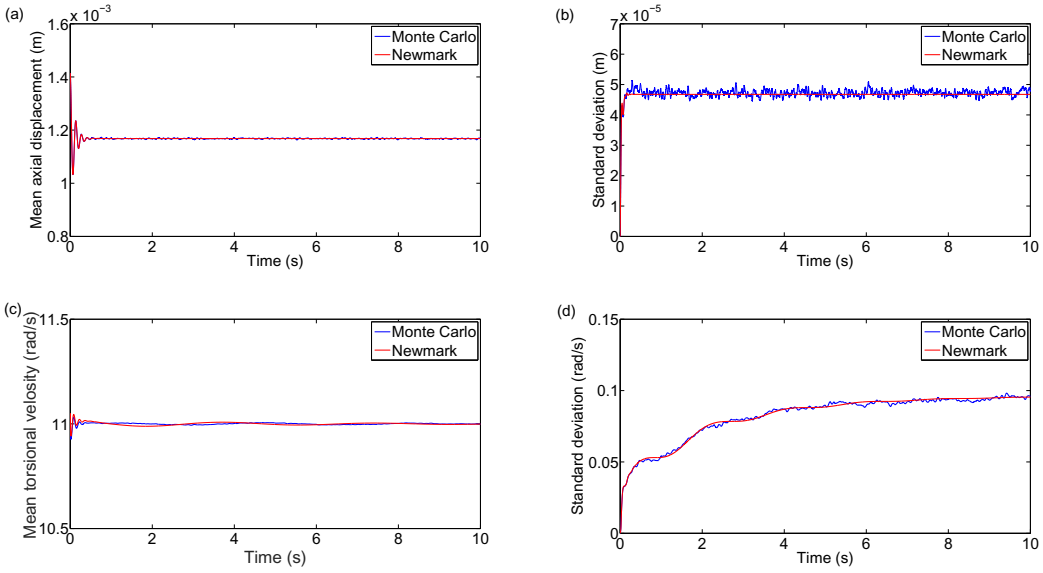

Figure 5.5: Statistical analysis in medium loading. (a) Bit axial displacement μ; (b) Bit axial displacement σ; (c) Bit torsional velocity μ; (d) Bit torsional velocity σ.

the weight on bit is computed as 160 KN. The simulation results with the Stochastic Newmark and MC in this case are presented in Fig. 5.5. The spectral density S_0 of the random excitation at the bit is taken as 1×10^5. It can be noticed that, the solutions from both methods become stationary after a short time (at most 10 seconds). Also the results from the two methods agree well except that the one from MC in Fig. 5.5(b) has larger fluctuation. It is proven that increase of sample size of MC can smooth out the result. However, this will increase the simulation time. In the paper, the sample size in MC is taken as 2000.

To check the range of the responses, we build the probability density distribution (PDD) of the bit axial displacement shown in Fig. 5.6(a). It is clearly seen that in

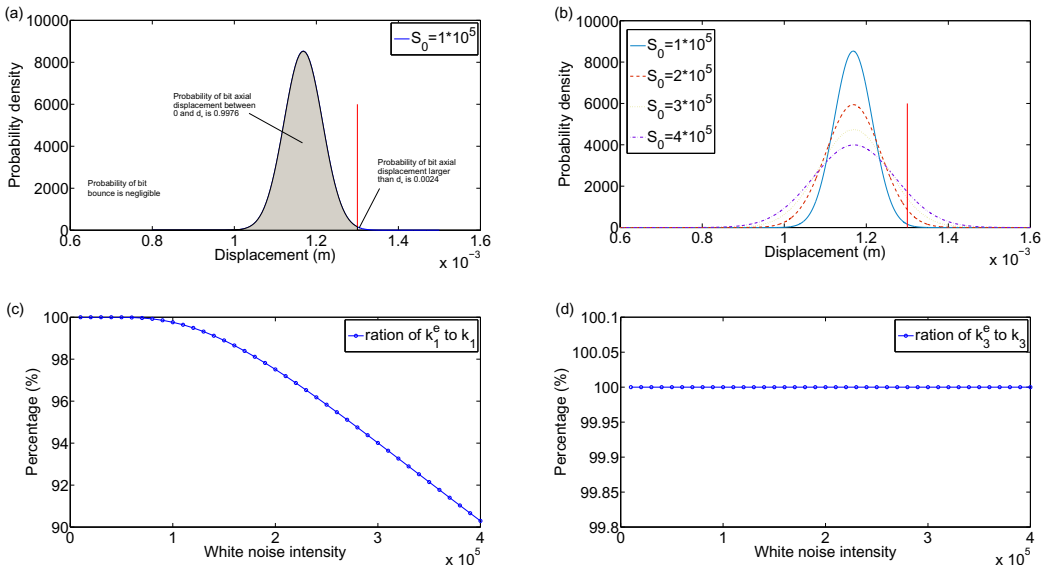

Figure 5.6: (a) PDD of bit axial displacement under medium loading with $S_0 = 10^5$ at $t = 10$s; (b) PDD of bit axial displacement under medium loading with different S_0 at $t = 10$s; (c) Ratio of k_1^e *to* k_1 in medium loading with varying white noise intensity; (d) Ratio of k_3^e *to* k_3 in medium loading with varying white noise intensity.

this case the majority of the axial displacement (99.76% falls between 0 and critical d_* represented by the red vertical line. Thus, it is almost linear. If the intensity of the white noise is changed, it can be expected the PDD of the response will change as well. The PDD of the bit axial displacement under 4 different noise intensities ($1 \times 10^5, 2 \times 10^5, 3 \times 10^5$ and 4×10^5) are given in Fig.5.6(b). As expected, with the increase of the noise intensity, the PDD becomes flatten out with larger distribution ranges. The consequence is that more responses will be beyond the critical axial displacement d_*. As a result more nonlinearity will occur. To verify this statement,

the ratios of k_1^e/k_1 and k_3^e/k_3 are given in Fig. 5.6(c) and 5.6(d). Clearly with the increase the nonlinearity becomes larger, but still minor.

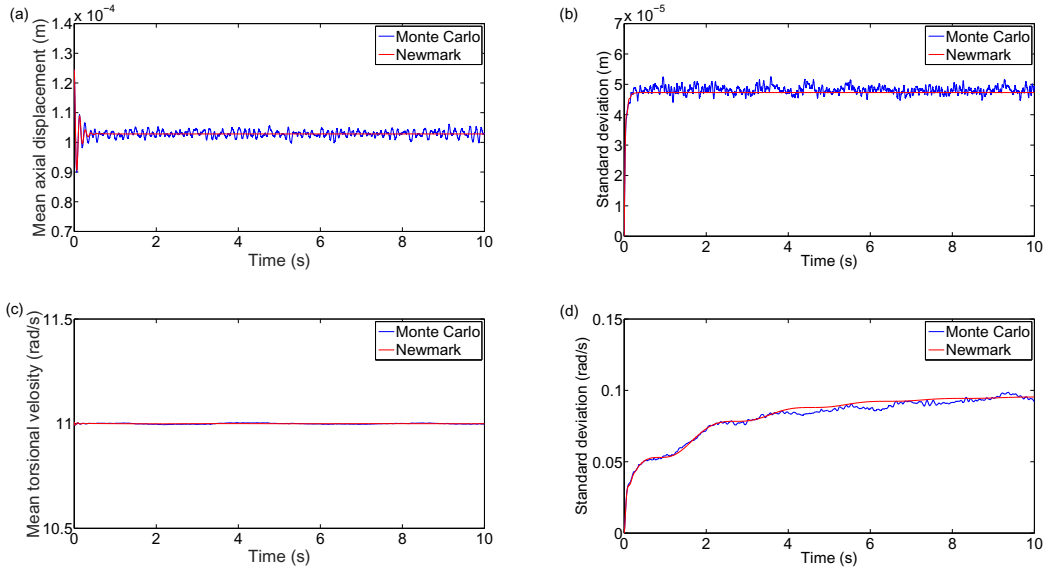

Figure 5.7: Statistical analysis in light loading. (a) Bit axial displacement μ; (b) Bit axial displacement σ; (c) Bit torsional velocity μ; (d) Bit torsional velocity σ.

In the case 2 with $F_h = 0.983$, the weight on bit ends up as 14 KN. Such a small weight on bit is not practical in real drilling; however, for illustration purpose we still present the results in Fig. 5.7 and 5.8. Due to the decrease of the WOB, the PDD of the bit axial displacement moves to the left with the left tail penetrating cross the critical value of 0 as shown in Fig.5.8(a). When the axial displacement becomes negative, the contact between the bit and the formation is lost and bit bounce happens. It can be seen that in this case under the noise intensity of 1×10^5, the

probability of bit bounce can be obtained by calculating the area shaded in Fig.5.8(a), which is about 1.5% at this instant $t = 10s$. This tiny part of responses won't affect the equivalent stiffness very much. However, with the increase of the noise intensity, the nonlinear effect becomes larger. This is shown in Fig.5.8(b), 5.8(c) and 5.8(d).

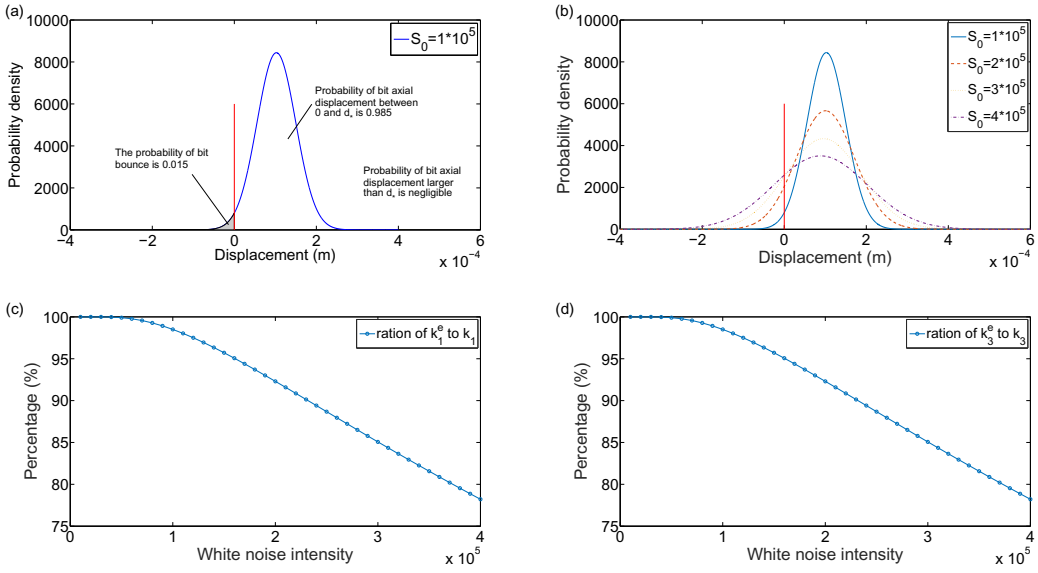

Figure 5.8: (a) PDD of bit axial displacement under light loading with $S_0 = 10^5$ at $t = 10$s; (b) PDD of bit axial displacement under light loading with different S_0 at $t = 10$s; (c) Ratio of k_1^e *to* k_1 in light loading with varying white noise intensity; (d) Ratio of k_3^e *to* k_3 in light loading with varying white noise intensity.

In the case 3, the hook load factor is taken as 0.768, which gives a WOB of 192 KN. The results of this case are given in Fig. 5.9 and 5.10. Contrast to the previous two cases, the main part of bit axial displacement (about 99.9% as shown in

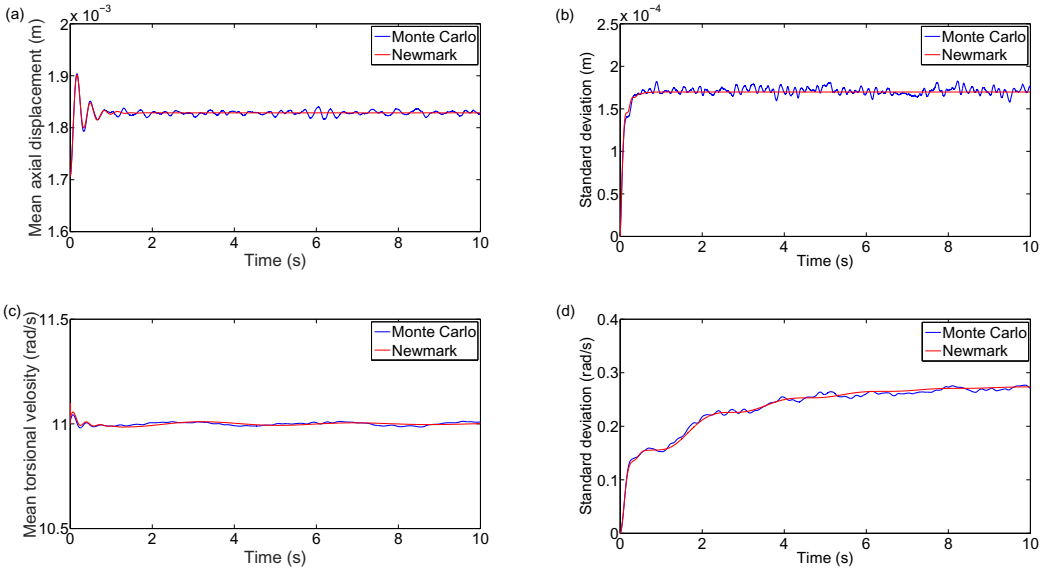

Figure 5.9: Statistical analysis in heavy loading. (a) Bit axial displacement μ; (b) Bit axial displacement σ; (c) Bit torsional velocity μ; (f) Bit torsional velocity σ.

Fig. 5.10(a)) is mainly located to the right of the critical depth d_* under the relatively heavy WOB. Correspondingly, the nonlinearity in axial direction (k_1^e/k_1) will be very large as shown in Fig. 5.10(c). While k_3^e is not affected that much as there is no such a critical threshold in k_3 and k_4 (Fig. 5.4(c) and 5.4(d)) . Also with the increase of noise intensity, the PDD of the axial displacement is also flatten out to a larger range as indicated in Fig. 5.10(b).

To get a closer look at the effect of hook load (or WOB) on the equivalent stiffness, we set F_h in between 0.98 and 0.745, and equally divide it into 43 steps. Then the ratios k_1^e/k_1 and k_3^e/k_3 are calculated and presented in Fig. 5.11. The vertical red lines in these figures represent the critical cutting depth d_*. In the deterministic case,

the stiffness k_1 would be 0 if the cutting depth exceeds d_*. The change from k_1 to 0 is abrupt. However, the switch in the probabilistic case is gradual as indicated by the points from A to F in Fig. 5.11(a). Given that the equivalent stiffness is a probabilistic average of the total stiffness, this is reasonable. Another observation is that the hook load affects k_3^e very little except at the very beginning, in Fig. 5.11(b), where the cutting depth is very small. In this case, the bit may get out of contact with the formation, and bit bounce happens. It is straightforward that bit bounce affects the equivalent stiffness.

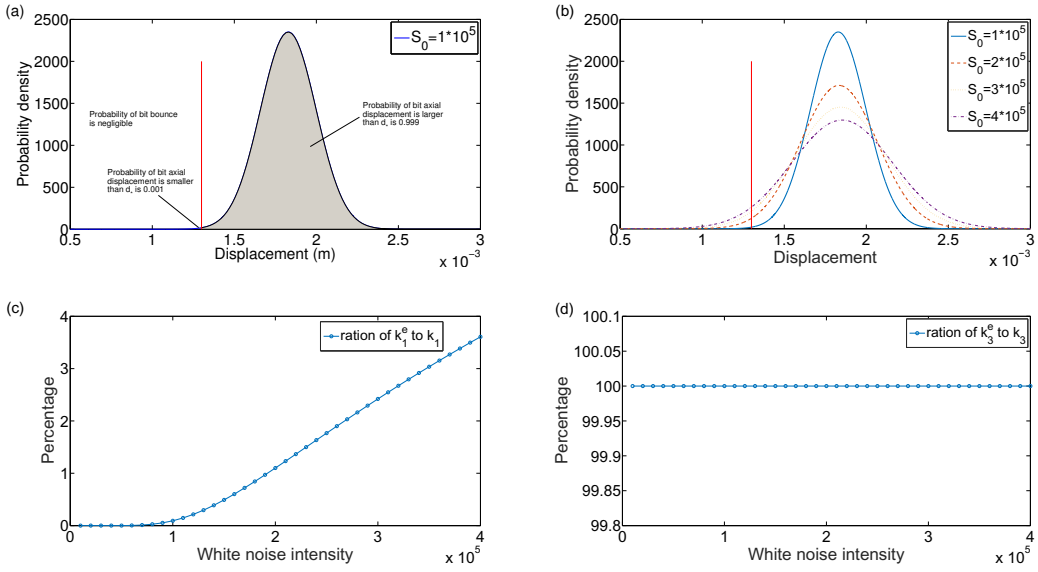

Figure 5.10: (a) PDD of bit axial displacement under heavy loading with $S_0 = 10^5$ at $t = 10$s; (b) PDF of bit axial displacement under heavy loading with different S_0 at $t = 10$s; (c) Ratio of k_1^e *to* k_1 in heavy loading with varying white noise intensity; (d) Ratio of k_3^e *to* k_3 in heavy loading with varying white noise intensity.

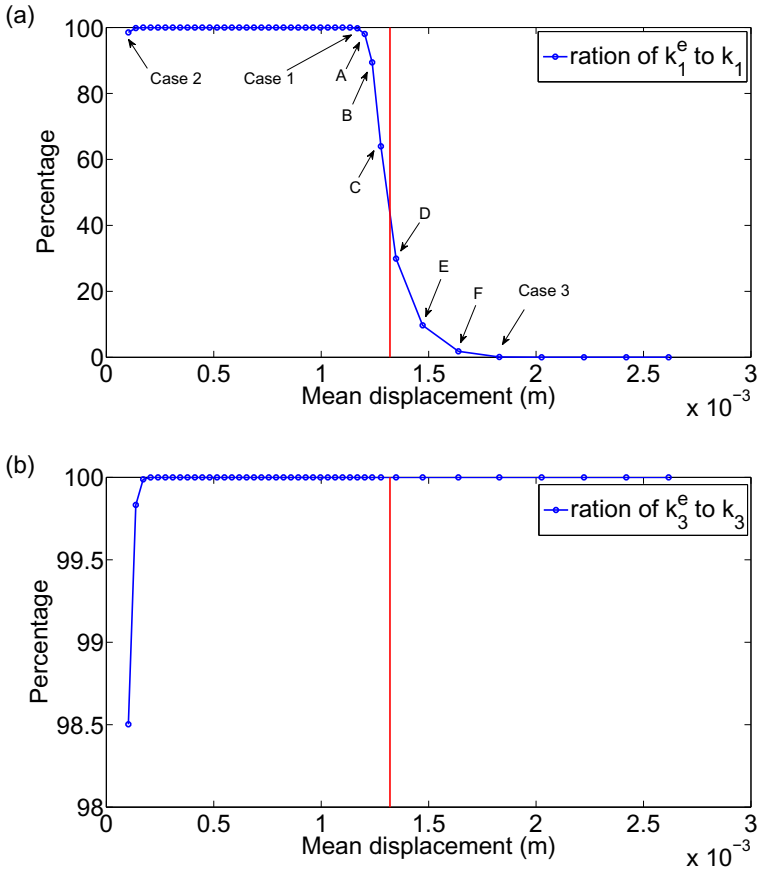

Figure 5.11: Results of k_1^e and k_3^e from light loading to heavy loading. (a) Ratio of k_1^e *to* k_1; (b) Ratio of k_3^e *to* k_3.

For the range of hook load above, the probability of bit bounce with 4 different noise intensities are computed and presented in Fig. 5.12. As can be seen the probability becomes larger with a stronger noise under the same hook load. On the other hand, if the noise intensity keeps constant, the bit bounce probability decreases with the increase of the WOB.

We also examined the distribution of torsional speed under the above parameters

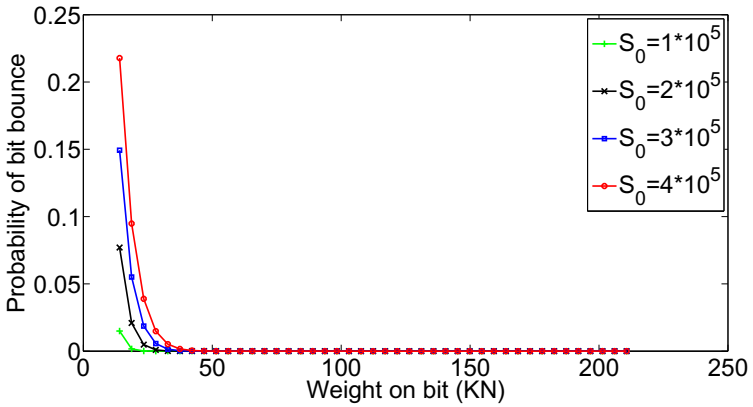

Figure 5.12: Probability of bit bounce with varying weight on bit under different random intensity.

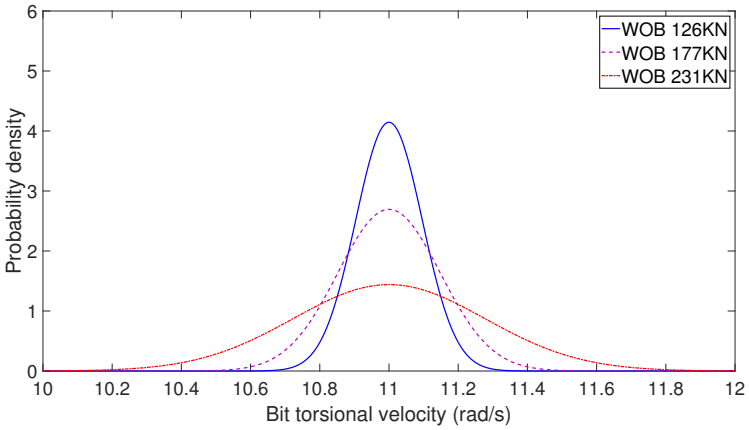

Figure 5.13: Distribution of bit rotary speed under different weight on bit.

with different WOB as shown in Fig. 5.13. Clearly, with the increase of WOB, the torsional speed distribution becomes scattered in larger ranges. Thus, larger WOB is more likely to cause stick slip. This is in agreement with the results reported in deterministic case.

Intuitively, stick slip happens if the bit torsional speed is below 0 at any moment. To observe the stick slip more clearly, we change the rotary speed on the top to 2 rad/s with $S_0 = 1 \times 10^5$ and $WOB = 177KN$. With the statistics calculated we construct the distribution of torsional speed at 4 discrete instants as shown in Fig. 5.14. At the instants $t = 8.5s$ and $t = 20.4s$, the probabilities of stick slip are almost negligible as shown in Fig. 5.14(a) and 5.14(d) respectively. While at $t = 11.7s$ and $t = 16.4s$, the probabilities become 38.9% and 11.5% respectively as indicated in Fig. 5.14(b) and 5.14(c).

5.7 Conclusion Remarks

This chapter investigates the vibration of a drillstring under combined deterministic and random excitations. Statistic linearization techniques are employed to get an equivalent linear replacement for the bit-rock interaction nonlinearity. Stochastic Newmark scheme is used to obtain the means and the standard deviations of the response. With this model, the probability of bit bounce and stick slip at any moment can be predicted. The main conclusions drawn from this work include:

1. White noise intensity has obvious effect on the distribution of the responses.

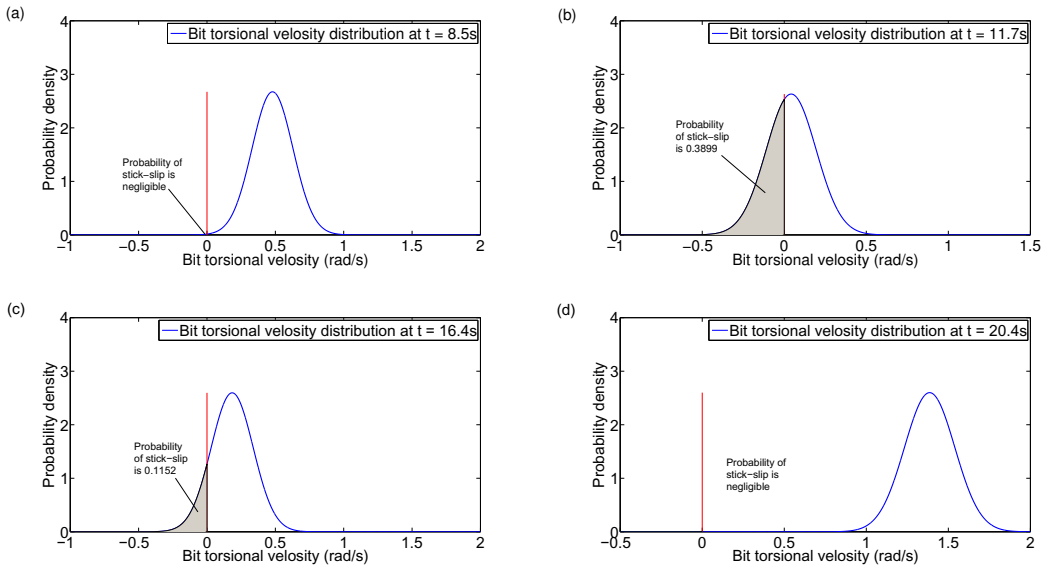

Figure 5.14: Prediction of stick-slip when rotary speed on the top is 2 rad/s, white noise intensity is 10^5 and WOB is 177 KN. (a) PDD of bit torsional velocity at $t = 8.5$s; (b) PDD of bit torsional velocity at $t = 11.7$s; (c) PDD of bit torsional velocity at $t = 16.4$s; (d) PDD of bit torsional velocity at $t = 20.4$s.

Stronger noise in general causes the distribution scattered in larger areas, but with lower probabilistic distribution density peak values.

2. If the axial load on the bit is classified into light, medium and heavy. In the medium loading condition, the drillstring model behaves basically as a linear system. A linear model is well suited to analyze the vibration response.

3. When the drillstring is lightly or heavily loaded, the nonlinearity in the bit-rock interaction becomes apparent and an equivalent stiffness needs to be sought, which is in general smaller than the actual stiffness.

There are many further investigations that could be performed with this system. For instance, a comprehensive modeling of stochastic excitations in drillstring axial, torsional and lateral directions.

Chapter 6

Static Study of Directional Drillstring from Random Viewpoint

The work of this chapter is partially based on a published conference paper: Hongyuan Qiu, Jianming Yang, Geoff Rideout, Stephen Butt. A random method for calculation of hoisting drag. In Proceedings of the *ASME 2020 39th International Conference on Ocean, Offshore & Arctic Engineering*, June 28-July 3, 2020.

6.1 Co-authorship Statement of Published Paper

Hongyuan Qiu: Dynamic Modeling, Methodology, Simulation, Data Processing, Result Analysis and Writing Manuscript. **Dr. Jianming Yang**: Supervision and

Reviewing. **Dr. Geoff Rideout**: Supervision and Reviewing. **Dr. Stephen Butt**: Supervision and Reviewing.

6.2 Abstract

In reality, downhole conditions are highly unpredictable due to many uncertain and inconsistent factors, such as the uncertainty of the friction and contact between drillstring and bore-hole. As friction and contact are crucial components in torque and drag calculation, it is meaningful and practical to consider their uncertainty. This paper presents a random method for calculation of hoisting drag. Firstly, the finite element method (FEM) is used for hoisting drag calculation of a directional drilling well in the deterministic case. Then two strategies are taken to model the random component in the downhole. The first strategy considers the randomness of the downhole friction. Instead of being a deterministic value, the friction coefficient is considered as Gaussian. The second strategy considers the randomness of contact between drillstring and wellbore. As a result, the drillstring is no longer continuously contacting with the wellbore in the curved section of well profile, which can help avoid overestimating torque and drag. Parametric studies on both strategies are conducted. Monte Carlo (MC) simulation is employed for statistical analysis. The probability density distributions and mean values of drag will be studied. The methodology can be extended into torque or drag calculation in lowering, ream in and ream out drilling conditions. Results from this paper indicate that surface hoisting drag is nearly Gaus-

sian when the friction coefficient is Gaussian. The contact loss leads to considerable reduction in the surface hoisting drag when contact uncertainty is considered. The skewness of the probability distribution of surface hoisting drag is influenced by the contact probability, length ratio of the hold section to all the other sections, and the inclination angle of the hold section when random contact is considered. The work of this paper will help estimate the range of surface drag and torque, which allows the well planner to develop a risk assessment for a challenging well trajectory.

6.3 Introduction

Directional drilling is of crucial importance in oil and gas industry due to its ability to increase drilling efficiency and maximize potential profit. For example, the number of offshore platforms has been greatly reduced by drilling long horizontal reach wells. The need for drilling deep and extended-reach wells is increasing. However, it is constrained by many factors such as the drilling torque and drag [78], which make drilling beyond a certain measured depth impossible. The estimation of torque and drag plays a critical role in well profile planning, real-time drilling and post analysis [79].

The existing torque and drag calculation methods are mainly based on two classical models: the soft-string model [80] and the stiff-string model [81]. The soft-string model developed by Johancsik et al. [80] has exerted a great influence over the petroleum industry. This method is based on the assumptions that the drillstring

lateral stiffness can be neglected and its body is continuously contacting with the wellbore. As a result, the value of friction coefficient is crucial to the application of this method and was usually found by Coulomb's friction model [82]. Based on the soft-string model, optimal well path design was addressed [82, 83] as well as the hydrodynamic influence on torque and drag calculation was considered [84, 85]. In recent years, Aadnoy et al. [86] developed analytical friction models for straight, build-up, drop-off, catenary profiles and side bends. In another work of Aadnoy et al. [87], new torque and drag equations for curved sections were developed and a tension dominant process was presented. However, the obvious shortcoming of soft-string model is the overestimation of torque and drag because the drillstring is in continuous contact with the wellbore.

Although many publications exist in the open literature dealing with torque and drag calculation theoretically or dynamically, one fundamental factor, the uncertainty in the downhole, has been neglected. In reality, downhole conditions are highly unpredictable due to many uncertain and inconsistent factors, such as the uncertainty of the friction between drillstring and bore-hole. Experiments in other areas have proven that the friction between two objects is random in essence, and better represented by a random process or random variables [158]. For example, Ibrahim et al [152] pointed out that both the static and kinetic friction coefficients show random time variations in the experiments. Besides, work of some researchers [166, 167] also indicated that the random component of friction force may be critical for successful

modeling in some applications. As friction is significant in torque and drag calculation, it is meaningful and practical to consider the uncertainty of friction in the model.

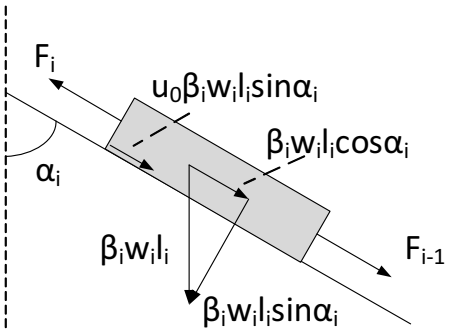

Figure 6.1: Drag force balance of drillstring element in straight section

6.4 Methodology

6.4.1 Hoisting drag calculation based on finite element method

The drillstring can be divided into many finite elements. The buoyancy factor β, drillstring component unit weight w, component length l, inclination angle α in different element may be not the same. Therefore, the parameters in the i th section of drillstring are marked with subscript i. If the i th element of drillstring is in straight section, drag force balance in the element is schematically shown in Fig. 6.1 with F_i

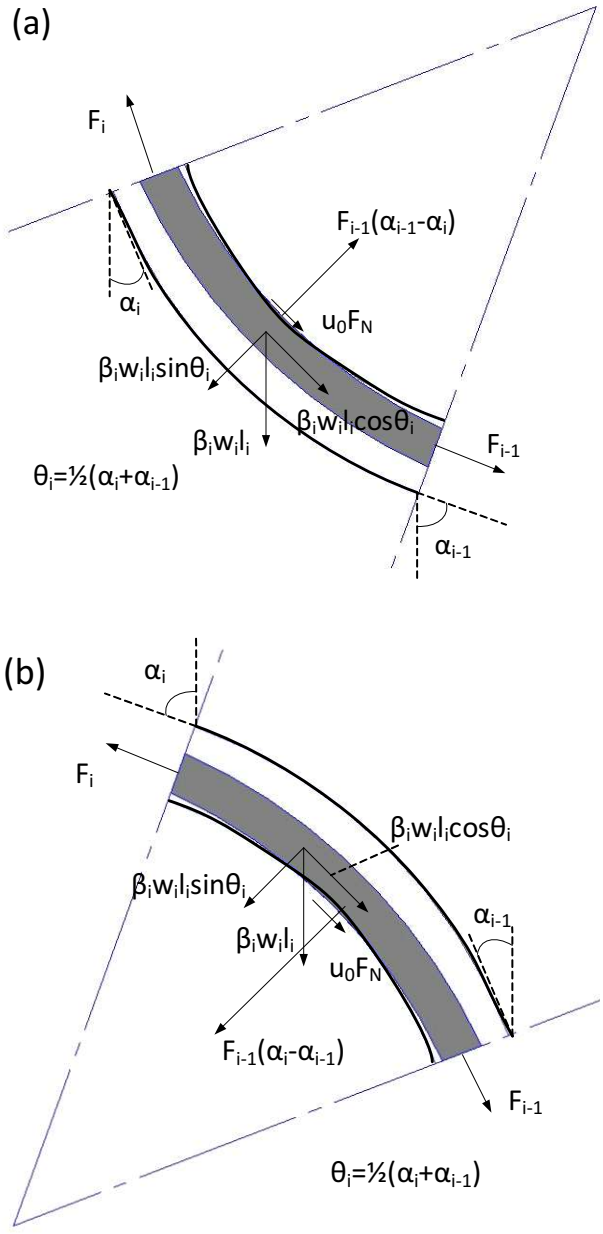

Figure 6.2: (a) Drag force balance of drillstring element in build-up section; (b) Drag force balance of drillstring element in drop-off section

given as:

$$F_i = F_{i-1} + \beta_i w_i l_i (cos\alpha_i + u_0 sin\alpha_i) \tag{6.1}$$

where u_0 is friction coefficient. If inclination α_i is equal to zero, the element is in vertical position and friction term in Eq. 6.1 will diminish. If inclination α_i is equal to 90 degree, the element is in horizontal position and weight term will diminish.

Fig. 6.2 shows the drag force balance when the i th element of drillstring is in curved section. In either build-up or drop-off, F_i can be represented as:

$$F_i = F_{i-1} + \beta_i w_i l_i cos(\frac{\alpha_i + \alpha_{i-1}}{2}) + u_0 F_{N_i} \tag{6.2}$$

where F_{N_i} is the normal force. When azimuth angle is zero, it is calculated as [80]:

$$F_{N_i} = F_{i-1}|\alpha_i - \alpha_{i-1}| \pm \beta_i w_i l_i sin(\frac{\alpha_i + \alpha_{i-1}}{2}) \tag{6.3}$$

where $+$ is for drop-off section and $-$ is for build-up section.

6.4.2 Random component

The modeling of random component in drag calculation is based on two strategies. The first strategy assumes that the friction coefficient is Gaussian. Therefore, for each drillstring section, the deterministic u_0 becomes a random variable u_1, which follows $N(\mu, \sigma)$. Thus, Eqs. 6.1 and 6.2 in strategy 1 becomes:

$$F_i = F_{i-1} + \beta_i w_i l_i (cos\alpha_i + u_1 sin\alpha_i) \tag{6.4}$$

$$F_i = F_{i-1} + \beta_i w_i l_i cos(\frac{\alpha_i + \alpha_{i-1}}{2}) + u_1 F_{N_i} \tag{6.5}$$

There are two reasons why the friction coefficient is assumed as Gaussian. The first is convenience, as one of the key features of the Gaussian distribution is the relatively simple form of its probability density function. The second reason is that Gaussian distribution often provides quite a good approximation to measured statistical data. Presumably, this is due to central limit theorem [119]. These are reasons why the Gaussian distribution is extensively used in applied probability.

In the second strategy, the contact between drillstring and wellbore in the curved section is modeled as Bernoulli distribution. The probability mass function of Bernoulli distribution is represented as:

$$f(x;p) = p^x(1-p)^{1-x} = \begin{cases} p & \text{if } x = 1 \\ 1-p & \text{if } x = 0 \end{cases} \tag{6.6}$$

The Bernoulli distribution gives two status, x = 1 or 0, which corresponding to two contact status in drillstring curved section: contact or non-contact. Therefore, if drillstring contacts with the wellbore, $x = 1$. p is the probability that contact happens. Based on this, a random variable γ, which has the probability of $1-p$ to be 0 (no contact) or probability of p to be 1 (contact), is used in Eqs. 6.2 for strategy 2:

$$F_i = F_{i-1} + \beta_i w_i l_i cos(\frac{\alpha_i + \alpha_{i-1}}{2}) + \gamma u_0 F_{N_i} \tag{6.7}$$

6.4.3 Solution strategy

Monte Carlo (MC) method is used to generate the samples for statistical analysis. Each sample is just a calculation of hoisting drag from drillstring bottom to the top

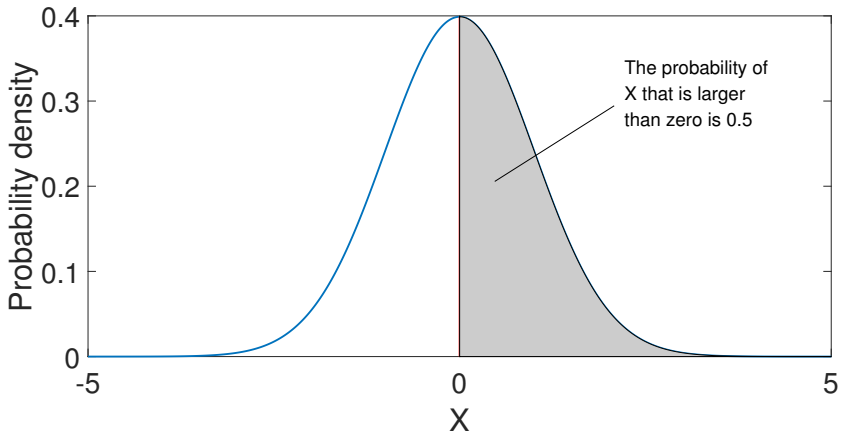

Figure 6.3: Probability of X that is larger than zero for $N(0,1)$

with uncertainty factor considered.

In strategy 1, the drag calculation of each sample is based on random friction coefficient. At each point of the finite element, when Eq. 6.4 or 6.5 is conducted, a Gaussian random variable u_1 is generated by Matlab built-in function, which follows $N(\mu, \sigma)$. μ is the mean and σ is the standard deviation of friction coefficient, respectively.

In strategy 2, γ is fulfilled by a Gaussian distribution and a logical statement. To make it clear, an example is given as follows. Assuming the probability of contact p between drillstring and wellbore is 0.5, for each sample, γ at each point of the finite element is generated by a logical judgment in Matlab:

$$\gamma = (N(0,1) > 0) \tag{6.8}$$

As can be seen in Fig. 6.3, for X that follows $N(0,1)$, the probability of X that

is larger than zero is 0.5. For each simulation, if the logical statement is true, γ is equal to 1, otherwise it is equal to 0. By changing the mean value of the Gaussian distribution in Eq. 6.8, different probability of contact can be simulated.

6.5 Simulation and result analysis

6.5.1 Well profile and specification

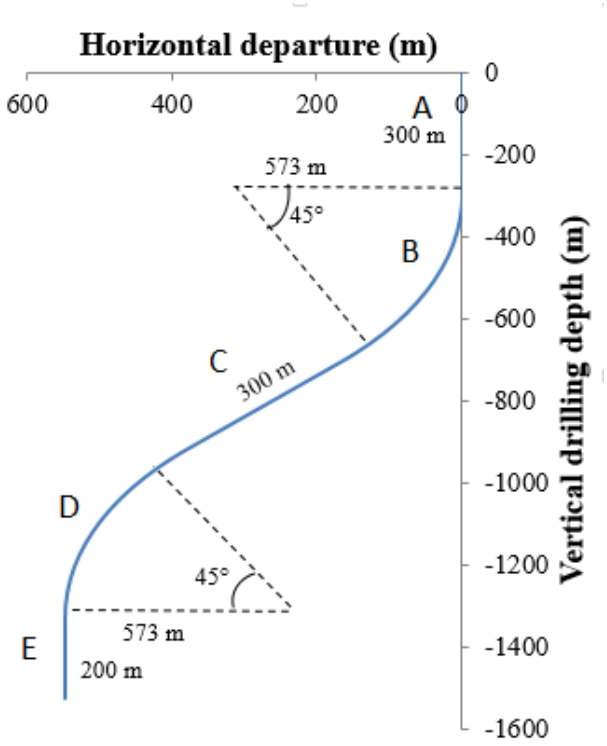

Figure 6.4: S-shaped well profile

An S-shaped well is considered in this paper for case study. For this case there is

no change in azimuth. The configuration of the well is shown in Fig. 6.4. As can be seen, the total drillstring can be separated into 5 parts. Part A is 300 m long and is vertical, which starts from the surface to the top of build-up section. Part B is the build-up section with the curve radius 573 m. Part C is a 300 m long hold section with a constant inclination angle 45°. Part D is the drop-off section with the curve radius 573 m. Part E is 200 m long, which starts out just below the drop-off section and is vertical. The build angle for both build-up and drop-off sections is 3°/30 m and is constant.

The total length of the drillstring is 1700 m, which consists of 200 m drillcollar (only part E) and 1500 m drillpipe. The drillcollar outer diameter is 0.2286 m and inner diameter is 0.0762 m. Drillpipe outer diameter is 0.127 m and inner diameter is 0.095 m. The well is filled with 1300 kg/m^3 drilling mud.

6.5.2 Results analysis and parametric study

For hoisting drag calculation, the drillstring is divided into 33 finite elements. The total curved section of build-up and drop-off is divided into 30 elements with each element 30 m long. Section A, C and E are represented by 1 element, respectively. The number of finite element in the straight section will not influence the static force. In the curved section, as the calculation becomes complicated, deterministic simulation is conducted to find out the sufficient number of finite elements. Figure 6.5 indicates that 30 elements are enough to represent the curved section. As can be seen

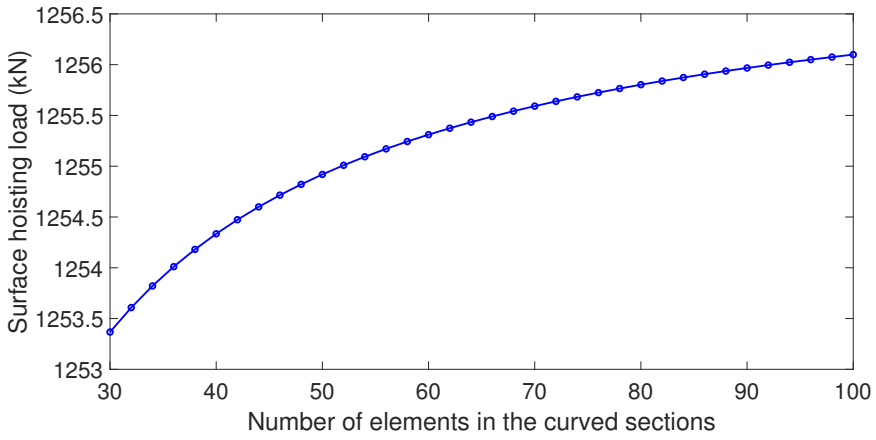

Figure 6.5: Surface hoisting drag with different finite elements in the curved section

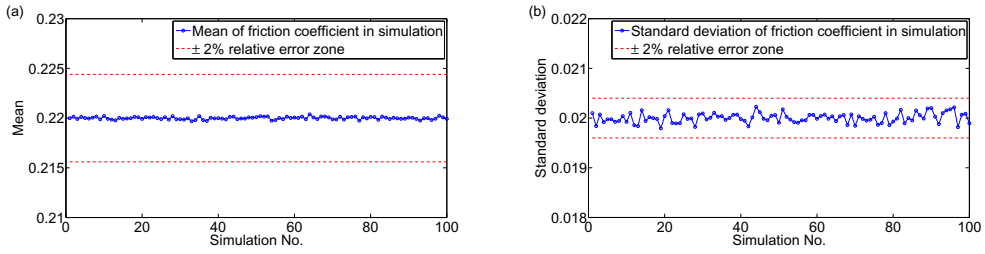

Figure 6.6: (a) Mean of friction coefficient in Monte Carlo simulation test; (b) Standard deviation of friction coefficient in Monte Carlo simulation test

in the figure, dividing the curved section into 100 elements only increase the surface hoisting drag by 0.2%, compared with the result from 30 elements. Considering MC method needs large computer memory, 30 elements are employed to represent the curved section.

The hoisting drag is firstly calculated by following strategy 1, in which a random friction coefficient is considered. It is assumed to be Gaussian with mean value 0.22

and standard deviation 0.02. Therefore, at each point of the finite element, friction coefficient is randomly chosen from $N(0.22, 0.02)$. MC method is employed to gather the results for statistic analysis and the sample size is taken as 20,000. Because the friction coefficient is randomly generated, its distribution may not be as planned if MC sample size is not enough. To verify the sample size, MC simulation test is conducted 100 times. Fig. 6.6 indicates that 20,000 sample size is enough to obtain satisfied mean and standard deviation of the random friction coefficient.

The hoisting drag is calculated from bottom to top. In Fig. 6.7(a), red line is the hoisting drag obtained from deterministic friction coefficient, the value of which is 0.22. Blue line represents the mean hoisting drag from MC simulation. Grey area marks the result from all the MC samples. It can be seen clearly that red line and blue line appear as one in the figure, and they are approximately in the center of the grey area.

For statistical analysis, the surface hoisting drag (when the drilling depth is zero) is selected. The probability density distribution of surface hoisting drag is presented in Fig. 6.7(b). Statistical information of the samples, like mean, standard deviation, kurtosis and skewness are calculated and listed in the figure. For an exact Gaussian distribution, the skewness is 0 and kurtosis is 3. Therefore, Fig. 6.7(b) indicates that surface hoisting drag is nearly Gaussian distributed when the friction coefficient is Gaussian.

Then, the standard deviation of the friction coefficient is changed to see its in-

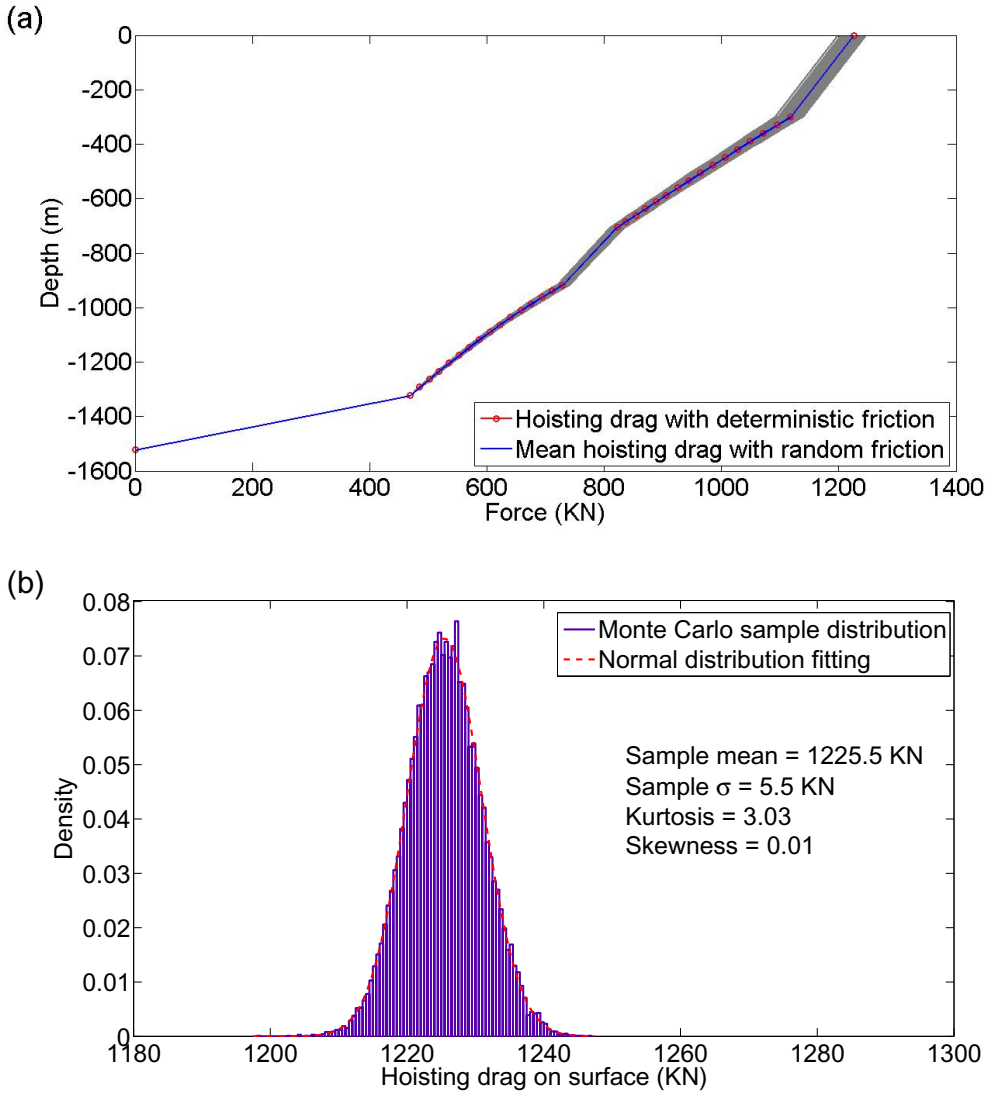

Figure 6.7: Monte Carlo simulation result with random friction: (a) Hoisting drag for all MC samples; (b) The probability density distribution of hoisting drag on the surface

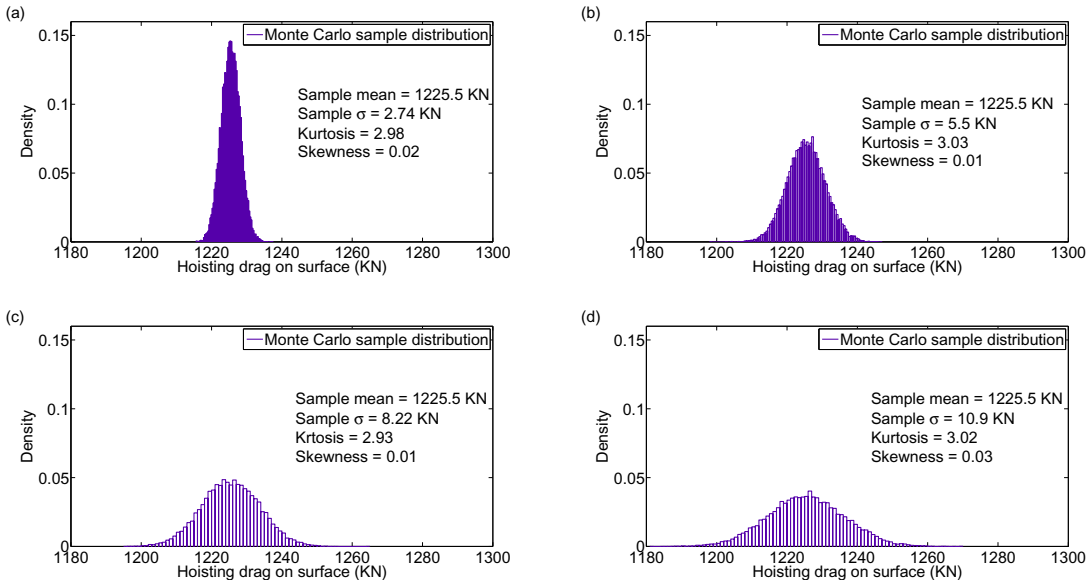

Figure 6.8: Monte Carlo simulation results with varying standard deviation of friction coefficient: (a) The probability density distribution of hoisting drag on the surface with $\sigma = 0.01$; (b) The probability density distribution of hoisting drag on the surface with $\sigma = 0.02$; (c) The probability density distribution of hoisting drag on the surface with $\sigma = 0.03$; (d) The probability density distribution of hoisting drag on the surface with $\sigma = 0.04$.

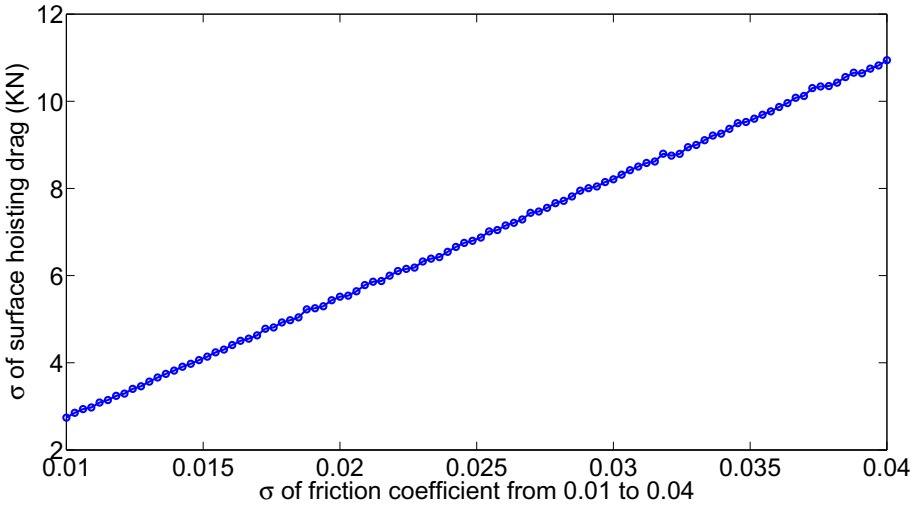

Figure 6.9: Relationship between σ of friction coefficient and σ of surface hoisting drag

fluence on the surface hoisting drag. Fig. 6.8 shows the statistical results based on standard deviation 0.01, 0.02, 0.03 and 0.04. As can be seen, the distributions are nearly Gaussian in all the sub-figures and mean values are the same. The standard deviation of the surface hoisting drag simultaneously increases as the standard deviation of friction coefficient changes from 0.01 to 0.04. Fig. 6.9 indicates a linear relationship between the standard deviation of friction coefficient and standard deviation of the surface hoisting drag.

In strategy 2, the hoisting drag is firstly calculated by considering the probability of contact between drillstring and wellbore in the curved section is 0.5. The contact probability is 1 for section C. For section A and E, as they are both vertical, the contact probability is assumed to be 0. Like what we did in strategy 1, MC simulation

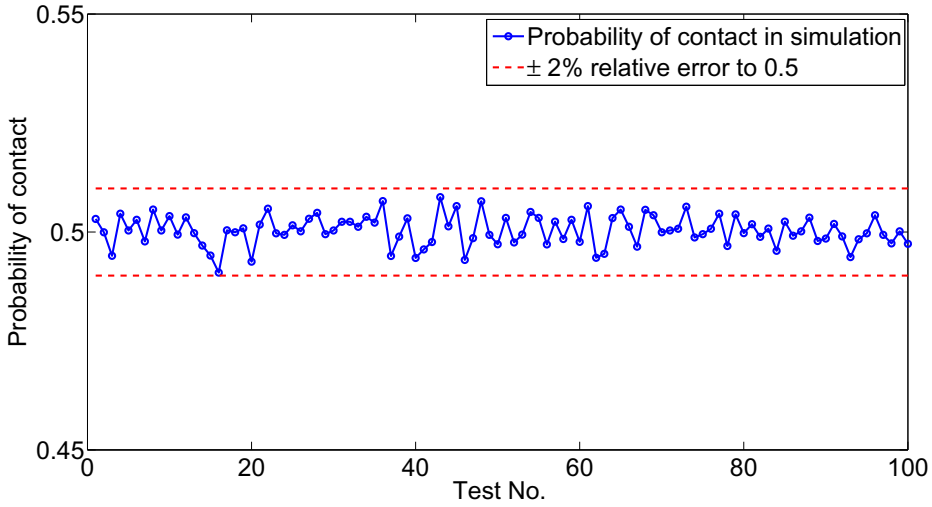

Figure 6.10: Probability of contact in the simulation test

test is conducted 100 times. Fig. 6.10 indicates that 20,000 sample size is enough to simulate 0.5 contact probability.

In Fig. 6.11(a), red line is the hoisting drag without considering random contact, thus the contact probability is 1.0. Blue line represents the mean hoisting drag from MC simulation with contact probability 0.5. Grey area marks the result from all the MC samples. It can be seen clearly that blue line appears approximately in the center of the grey area. The contact loss leads to considerably reduction in the surface hoisting drag.

The probability density distribution of surface hoisting drag is presented in Fig. 6.11(b). Statistical information of the samples, like mean, standard deviation, kurtosis and skewness are also calculated and listed in the figure. As can be noticed, the distribution is still approximately Gaussian.

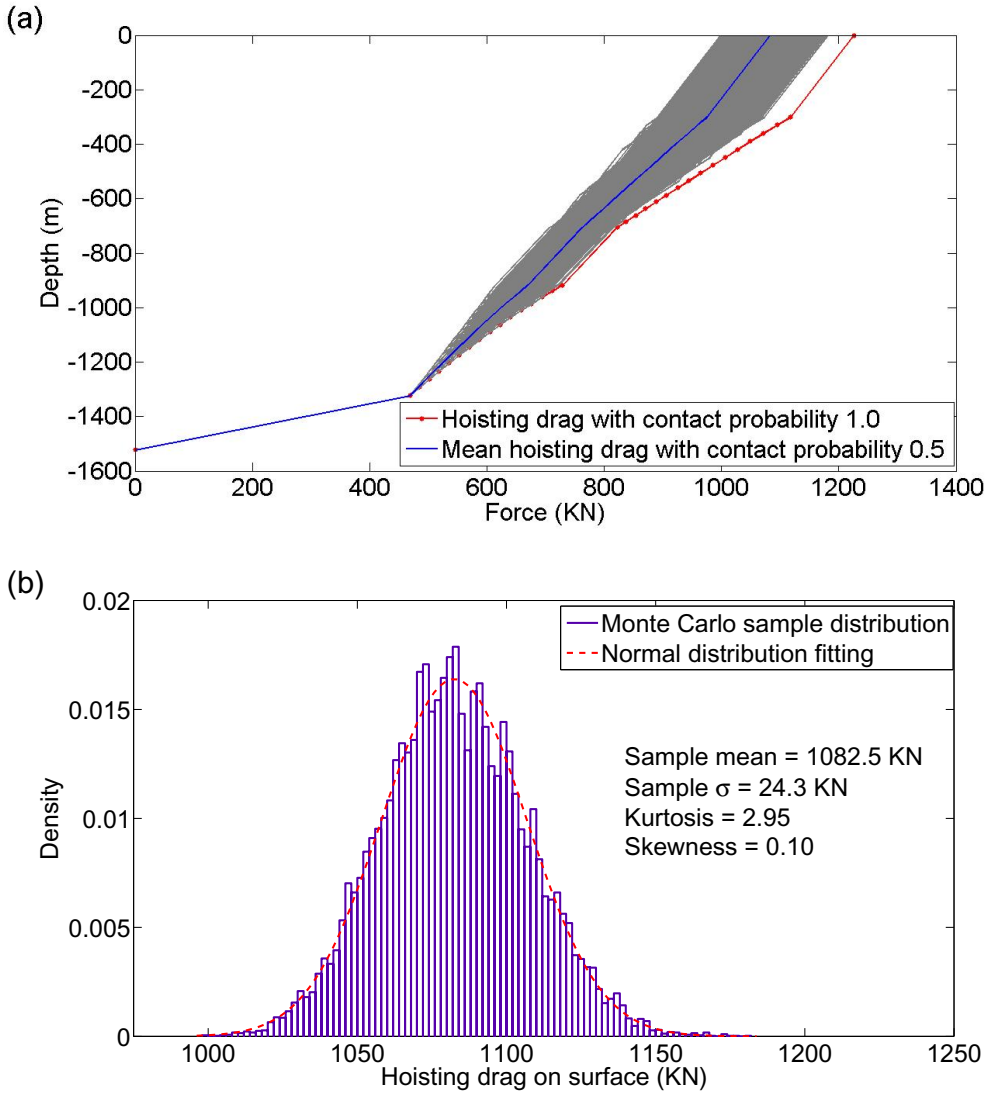

Figure 6.11: Monte Carlo simulation result with contact probability 0.5: (a) Hoisting drag for all MC samples; (b) The probability density distribution of hoisting drag on the surface

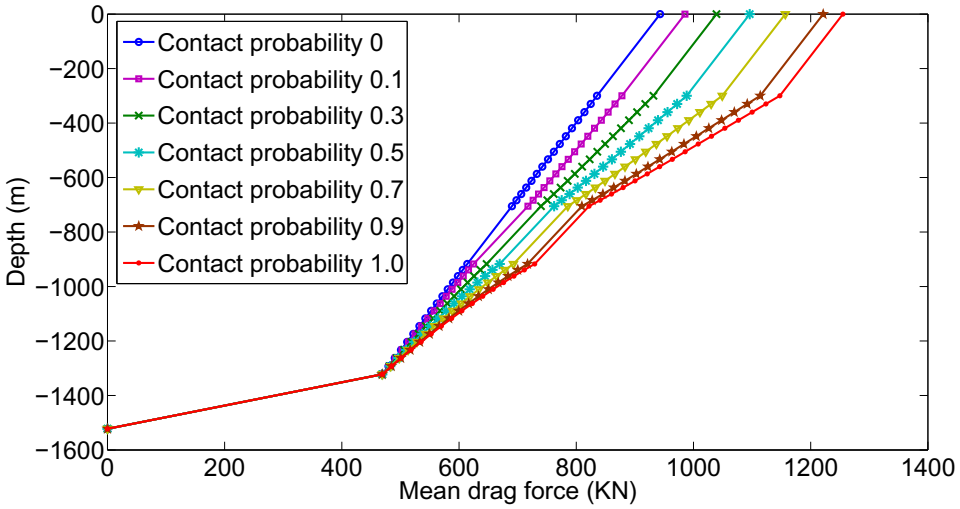

Figure 6.12: Mean hoisting drag with different contact probability

Then, the contact probability between drillstring and wellbore is going to be changed to see its influence on the surface hoisting drag. When the contact probability is small, meaning that friction term in Eq. 6.7 is negligible, we expect that the majority of the hoisting drag in MC samples are close to the static drag. On the other hand, as contact probability probability grows, we expect that the majority of the hoisting drag are more and more likely to be the deterministic hoisting drag. In Fig. 6.12, blue line on the left represents the static drag. Red line on the right is maximum hoisting drag. As the contact probability changes from 0.1 to 0.9, the mean hoisting drag is shifting from left to right as expected. Meanwhile, the probability density distribution of the surface hoisting drag with different contact probability is shown in Fig. 6.13. Like the transition of the mean, the distribution shifts from the left to right as contact probability increases.

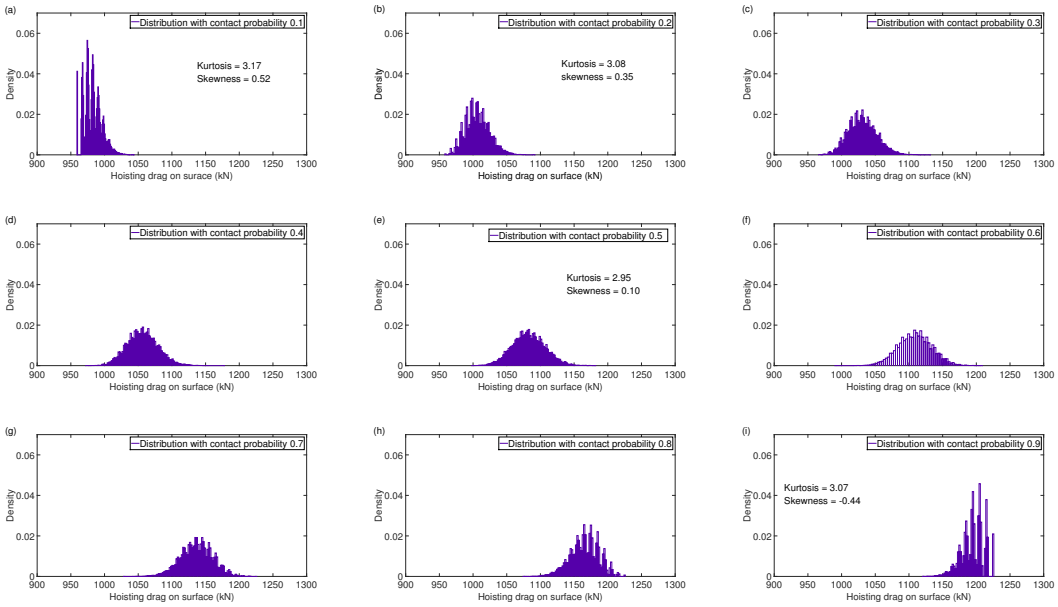

Figure 6.13: Probability density distribution of surface hoisting drag with different contact probability: (a) Contact probability 0.1; (b) Contact probability 0.2; (c) Contact probability 0.3; (d) Contact probability 0.4; (e) Contact probability 0.5; (f) Contact probability 0.6; (g) Contact probability 0.7; (h) Contact probability 0.8; (i) Contact probability 0.9.

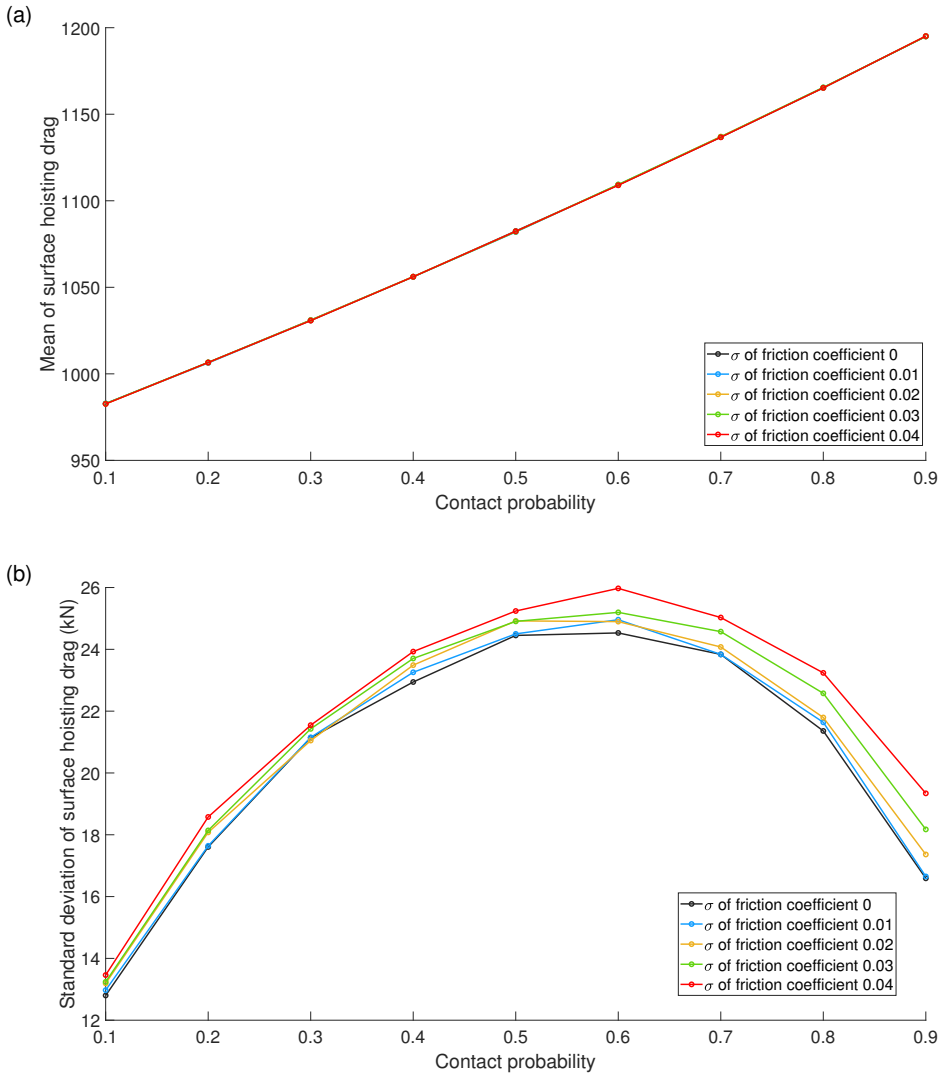

Figure 6.14: Statistic results of surface hoisting drag with all random component considered: (a) Mean; (b) Standard deviation

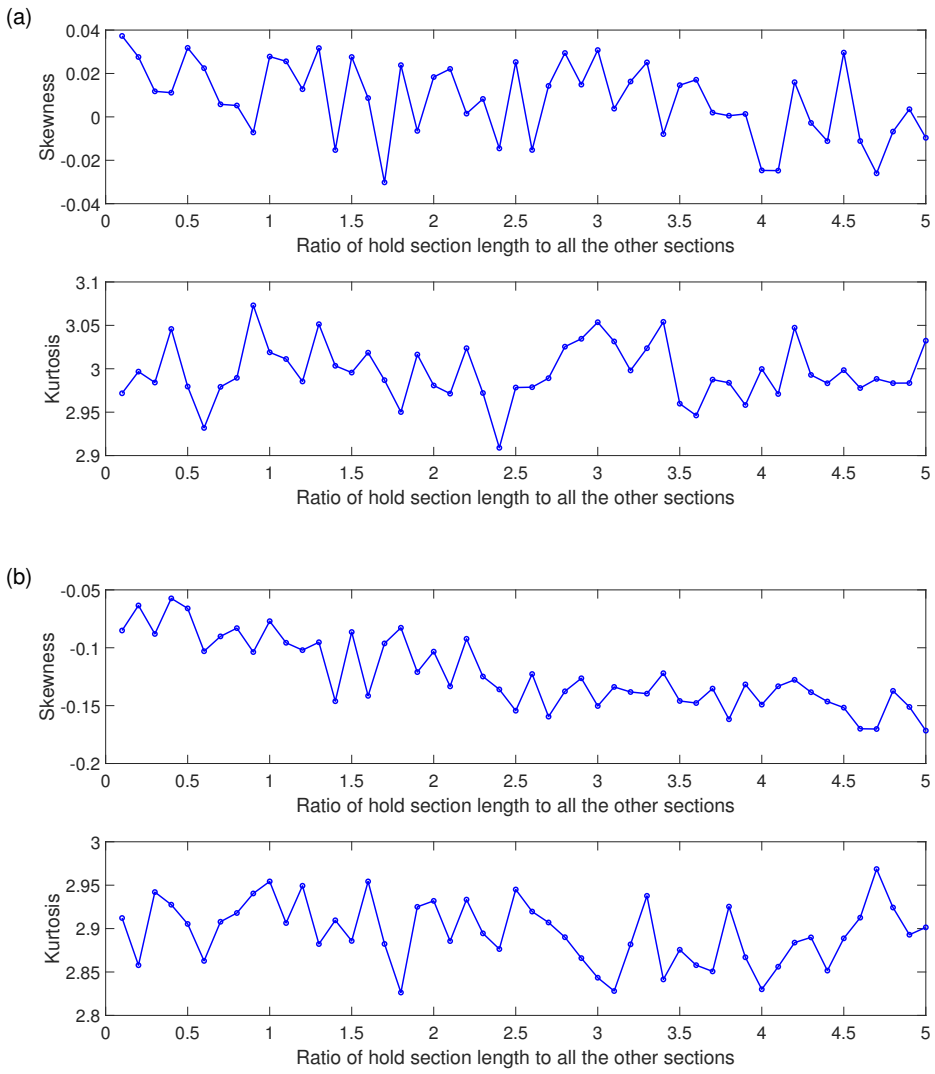

Figure 6.15: Skewness and kurtosis of surface hoisting drag under different length ratio: (a) only consider random friction coefficient, which follows $N(0.22, 0.02)$; (b) only consider random contact with contact probability 0.7

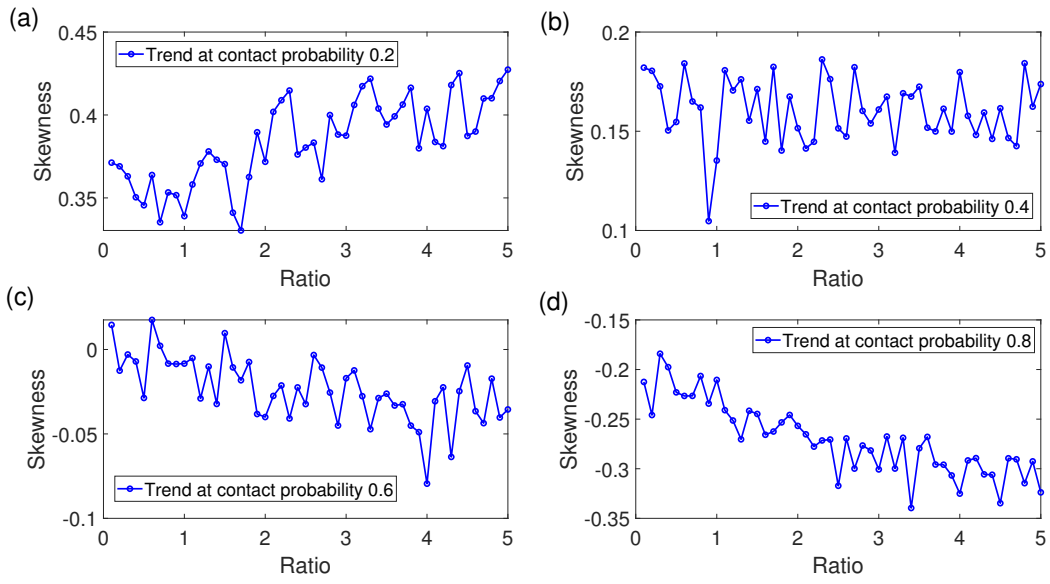

Figure 6.16: Skewness of surface hoisting drag under different length ratio: (a) contact probability 0.2; (b) contact probability 0.4; (c) contact probability 0.6; (d) contact probability 0.8

Fig. 6.14 shows the mean and standard deviation of surface hoisting drag with both random friction and random contact considered. The contact probability varies from 0.1 to 0.9, and the standard deviation of the friction coefficient changes from 0 to 0.04. As can be seen in Fig. 6.14(a), with the increase in contact probability, the mean value increases as well; however, the changing standard deviation of the friction coefficient does not make any significant changes to the mean value. In Fig. 6.14(b), a larger standard deviation of friction coefficient generally increases the standard deviation of surface hoisting drag. The simulation results resemble downward parabola with peak values around the contact probability of 0.6.

All the simulations above are based on a 1700-meter long S-shaped well with a hold section of 300 meters. In the following, different hold section lengths will be chosen to change the length ratio of this section to all the other sections. By doing so, the effect of changing the length ratio on the probability density distribution of the surface hoisting drag will be analyzed. Fig. 6.15(a) shows the skewness and kurtosis of the distribution from MC simulation with only random friction coefficient considered. As can be seen in the figure, the skewness and kurtosis are slightly changing around 0 and 3, respectively. It indicates that the distribution of surface hoisting drag may be nearly Gaussian when the friction coefficient is Gaussian, regardless of the length ratio. Fig. 6.15(b) shows the statistic results of skewness and kurtosis from simulation only considering random contact. As can be seen from the result, when the contact probability is 0.7, the distribution of surface hoisting drag shows negative skewness.

Further, with the increase in length ratio, the negative value decreases. It indicates that the left tail of the distribution may get longer.

Fig. 6.15(b) presents a trend of skewness when contact probability is 0.7. Further, the trend of skewness will be studied by calculating the skewness of the probability density distribution of the surface hoisting drag under different length ratios at contact probability 0.2, 0.4, 0.6, and 0.8, respectively. As can be seen in Fig. 6.16, at low contact probability like 0.2 (Fig. 6.16(a)), the positive skewness is getting larger as the length ratio increases. While at high contact probability like 0.8 (Fig. 6.16(d)), the negative skewness decreases as the length ratio increases. It can also be observed in Fig. 6.16 that, at the same length ratio, the skewness decreases as the contact probability increases. A similar observation could be found in Fig. 6.13 as well. The results of Fig. 6.16 indicate that the skewness of the probability distribution of surface hoisting drag is influenced by the length ratio and contact probability when random contact is considered.

The inclination angle of the hold section is another parameter to be studied. Statistic analysis of surface hoisting drag is conducted based on the MC simulation with random friction coefficient, different length ratio of hold section to all the other sections and varying inclination angle from 21 to 90 degrees. The corresponding results are presented in Fig. 6.17. Further, to make it clear, statistic results at one specific hold section length (300 m) are presented in Fig. 6.18. As can be seen in Fig. 6.17 and 6.18, the skewness and kurtosis are just changing around 0 and 3,

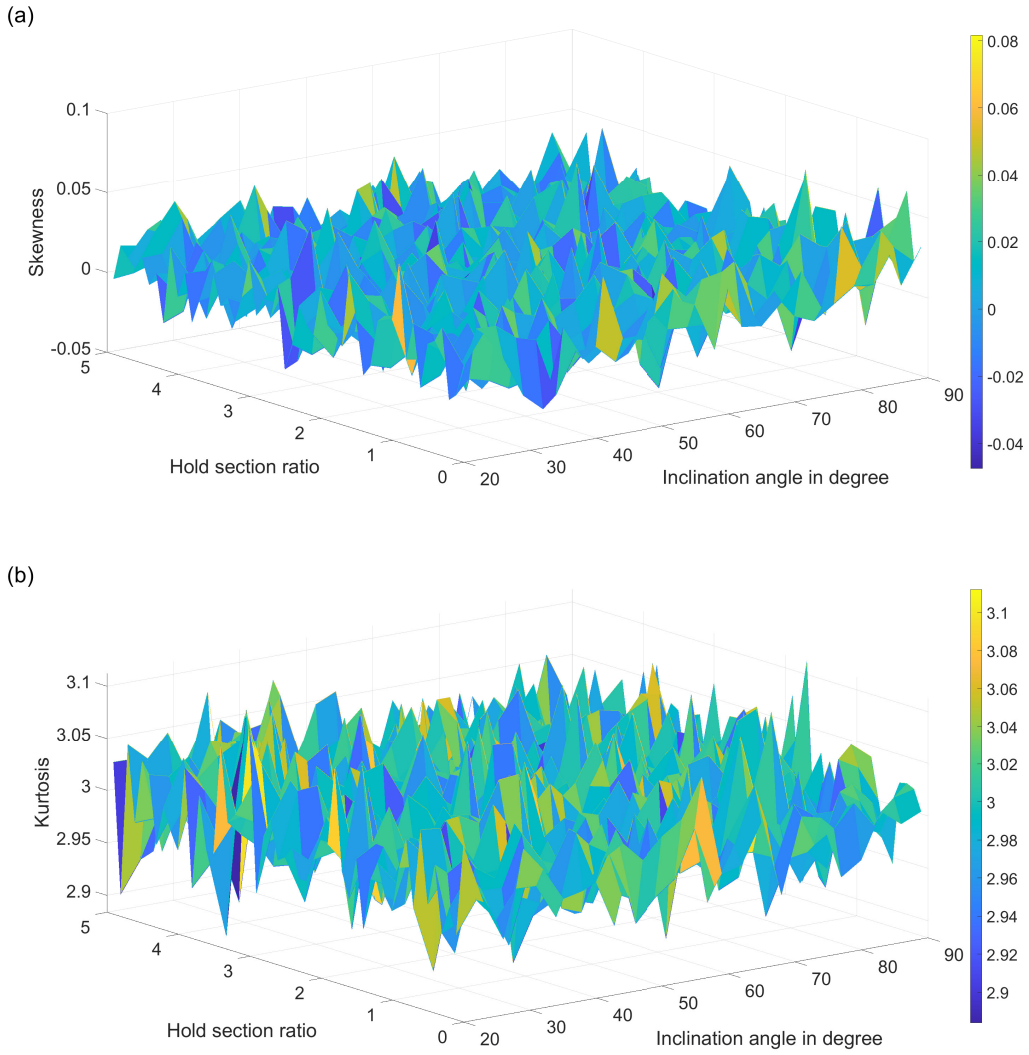

Figure 6.17: Skewness and kurtosis of surface hoisting drag under different length ratio and inclination angle, with only random friction coefficient considered, which follows $N(0.22, 0.02)$: (a) Skewness; (b) Kurtosis

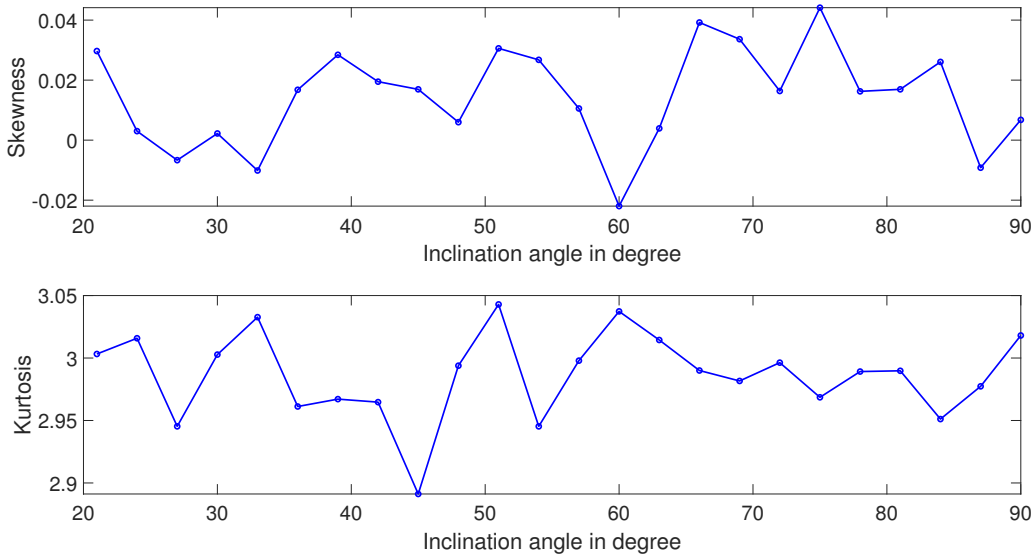

Figure 6.18: Skewness and kurtosis of surface hoisting drag when hold section is 300 meters, considering only random friction coefficient, which follows $N(0.22, 0.02)$

respectively. It indicates that the inclination angle of the hold section does not have any significant influence on the skewness or kurtosis of the distribution of surface hoisting drag, when random friction coefficient is considered.

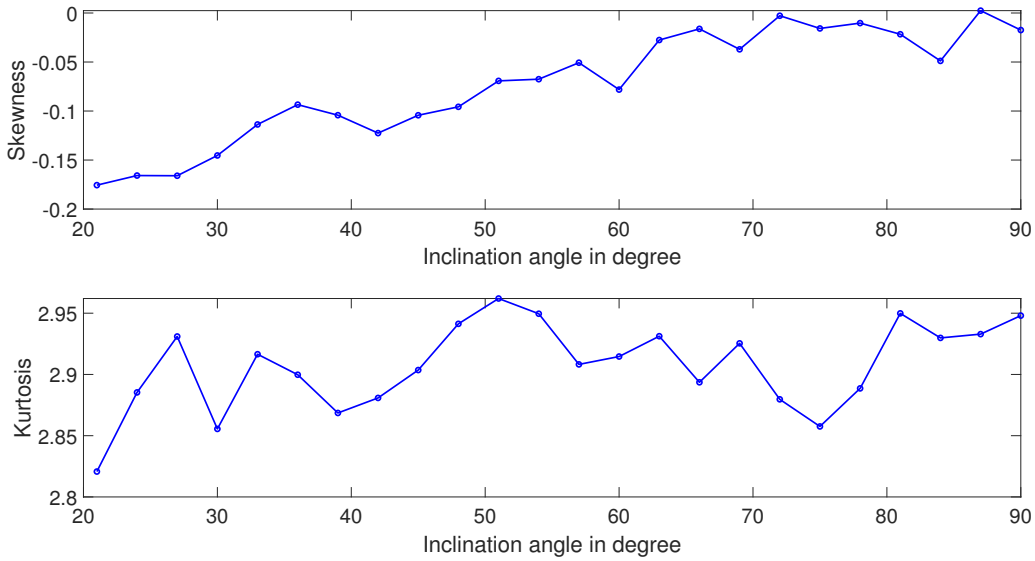

Figure 6.19: Skewness and kurtosis of surface hoisting drag under different inclination angles with contact probability 0.7

The following parameter study of inclination angle will only consider random contact for calculating surface hoisting drag. Fig. 6.19 presents the skewness and kurtosis of the result distribution when the contact probability is 0.7. As can be seen, the probability distribution has negative skewness and its value increases as the inclination angle increases. Further, in Fig. 6.20, the trend of the skewness is presented for contact probability at 0.2, 0.3, 0.7 and 0.8. Simulation results indicate

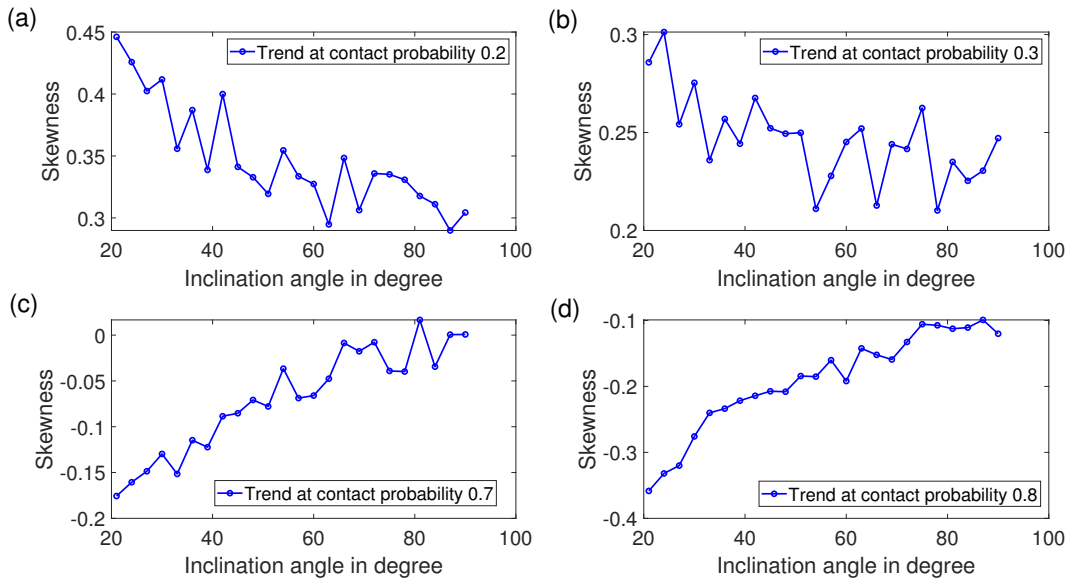

Figure 6.20: Skewness of surface hoisting drag under different inclination angle: (a) contact probability 0.2; (b) contact probability 0.3; (c) contact probability 0.7; (d) contact probability 0.8

that, at low contact probability, skewness of the probability distribution of surface hoisting drag is positive. Its value can be decreased if the inclination angle of the hold section increases. While contact probability is high, skewness of the probability distribution of surface hoisting drag is negative. Its value can be increased with the increasing of inclination angle. The results of Fig. 6.20 indicate that the skewness of the probability distribution of surface hoisting drag is influenced by the inclination angle when random contact is considered.

6.6 Conclusion and remarks

This chapter studies the calculation of drillstring hoisting drag from a random viewpoint. Two strategies are taken to model the random component. The first strategy considers the randomness of the downhole friction. The second strategy considers the randomness of contact between drillstring and wellbore. MC simulation is employed to estimate the statistics for them. A parameter study is conducted to determine how the statistics vary with the parameters.

When the friction coefficient is Gaussian, surface hoisting drag is also Gaussian distributed, with its mean the same as the deterministic case. There is a linear relationship between the standard deviation of friction coefficient and standard deviation of the surface hoisting drag.

When contact probability between the drillstring and wellbore is considered, the contact loss leads to considerable reduction in the surface hoisting drag. As the

contact probability grows, the mean and distribution of the surface hoisting drag is shifting from the side of static drag to the side of deterministic hoisting drag.

The skewness of the probability distribution of surface hoisting drag is influenced by the contact probability, length ratio of the hold section to all the other sections, and the inclination angle of the hold section when random contact is considered. The skewness value changes from positive to negative as the contact probability increases. Further, at low contact probability, the positive skewness can be enlarged by increasing the length ratio or decreasing the inclination angle. While at high contact probability, the negative skewness can be decreased by increasing the length ratio or decreasing the inclination angle.

The methodology can be extended into torque or drag calculation in lowering, ream in and ream out drilling conditions. The work of this chapter will help estimate the range of surface drag and torque, which allows the well planner to develop a risk assessment for a challenging well trajectory. Based on the assessment, drilling devices, such as top drive and motor, can be safely and wisely chosen.

Chapter 7

Conclusion

7.1 Summary

The research work from this dissertation studies the stick-slip, bit-bounce and hoisting drag calculation of drillstring from random viewpoint. Different downhole uncertainties are considered. The random friction coefficients are used in drillstring torsional stick-slip analysis. Gaussian white noise on the bit in the axial direction is employed in an axial-torsional coupled model. While studying the hoisting drag calculation of directional drilling, the random contact between the drillstring and the wellbore is considered.

7.2 Concluding Remarks and Highlights

Concluding remarks and highlights of each chapter are given below.

7.2.1 Conclusion and highlights from Chapter 3

Chapter 3 analyzes the stochastic torsional stick-slip vibration of a drill bit using a finite element model of drillstring. The random excitation is caused by the random friction coefficient in the bit-rock interaction. The two points, which represent entering and leaving the stick stage, are examined with special attention. The highlights of this chapter include:

- Phase plane of the stick-slip response become diffused in a range in the random cases.
- The two points, which represent entering and leaving the stick stage, become diffused in the random cases.
- Due to the nonlinearity caused by the friction, the probabilistic distributions of the two points are not normal even when the excitation is assumed as Gaussian white noise.

7.2.2 Conclusion and highlights from Chapter 4

Chapter 4 investigates stick-slip with the friction considered random by using a single degree of freedom (DOF) drillstring model. In the stick stage, the static friction is treated as either a deterministic value or a random variable. While in the slip stage, the kinetic friction is treated as a combination of deterministic and random components. Then path integration (PI) method is firstly used to obtain the probability

density evolution of the response. Monte Carlo (MC) simulation is then used for validation of the PI results and statistical analysis. In addition, parametric studies on damping, rotary speed, weight on bit, drillstring length and different combinations of pipe and collar are conducted for both deterministic and random cases. The highlights of this chapter include:

- Analyzing drillstring stick-slip response based on random static and kinetic frictions.
- Random static friction influences the period of stick-slip motion.
- Random kinetic friction influences the moment entering the stick stage.
- Parametric study also indicates the necessity of research from stochastic viewpoint.

7.2.3 Conclusion and highlights from Chapter 5

In Chapter 5, a two DOFs drillstring model, considering both axial and torsional direction, is used for stochastic dynamic analysis. Finite element method is used to build the drillstring model. The random excitation at the bit-rock interaction, which is considered in the bit axial direction, is treated as Gaussian white noise. The nonlinear bit-rock interaction is replaced with an equivalent linear term by statistic linearization. The linear dynamic system is then solved with the stochastic Newmark algorithm. The highlights of this chapter include:

- Stochastic Newmark strategy yields reliable results when comparing to MC.
- Work of this chapter will help predict the probability of the bit bounce and stick slip at any moment more effectively.

7.2.4 Conclusion and highlights from Chapter 6

Chapter 6 studies the calculation of drillstring hoisting drag from random viewpoint by considering the randomness of the downhole friction and the randomness of contact between drillstring and wellbore. Statistical analysis and parameter study are conducted based on MC simulations. The highlights of this chapter include:

- When the friction coefficient is Gaussian, surface hoisting drag is also Gaussian distributed, with its mean the same as the deterministic case.
- When contact probability between the drillstring and well-bore is considered, as the contact probability grows, the mean and distribution of the surface hoisting drag is shifting from the side of static drag to the side of deterministic hoisting drag. The contact probability influences the range and shape of the surface hoisting drag distribution.
- The skewness of the probability distribution of surface hoisting drag is influenced by the contact probability, length ratio of the hold section to all the other sections, and the inclination angle of the hold section when random contact is considered.

- Work of this chapter will help estimate the range of surface drag and torque, which allows the well planner to develop a risk assessment for a challenging well trajectory.

7.3 Recommendations for Future Work

Based on the current research, some recommendations can be offered.

7.3.1 Stochastic dynamics modeling of directional drilling

As suggested by the literature review, works on stochastic dynamics of directional drilling are necessary. Therefore, a whole directional drillstring dynamic model is highly recommended. The randomness of the downhole friction is suggested to be considered. As friction is really significant in producing torque and drag in directional drilling [78], it is meaningful to consider the uncertainty of friction when predicting the dynamic responses in the downhole.

It is reported by Ritto et al. [136] that drilling fluid can lead to a significant change in system mass and stiffen the drillstring at the bottom. It is also proved that the drilling fluid is critical to the drilling dynamics, especially for the lateral vibrations [183]. As the contact between drillstring and borehole in directional drilling is critical, considering the fluid-structure interaction is recommended.

7.3.2 Research on control strategies

It is highly recommended to analyze control strategies for suppressing stick-slip vibration of drillstrings by using a stochastic dynamic drillstring model with the consideration of uncertainties in the bit-rock interaction. It is recommended to calibrate the uncertainties with field data to improve its reliability.

Bibliography

[1] Bernt S Aadnoy, Iain Cooper, Stefan Miska, Robert F Mitchell, and Michael L Payne. *Advanced drilling and well technology*. SPE Houston, TX, 2009.

[2] Don W Dareing. *Mechanics of drillstrings and marine risers*. ASME Press, 2012.

[3] MT Albdiry and MF Almensory. Failure analysis of drillstring in petroleum industry: a review. *Engineering Failure Analysis*, 65:74–85, 2016.

[4] Ahmad Ghasemloonia, D Geoff Rideout, and Stephen D Butt. A review of drillstring vibration modeling and suppression methods. *Journal of Petroleum Science and Engineering*, 131:150–164, 2015.

[5] Wermac. (n.d.). Drilling rig, online; accessed Oct 10, 2022. https://www.wermac.org/others/oilandgaswelldrilling.html.

[6] J. J. Azar and G. R. Samuel. *Drilling engineering*. PennWell Books, 2007.

[7] Discovery Drilling Funds. (n.d.). Anatomy of a land based

drilling rig - hoisting system, online; accessed Oct 21, 2012. http://www.drillingfunds.com/hoisting.html.

[8] DA Simpson. Wellbore construction (drilling and completions). *Practical Onshore Gas Field Engineering*, pages 85–134, 2017.

[9] Wikipedia. (n.d.). Tricone bit, online; accessed Oct 20, 2013. http://ffden-2.phys.uaf.edu/211-fall2010.web.dir/Jared-Boerger/Technique.html.

[10] Wikipedia. (n.d.). A pdc bit, online; accessed April 7, 2014. http://varelintl.com/Oil-and-Gas-Home/PDC-Drill-Bits/ToughDrill-Bits/.

[11] Alibaba. (n.d.). Bottom view of hybrid bit, online; accessed Mar 28, 2022. https://www.alibaba.com/product-detail/High-Quality-And-Good-Price-Hybrid-50045783529.html.

[12] Kuilin Huang, Yingxin Yang, Gao Li, Yuntian Wang, Haitao Ren, and Shiwei Niu. Torsion and vibration reduction mechanism of roller pdc hybrid bit. *Journal of Petroleum Science and Engineering*, 208:109491, 2022.

[13] DK Ashley, XM McNary, and JC Tomlinson. Extending bha life with multi-axis vibration measurements. In *SPE/IADC drilling conference*. OnePetro, 2001.

[14] Amjad A Besaisow and Mike L Payne. A study of excitation mechanisms and resonances inducing bottomhole-assembly vibrations. *SPE drilling engineering*, 3(01):93–101, 1988.

[15] PD Spanos, AK Sengupta, RA Cunningham, and PR Paslay. Modeling of roller cone bit lift-off dynamics in rotary drilling. *Journal of Energy Resources Technology*, 117(3):197–207, 1995.

[16] Ahmet S Yigit and Andreas P Christoforou. Stick-slip and bit-bounce interaction in oil-well drillstrings. *Journal of Energy Resources Technology*, 128(6):268–274, 2006.

[17] J. M. Kamel and A. S. Yigit. Modeling and analysis of stick-slip and bit bounce in oil well drillstrings equipped with drag bits. *Journal of Sound and Vibration*, 333(25):6885–6899, 2014.

[18] Marian Wiercigroch, K Nandakumar, Lijun Pei, M Kapitaniak, and Vahid Vaziri. State dependent delayed drill-string vibration: theory, experiments and new model. *Procedia IUTAM*, 22:39–50, 2017.

[19] Xueying Wang, Hongjian Ni, and Ruihe Wang. Experimental study on toolface disorientation and correction during slide drilling. *Journal of Petroleum Science and Engineering*, 173:853–860, 2019.

[20] Xueying Wang, Hongjian Ni, Ruihe Wang, Tianke Liu, and Jingguo Xu. Modeling and analyzing the movement of drill string while being rocked on the ground. *Journal of Natural Gas Science and Engineering*, 39:28–43, 2017.

[21] Arnaud Chevallier. *'Nonlinear Stochastic Drilling Vibrations.* PhD thesis, Ph.

D. thesis, Rice University, Department of Mechanical Engineering, Houston, Texas, 2000.

[22] E Skaugen et al. The effects of quasi-random drill bit vibrations upon drillstring dynamic behavior. In *SPE Annual Technical Conference and Exhibition*. Society of Petroleum Engineers, 1987.

[23] Xianping Wu, Luis Carlos Paez, Uyen Tran Partin, Mukul Agnihotri, et al. Decoupling stick/slip and whirl to achieve breakthrough in drilling performance. In *IADC/SPE Drilling Conference and Exhibition*. Society of Petroleum Engineers, 2010.

[24] LW Ledgerwood, OJ Hoffmann, JR Jain, C El Hakam, C Herbig, and RW Spencer. Downhole measurement, monitoring, and modeling reveal stick-slip as a primary cause of pdc bit damage in today's applications. In *Paper SPE-134488 presented at SPE Annual Technical Conference and Exhibition, Florence, Italy*, 2010.

[25] Rapier Dawson, YQ Lin, and PD Spanos. Drill string stick-slip oscillations. In *Spring Conference of the Society for Experimental Mechanics, Houston, Texas*, 1987.

[26] Jens Rudat and Dmitriy Dashevskiy. Development of an innovative model-based stick/slip control system. In *SPE/IADC drilling conference and exhibition*. OnePetro, 2011.

[27] JF Brett. The genesis of torsional drillstring vibrations, spe drilling engineering. *SPE Drilling Engineering (Society of Petroleum Engineers);(United States); Journal*, 7(3):168–174, 1992.

[28] BL Van de Vrande, DH Van Campen, and A De Kraker. An approximate analysis of dry-friction-induced stick-slip vibrations by a smoothing procedure. *Nonlinear Dynamics*, 19(2):159–171, 1999.

[29] Hector Puebla and Jose Alvarez-Ramirez. Suppression of stick-slip in drillstrings: A control approach based on modeling error compensation. *Journal of Sound and Vibration*, 310(4):881–901, 2008.

[30] Eva M Navarro-López and Eduardo Licéaga-Castro. Non-desired transitions and sliding-mode control of a multi-dof mechanical system with stick-slip oscillations. *Chaos, Solitons & Fractals*, 41(4):2035–2044, 2009.

[31] Eva M Navarro-López and Domingo Cortés. Avoiding harmful oscillations in a drillstring through dynamical analysis. *Journal of Sound and Vibration*, 307(1):152–171, 2007.

[32] Thomas Richard, Christophe Germay, and Emmanuel Detournay. A simplified model to explore the root cause of stick–slip vibrations in drilling systems with drag bits. *Journal of Sound and Vibration*, 305(3):432–456, 2007.

[33] YA Khulief, FA Al-Sulaiman, and S Bashmal. Vibration analysis of drill-

strings with self-excited stick–slip oscillations. *Journal of Sound and Vibration*, 299(3):540–558, 2007.

[34] R Sampaio, MT Piovan, and G Venero Lozano. Coupled axial/torsional vibrations of drill-strings by means of non-linear model. *Mechanics Research Communications*, 34(5):497–502, 2007.

[35] M Sarker, DG Rideout, and SD Butt. Dynamic model of an oilwell drillstring with stick-slip and bit-bounce interaction. In *Submitted to 10th International Conference on Bond Graph Modeling and Simulation. Genoa, Italy*, 2012.

[36] Martha Belem Saldivar, Sabine Mondié, and Jean Jacques Loiseau. Reducing stick-slip oscillations in oilwell drillstrings. In *2009 6th International Conference on Electrical Engineering, Computing Science and Automatic Control (CCE)*, pages 1–6. IEEE, 2009.

[37] E Kreuzer and M Steidl. Controlling torsional vibrations of drill strings via decomposition of traveling waves. *Archive of Applied Mechanics*, 82(4):515–531, 2012.

[38] Eva María Navarro-López and Rodolfo Suárez. Practical approach to modelling and controlling stick-slip oscillations in oilwell drillstrings. In *Proceedings of the 2004 IEEE International Conference on Control Applications, 2004.*, volume 2, pages 1454–1460. IEEE, 2004.

[39] AFA Serrarens, MJG Van De Molengraft, JJ Kok, and L Van Den Steen. H/-sub/spl infin//control for suppressing stick-slip in oil well drillstrings. *IEEE Control Systems Magazine*, 18(2):19–30, 1998.

[40] Nenad Mihajlovic. Torsional and lateral vibrations in flexible rotor systems with friction. 2005.

[41] Christophe Germay, Nathan Van de Wouw, Henk Nijmeijer, and Rodolphe Sepulchre. Nonlinear drillstring dynamics analysis. *SIAM Journal on Applied Dynamical Systems*, 8(2):527–553, 2009.

[42] Yevhen Kovalyshen. Understanding root cause of stick–slip vibrations in deep drilling with drag bits. *International Journal of Non-Linear Mechanics*, 67:331–341, 2014.

[43] Mejbahul Sarker, D Geoff Rideout, and Stephen D Butt. Dynamic model for longitudinal and torsional motions of a horizontal oilwell drillstring with wellbore stick-slip friction. *Journal of Petroleum Science and Engineering*, 150:272–287, 2017.

[44] MP Dufeyte, H Henneuse, et al. Detection and monitoring of the slip-stick motion: Field experiments. In *SPE/IADC drilling conference*. Society of Petroleum Engineers, 1991.

[45] SL Chen, K Blackwood, and E Lamine. Field investigation of the effects of

stick-slip, lateral, and whirl vibrations on roller cone bit performance. In *SPE Annual Technical Conference and Exhibition*. OnePetro, 1999.

[46] Mokhtar Yaveri, Karan Damani, and Harshad Kalbhor. Solutions to the down hole vibrations during drilling. In *Nigeria Annual International Conference and Exhibition*. OnePetro, 2010.

[47] Rong-Juin Shyu. *Bending vibration of rotating drill strings*. PhD thesis, Massachusetts Institute of Technology, 1989.

[48] G Heisig and M Neubert. Lateral drillstring vibrations in extended-reach wells. In *IADC/SPE drilling conference*. OnePetro, 2000.

[49] M BBHA Allen. Bha lateral vibrations: case studies and evaluation of important parameters. In *SPE/IADC drilling conference*. OnePetro, 1987.

[50] TM Burgess, GL McDaniel, and PK Das. Improving bha tool reliability with drillstring vibration models: field experience and limitations. In *SPE/IADC drilling conference*. OnePetro, 1987.

[51] Robert F Mitchell and Michael B Allen. Lateral vibration: the key to bha failure analysis. *World Oil;(United States)*, 200(4), 1985.

[52] Robert F Mitchell and Michael B Allen. A practical method to predict dynamic bottom hole assembly failures. In *Proceedings 9th ASME Energy-Sources Technology Conference*, pages 31–36, 1986.

[53] RF Mitchell and MB Allen. Case studies of bha vibration failure. In *SPE Annual Technical Conference and Exhibition*. OnePetro, 1987.

[54] Kim J Vandiver, James W Nicholson, and Rong-Juin Shyu. Case studies of the bending vibration and whirling motion of drill collars. *SPE Drilling Engineering*, 5(04):282–290, 1990.

[55] Andreas Hohl, Carsten Hohl, Christian Herbig, Hatem Oueslati, and Hanno Reckmann. Characterization and mitigation of mud motor vibrations. In *SPE/IADC Drilling Conference and Exhibition*. OnePetro, 2017.

[56] AP Christoforou and AS Yigit. Dynamic modelling of rotating drillstrings with borehole interactions. *Journal of sound and vibration*, 206(2):243–260, 1997.

[57] K Vijayan, N Vlajic, and MI Friswell. The influence of drillstring-borehole interaction on backward whirl. In *International conference on noise and vibration engineering, ISMA*, 2014.

[58] Nabil W Musa, VI Gulyayev, LV Shevchuk, Hasan Aldabas, et al. Whirl interaction of a drill bit with the bore-hole bottom. *Modern Mechanical Engineering*, 5(03):41, 2015.

[59] Andreas P Christoforou, Ahmet S Yigit, et al. Active control of stick-slip vibrations: The role of fully coupled dynamics. In *SPE middle east oil show*. Society of Petroleum Engineers, 2001.

[60] AP Christoforou and AS Yigit. Fully coupled vibrations of actively controlled drillstrings. *Journal of Sound and Vibration*, 267(5):1029–1045, 2003.

[61] AS Yigit and AP Christoforou. Coupled axial and transverse vibrations of oilwell drillstrings. *Journal of sound and vibration*, 195(4):617–627, 1996.

[62] AS Yigit and AP Christoforou. Coupled torsional and bending vibrations of drillstrings subject to impact with friction. *Journal of Sound and Vibration*, 215(1):167–181, 1998.

[63] JD Jansen. Whirl and chaotic motion of stabilized drill collars. *SPE Drilling Engineering*, 7(02):107–114, 1992.

[64] SJ Kotsonis and PD Spanos. Chaotic and random whirling motion of drillstrings. *Journal of Energy Resources Technology*, 119(4):217–222, 1997.

[65] Gert HM Van Der Heijden. Bifurcation and chaos in drillstring dynamics. *Chaos, Solitons & Fractals*, 3(2):219–247, 1993.

[66] John D Macpherson, Pastusek Paul, Michael Behounek, and Richard Harmer. A framework for transparency in drilling mechanics and dynamics measurements. In *SPE Annual Technical Conference and Exhibition*. OnePetro, 2015.

[67] Keith K Millheim and Michael C Apostal. The effect of bottomhole assembly dynamics on the trajectory of a bit. *Journal of Petroleum Technology*, 33(12):2323–2338, 1981.

[68] JA Baird, BC Caskey, MA Tinianow, and CM Stone. Geodyn: A geological formation/drillstring dynamics computer program. In *SPE Annual Technical Conference and Exhibition*. OnePetro, 1984.

[69] Johannes Daniel Brakel and JJ Azar. Prediction of wellbore trajectory considering bottomhole assembly and drill-bit dynamics. *SPE Drilling Engineering*, 4(02):109–118, 1989.

[70] JD Jansen. Non-linear rotor dynamics as applied to oilwell drillstring vibrations. *Journal of sound and vibration*, 147(1):115–135, 1991.

[71] Mark W Dykstra, M Neubert, JM Hanson, and MJ Meiners. Improving drilling performance by applying advanced dynamics models. In *SPE/IADC drilling conference*. OnePetro, 2001.

[72] A The´ ron, Emmanuel de Langre, and C Putot. The effect of dynamical parameters on precession in rotary drilling. *J. Energy Resour. Technol.*, 123(3):181–186, 2001.

[73] Ilja Gorelik, Marcus Neubauer, Jörg Wallaschek, and Oliver Höhn. Model and method for a time-efficient analysis of lateral drillstring dynamics. In *Turbo Expo: Power for Land, Sea, and Air*, volume 56802, page V009T24A006. American Society of Mechanical Engineers, 2015.

[74] Timothy Popp, Holger Stibbe, Dennis Heinisch, Hanno Reckmann, and Pol Spanos. Backward whirl testing and modeling with realistic borehole contacts

for enhanced drilling tool reliability. In *IADC/SPE Drilling Conference and Exhibition*. OnePetro, 2018.

[75] VA Dunayevsky, A Judzis, and WH Mills. Onset of drillstring precession in a directional borehole. In *SPE Annual Technical Conference and Exhibition*. OnePetro, 1984.

[76] AS Yigit and AP Christoforou. Coupled torsional and bending vibrations of actively controlled drillstrings. *Journal of Sound and Vibration*, 234(1):67–83, 2000.

[77] SA Al-Hiddabi, B Samanta, and A Seibi. Non-linear control of torsional and bending vibrations of oilwell drillstrings. *Journal of sound and vibration*, 265(2):401–415, 2003.

[78] Thor Viggo Aarrestad et al. Torque and drag-two factors in extended-reach drilling. *Journal of Petroleum Technology*, 46(09):800–803, 1994.

[79] Juergen Maehs, Steve Renne, Brian Logan, Nerwing Diaz, et al. Proven methods and techniques to reduce torque and drag in the pre-planning and drilling execution of oil and gas wells. In *IADC/SPE Drilling Conference and Exhibition*. Society of Petroleum Engineers, 2010.

[80] CA Johancsik, DB Friesen, Rapier Dawson, et al. Torque and drag in directional wells-prediction and measurement. *Journal of Petroleum Technology*, 36(06):987–992, 1984.

[81] HS Ho et al. An improved modeling program for computing the torque and drag in directional and deep wells. In *SPE Annual Technical Conference and Exhibition*. Society of Petroleum Engineers, 1988.

[82] MC Sheppard, C Wick, T Burgess, et al. Designing well paths to reduce drag and torque. *SPE Drilling Engineering*, 2(04):344–350, 1987.

[83] SM Banks, TW Hogg, JL Thorogood, et al. Increasing extended-reach capabilities through wellbore profile optimisation. In *SPE/IADC Drilling Conference*. Society of Petroleum Engineers, 1992.

[84] Eric E Maidla and Andrew K Wojtanowicz. A field method for assessing borehole friction for directional well casing. *Journal of Petroleum Science and Engineering*, 1(4):323–333, 1988.

[85] Mohammad Fazaelizadeh, Geir Hareland, and Bernt Aadnoy. Application of new 3-d analytical model for directional wellbore friction. *Modern applied science*, 4(2):2, 2010.

[86] Bernt S Aadnøy and Ketil Andersen. Design of oil wells using analytical friction models. *Journal of petroleum Science and Engineering*, 32(1):53–71, 2001.

[87] Bernt S Aadnoy, Mohammad Fazaelizadeh, Geir Hareland, et al. A 3d analytical model for wellbore friction. *Journal of Canadian Petroleum Technology*, 49(10):25–36, 2010.

[88] Anas Sikal, Stephane Menand, Jean Boulet, and Hedi Sellami. Drill pipe stress and cumulative fatigue analysis in complex wells drilling: new approach in fatigue optimization. In *Annual Technical Conference and Exhibition*, page SPE116029, 2008.

[89] You-zhen Zhang, Jian-ming Zhang, and Zhi-jun Shi. Application and development of numerical simulation for underground horizontal directional drilling. *Journal of Coal Science and Engineering (China)*, 18(1):101–107, 2012.

[90] Andrew Wu, Geir Hareland, and Mohammad Fazaelizadeh. Torque & drag analysis using finite element method. *Modern Applied Science*, 5(6):13, 2011.

[91] Mohammad Fazaelizadeh. *Real Time Torque and Drag Analysis during Directional Drilling*. PhD thesis, University of Calgary, 2013.

[92] Yang Caijin, Cheng Zaibin, Jang Wei, Jiang Shiquan, and Ren Gexue. A multibody dynamic model of drillstring for torque and drag analysis. *Journal of Offshore Mechanics and Arctic Engineering*, 137(3):031403, 2015.

[93] Siamak Arbatani, Alfonso Callejo, József Kövecses, Masoud Kalantari, Nick R Marchand, and Javad Dargahi. An approach to directional drilling simulation: finite element and finite segment methods with contact. *Computational Mechanics*, 57(6):1001–1015, 2016.

[94] Mejbahul Sarker, D Geoff Rideout, and Stephen D Butt. Dynamic model for

longitudinal and torsional motions of a horizontal oilwell drillstring with wellbore stick-slip friction. *Journal of Petroleum Science and Engineering*, 2016.

[95] Anatoly Baryshnikov, Angelo Calderoni, Angelo Ligrone, and Paola Ferrara. A new approach to the analysis of drillstring fatigue behaviour. *SPE Drilling & Completion*, 12(2):77–84, 1997.

[96] TH Hill, PV Seshadri, KS Durham, et al. A unified approach to drillstem-failure prevention (includes associated papers 26205 and 26213). *SPE drilling engineering*, 7(04):254–260, 1992.

[97] JP Pitts. Trip inspection, testing gain favor as insurance. *Drill Bit*, 303:885.

[98] WS Bachman. Fatigue testing and development of drill pipe to tool joint connection. *World Oil*, 132:104, 1951.

[99] R. P. Morgan and M. J. Robin. A method for the investigation of fatigue strength in seamless drillpipe. 1969.

[100] Gilbert Yves Grondin and University of Alberta. Dept. of Civil Engineering Kulak, GL. *Fatigue of drill pipe*. Department of Civil Engineering, University of Alberta, 1991.

[101] KA Macdonald and JV Bjune. Failure analysis of drillstrings. *Engineering Failure Analysis*, 14(8):1641–1666, 2007.

[102] S Moradi and K Ranjbar. Experimental and computational failure analysis of drillstrings. *Engineering Failure Analysis*, 16(3):923–933, 2009.

[103] Rui-he Wang, Yan-bin Zang, Rui Zhang, Yu-huan Bu, and Hua-zhou Li. Drillstring failure analysis and its prevention in northeast sichuan, china. *Engineering Failure Analysis*, 18(4):1233–1241, 2011.

[104] GY Grondin, GL Kulak, et al. Fatigue testing of drillpipe. *SPE Drilling and Completion*, 9(2):95–102, 1994.

[105] David R Bert, Anders Storaune, Nanjiu Zheng, et al. Case study: Drillstring failure analysis and new deep-well guidelines lead to success. In *SPE Annual Technical Conference and Exhibition*. Society of Petroleum Engineers, 2007.

[106] Kazimierz Sobczyk and BF Spencer Jr. *Random fatigue: from data to theory*. Access Online via Elsevier, 1992.

[107] O Vaisberg, O Vincke, G Perrin, JP Sarda, and JB Fay. Fatigue of drillstring: state of the art. *Oil & Gas Science and Technology*, 57(1):7–37, 2002.

[108] Tom PE, Ellis Sean, Kang PhD, Reynolds Nicholas, and Zheng Nanjiu. An innovative design approach to reduce drill string fatigue. In *IADC/SPE Drilling Conference*, 2004.

[109] Ai Chi, Jinan Zhang, Weitao Ge, Boyun Guo, et al. Prediction of fatigue life of

drillstring under axial-torsional combined vibrations. In *SPE Gas Technology Symposium*. Society of Petroleum Engineers, 2006.

[110] Arthur Lubinski. Maximum permissible dog-legs in rotary boreholes. *Journal of Petroleum Technology*, 13(2):175–194, 1961.

[111] John E Hansford and Arthur Lubinski. Cumulative fatigue damage of drill pipe in dog-legs. *Journal of Petroleum Technology*, 18(3):359–363, 1966.

[112] Jiang Wu. Drill-pipe bending and fatigue in rotary drilling of horizontal wells. In *SPE Eastern Regional Meeting*, 1996.

[113] Jiang Wu. Model predicts drill pipe fatigue in horizontal wells. *Oil and gas Journal*, 95(5), 1997.

[114] Anas Sikal, Jean Boulet, Stephane Menand, and Hedi Sellami. Drillpipe stress distribution and cumulative fatigue analysis in complex well drilling: New approach in fatigue optimization. In *SPE Annual Technical Conference and Exhibition*, 2008.

[115] UB Sathuvalli, ML Payne, PD Pattillo, RB Livesay, et al. Advanced assessment of drillpipe fatigue and application to critical well engineering. In *SPE/IADC Drilling Conference*. Society of Petroleum Engineers, 2005.

[116] A Baryshnikov, S Poli, F Stewart, P Ferrara, et al. Downhole tool serviceability

under dynamic loads. In *SPE/IADC Drilling Conference*. Society of Petroleum Engineers, 1997.

[117] MK Rahman, MM Hossain, and SS Rahman. Stress concentration incorporated fatigue analysis of die-marked drill pipes. *International journal of Fatigue*, 21(8):799–811, 1999.

[118] Hongwei Shen, Jizhong Lin, and Ensheng Mu. Probabilistic model on stochastic fatigue damage. *International Journal of Fatigue*, 22(7):569–572, 2000.

[119] Loren D Lutes and Shahram Sarkani. *Random Vibrations: Analysis of Structural and Mechanical Systems*. Butterworth-Heinemann, 2004.

[120] Jung Gu Lee and Alan Palazzolo. Catcher bearing life prediction using a rainflow counting approach. *Journal of tribology*, 134(3):031101, 2012.

[121] Jiahao Zheng, Hongyuan Qiu, Jianming Yang, and Stephen Butt. Fatigue life prediction of drill-string subjected to random loadings. In *ASME 2014 International Mechanical Engineering Congress and Exposition*, volume 46483, page V04BT04A024. American Society of Mechanical Engineers, 2014.

[122] John W Miles. On structural fatigue under random loading. *Journal of the Aeronautical Sciences*, 21(11):753–762, 1954.

[123] Loren D Lutes, Miguel Corazao, Sau-lon James Hu, and James Zimmerman.

Stochastic fatigue damage accumulation. *Journal of Structural Engineering*, 110(11):2585–2601, 1984.

[124] Loren D Lutes and Curtis E Larsen. Improved spectral method for variable amplitude fatigue prediction. *Journal of Structural Engineering*, 116(4):1149–1164, 1990.

[125] K Ortiz and NK Chen. Fatigue damage prediction for stationary wideband processes. In *In 'Fifth Int. Conf. on Applications of Statistics and Probability in Civil Engrg*, 1987.

[126] Paul H Wirsching and Mark C Light. Fatigue under wide band random stresses. *Journal of the Structural Division*, 106(7):1593–1607, 1980.

[127] S Sarkani, DP Kihl, and JE Beach. Fatigue of welded joints under narrow-band non-gaussian loadings. *Probabilistic Engineering Mechanics*, 9(3):179–190, 1994.

[128] Steven R Win t´ erstein. Nonlinear vibration models for extremes and fatigue. *Journal of Engineering Mechanics*, 114(10):1772–1790, 1988.

[129] D Benasciutti and R Tovo. Cycle distribution and fatigue damage assessment in broad-band non-gaussian random processes. *Probabilistic Engineering Mechanics*, 20(2):115–127, 2005.

[130] G Petrucci and B Zuccarello. Fatigue life prediction under wide band ran-

dom loading. *Fatigue & Fracture of Engineering Materials & Structures*, 27(12):1183–1195, 2004.

[131] B Zuccarello and NF Adragna. A novel frequency domain method for predicting fatigue crack growth under wide band random loading. *International journal of fatigue*, 29(6):1065–1079, 2007.

[132] JL Bogdanoff and JE Goldberg. A new analytical approach to drill pipe breakage ii. *Journal of Manufacturing Science and Engineering*, 83(2):101–106, 1961.

[133] P.D. Spanos and A.M. Chevallier. Nonlinear stochastic drill-string vibrations. In *8th ASCE Specialty Conference on Probabilistic Mechanics and Structural Reliability*, pages 1–6. Notre Dame, Indiana, 2000.

[134] PD Spanos, AM Chevallier, and NP Politis. Nonlinear stochastic drill-string vibrations. *J. Vib. Acoust.*, 124(4):512–518, 2002.

[135] TG Ritto, C Soize, R Sampaio, et al. Drill-string with uncertainty in the bit-rock interaction. *Proceedings of PACAM XI*, 2010.

[136] TG Ritto, C Soize, and R Sampaio. Non-linear dynamics of a drill-string with uncertain model of the bit–rock interaction. *International Journal of Non-Linear Mechanics*, 44(8):865–876, 2009.

[137] TG Ritto, C Soize, R Sampaio, et al. Modeling uncertainties for local nonlin-

earities: application to the drill-string dynamics. *Proceedings of COMPDYN 2009*, 2009.

[138] TG Ritto, C Soize, and R Sampaio. Probabilistic model identification of the bit–rock-interaction-model uncertainties in nonlinear dynamics of a drill-string. *Mechanics Research Communications*, 37(6):584–589, 2010.

[139] TG Ritto, C Soize, R Sampaio, et al. Stochastic drill-string dynamics-random weight-on-hook (woh). In *Proceedings of the XIII International Symposium on Dynamic Problems of Mechanics (DINAME 2009)*, 2009.

[140] TG Ritto, C Soize, and Rubens Sampaio. Stochastic dynamics of a drill-string with uncertain weight-on-hook. *Journal of the Brazilian Society of Mechanical Sciences and Engineering*, 32(3):250–258, 2010.

[141] TG Ritto, Christian Soize, and R Sampaio. Robust optimization of the rate of penetration of a drill-string using a stochastic nonlinear dynamical model. *Computational Mechanics*, 45(5):415–427, 2010.

[142] Hongyuan Qiu and Jianming Yang. Stochastic and deterministic vibration analysis on drill-string with finite element method. In *ASME International Mechanical Engineering Congress and Exposition*, volume 56246, page V04AT04A004. American Society of Mechanical Engineers, 2013.

[143] Eleazar Marquez. *Stochastic Dynamics in Rotary and Vibration-assisted Drilling*. PhD thesis, Ph.D. Dissertation, Rice University, 2016.

[144] DM Lobo, TG Ritto, and DA Castello. A novel stochastic process to model the variation of rock strength in bit-rock interaction for the analysis of drill-string vibration. *Mechanical Systems and Signal Processing*, 141:106451, 2020.

[145] Timothy Michael Popp. *Stochastic Analysis of Whirl in Drillstrings*. PhD thesis, Ph. D. thesis, Rice University, Department of Mechanical Engineering and Civil Engineering, Houston, Texas, 2020.

[146] Lucas P Volpi, Daniel M Lobo, and Thiago G Ritto. A stochastic analysis of the coupled lateral–torsional drill string vibration. *Nonlinear Dynamics*, 103(1):49–62, 2021.

[147] DM Lobo, TG Ritto, DA Castello, and A Batou. On the stochastic bit–rock interaction disturbances and its effects on the performance of two commercial control strategies used in drill strings. *Mechanical Systems and Signal Processing*, 164:108229, 2022.

[148] TG Ritto, MR Escalante, Rubens Sampaio, and MB Rosales. Drill-string horizontal dynamics with uncertainty on the frictional force. *Journal of Sound and Vibration*, 332(1):145–153, 2013.

[149] Jialin Tian, Yinglin Yang, and Lin Yang. Vibration characteristics analysis and experimental study of horizontal drill string with wellbore random friction force. *Archive of Applied Mechanics*, 87(9):1439–1451, 2017.

[150] Niek Antonius Henricus Kremers, Emmanuel Detournay, and Nathan van de Wouw. Model-based robust control of directional drilling systems. *IEEE Transactions on Control Systems Technology*, 24(1):226–239, 2016.

[151] Americo Cunha, Christian Soize, and Rubens Sampaio. Computational modeling of the nonlinear stochastic dynamics of horizontal drillstrings. *Computational Mechanics*, 56(5):849–878, 2015.

[152] RA Ibrahim, SA Zielke, and K Popp. Characterization of interfacial forces in metal-to-metal contact under harmonic excitation. *Journal of sound and vibration*, 220(2):365–377, 1999.

[153] M Zamanian, SE Khadem, and MR Ghazavi. Stick-slip oscillations of drag bits by considering damping of drilling mud and active damping system. *Journal of Petroleum Science and Engineering*, 59(3):289–299, 2007.

[154] Thomas Richard, Christophe Germay, and Emmanuel Detournay. Self-excited stick–slip oscillations of drill bits. *Comptes rendus MECANIQUE*, 332(8):619–626, 2004.

[155] Marcelo A Trindade, Claudio Wolter, and Rubens Sampaio. Karhunen–loève decomposition of coupled axial/bending vibrations of beams subject to impacts. *Journal of Sound and Vibration*, 279(3):1015–1036, 2005.

[156] YA Khulief and H Al-Naser. Finite element dynamic analysis of drillstrings. *Finite elements in analysis and design*, 41(13):1270–1288, 2005.

[157] Hongyuan Qiu. Dynamic analysis of a drill-string under deterministic and random excitations. Master's thesis, Memorial University, Department of Mechanical Engineering, St. John's, Newfoundland, Canada, 2014.

[158] RF Kilburn. Friction viewed as a random process. *Journal of Tribology*, 96(2):291–299, 1974.

[159] N Challamel, H Sellami, E Chenevez, and L Gossuin. A stick/slip analysis based on rock/bit interaction. *Journal of petroleum technology*, 52(12):30–31, 2000.

[160] CWS To and ML Liu. Large nonstationary random responses of shell structures with geometrical and material nonlinearities. *Finite elements in analysis and design*, 35(1):59–77, 2000.

[161] Christian Bucher. *Computational Analysis of Randomness in Structural Mechanics: Structures and Infrastructures Book Series*, volume 3. CRC Press, 2009.

[162] PC Kriesels, WJG Keultjes, P Dumont, Issam Huneidi, OO Owoeye, and RA Hartmann. Cost savings through an integrated approach to drillstring vibration control. In *SPE/IADC Middle East drilling technology. Symposium*, pages 139–150, 1999.

[163] Parimal Arjun Patil and Catalin Teodoriu. Model development of torsional

drillstring and investigating parametrically the stick-slips influencing factors. *Journal of Energy Resources Technology*, 135(1):1–7, 2013.

[164] Régis Viguié, Gaëtan Kerschen, J-C Golinval, DM McFarland, LA Bergman, AF Vakakis, and N Van de Wouw. Using passive nonlinear targeted energy transfer to stabilize drill-string systems. *Mechanical Systems and Signal Processing*, 23(1):148–169, 2009.

[165] JD Jansen and L Van den Steen. Active damping of self-excited torsional vibrations in oil well drillstrings. *Journal of sound and vibration*, 179(4):647–668, 1995.

[166] SL Qiao and RA Ibrahim. Stochastic dynamics of systems with friction-induced vibration. *Journal of sound and vibration*, 223(1):115–140, 1999.

[167] RA Ibrahim, S Madhavan, SL Qiao, and WK Chang. Experimental investigation of friction-induced noise in disc brake systems. *International Journal of Vehicle Design*, 23(3-4):218–240, 2000.

[168] Yao-Qun Lin and Yu-Hwa Wang. Stick-slip vibration of drill strings. *Journal of Manufacturing Science and Engineering*, 113(1):38–43, 1991.

[169] Hongyuan Qiu, Jianming Yang, and Stephen Butt. Stick-slip analysis of a drill string subjected to deterministic excitation and stochastic excitation. *Shock and Vibration*, 2016.

[170] Don W Dareing. *Mechanics of Drillstrings and Marine Risers*. ASME Press, 2012.

[171] Yubing Wen, Jianming Yang, and Shiyu Wang. Random dynamics of a non-linear spur gear pair in probabilistic domain. *Journal of Sound and Vibration*, 333(20):5030–5041, 2014.

[172] Jianqiao Sun. *Stochastic dynamics and control*, volume 4. Elsevier, 2006.

[173] JS Yu, GQ Cai, and YK Lin. A new path integration procedure based on gauss-legendre scheme. *International journal of non-linear mechanics*, 32(4):759–768, 1997.

[174] Arvid Naess, FE Kolnes, and Eirik Mo. Stochastic spur gear dynamics by numerical path integration. *Journal of Sound and Vibration*, 302(4):936–950, 2007.

[175] JQ Sun and CS T Hsu. The generalized cell mapping method in nonlinear random vibration based upon short-time gaussian approximation. *Journal of applied mechanics*, 57(4):1018–1025, 1990.

[176] JS Yu and YK Lin. Numerical path integration of a non-homogeneous markov process. *International Journal of Non-Linear Mechanics*, 39(9):1493–1500, 2004.

[177] CWS To. Recursive expressions for random response of nonlinear systems. *Computers & structures*, 29(3):451–457, 1988.

[178] Hongyuan Qiu, Jianming Yang, Stephen Butt, and Jinghan Zhong. Investigation on random vibration of a drillstring. *Journal of Sound and Vibration*, 406:74–88, 2017.

[179] Khaja Zameeruddin Khan. *Longitudinal and torsional vibration of drill strings*. PhD thesis, Massachusetts Institute of Technology, 1986.

[180] Brian Armstrong-Hélouvry, Pierre Dupont, and Carlos Canudas De Wit. A survey of models, analysis tools and compensation methods for the control of machines with friction. *Automatica*, 30(7):1083–1138, 1994.

[181] Jasem M Kamel and Ahmet S Yigit. Modeling and analysis of stick-slip and bit bounce in oil well drillstrings equipped with drag bits. *Journal of Sound and Vibration*, 333(25):6885–6899, 2014.

[182] P Bernard and G Fleury. Stochastic newmark scheme. *Probabilistic Engineering Mechanics*, 17(1):45–61, 2002.

[183] TG Ritto, C Soize, R Sampaio, et al. Drill-string dynamics with uncertainty in the bit-rock nonlinear interaction model. In *Proceedings of the 2nd International Conference on Uncertainty in Structural Dynamics*, 2009.

Appendix A

The drillstring model is made up of drillpipe and drillcollar. Drillpipe is 1000 m and is evenly divided into 20 finite elements. Drillcollar is 200 m and is evenly divided into 10 finite elements. Therefore we have 62×62 global stiffness matrix $\mathbf{K}$ and 62×62 global mass matrix $\mathbf{M}$.

$\mathbf{Q}(t)$ is the 62×1 random general coordinate vector:

$$\mathbf{Q}(t) = \begin{bmatrix} Q_1(t) & Q_2(t) & Q_3(t) & \cdots & Q_{60}(t) & Q_{61}(t) & Q_{62}(t) \end{bmatrix}^T \tag{A1}$$

$\mathbf{F}(\mathbf{Q})$ is a 62×1 excitation vector including WOB, TOB, buoyant weight f_b,

drilling fluid axial force f_d and constant hookload f_0, which is given as:

$$\mathbf{F}(\mathbf{Q}) = \begin{bmatrix} -f_0 + f_b + f_d \\ 0 \\ 2f_b + 2f_d \\ 0 \\ 2f_b + 2f_d \\ 0 \\ \vdots \\ 2f_b + 2f_d \\ 0 \\ f_b + f_d - WOB \\ -TOB \end{bmatrix} \tag{A2}$$

$\mathbf{W}(t)$ represents an array of Gaussian white noise:

$$\mathbf{W}(t) = \begin{bmatrix} 0 & 0 & 0 & 0 & \cdots & 0 & 0 & w(t) & 0 \end{bmatrix}^T \tag{A3}$$

where $w(t)$ is Gaussian white noise.

$\mathbf{B}$ is a 62×62 matrix representing the intensity of the white noise:

$$\mathbf{B} = \begin{bmatrix} 0 & 0 & 0 & \cdots & 0 & 0 & 0 \\ 0 & 0 & 0 & \cdots & 0 & 0 & 0 \\ 0 & 0 & 0 & \cdots & 0 & 0 & 0 \\ \vdots & \vdots & \vdots & \ddots & \vdots & \vdots & \vdots \\ 0 & 0 & 0 & \cdots & 0 & 0 & 0 \\ 0 & 0 & 0 & \cdots & 0 & \sqrt{2\pi S_0} & 0 \\ 0 & 0 & 0 & \cdots & 0 & 0 & 0 \end{bmatrix} \tag{A4}$$

It is worth noting that Stochastic Newmark method [182] has already considered the time step affection in the White noise when deriving Eqs. (5.33) and (5.34). Therefore, $G = 2\pi S_0$, rather than $G = \frac{2\pi S_0}{\Delta t}$, is used in the simulation.

Appendix B

$$f_1(x) = W_f = \begin{cases} 0 & \text{if } x \leq 0 \\ k_c n x & \text{if } x < d_* \\ R_b \sigma n l & \text{if } x > d_* \end{cases} \quad g(x) = \frac{1}{\sqrt{2\pi}\sigma} e^{\frac{-(x-\mu)^2}{2\sigma^2}} \tag{B1}$$

$$k_1^e = E(\frac{df_1(x)}{dx}) = \int_{-\infty}^{+\infty} \frac{df_1(x)}{dx} \frac{1}{\sqrt{2\pi}\sigma} e^{\frac{-(x-\mu)^2}{2\sigma^2}} dx = \int_0^{d*} k_c n \frac{1}{\sqrt{2\pi}\sigma} e^{\frac{-(x-\mu)^2}{2\sigma^2}} dx \tag{B2}$$

Letting

$$y = \frac{x-\mu}{\sqrt{2}\sigma} \tag{B3}$$

Then

$$dx = \sqrt{2}\sigma dy \tag{B4}$$

Substituting Eqs. (B3) and (B4) into Eq. (B2) leads to

$$\int_0^{d*} k_c n \frac{1}{\sqrt{2\pi}\sigma} e^{\frac{-(x-\mu)^2}{2\sigma^2}} dx = \frac{k_c n}{2} \frac{2}{\sqrt{\pi}} \int_{y_2}^{y_1} e^{-y^2} dy = \frac{k_c n}{2} (erf(y_2) - erf(y_1)) \tag{B5}$$

where

$$y_1 = -\frac{\mu}{\sqrt{2}\sigma} \tag{B6}$$

$$y_2 = \frac{d_* - \mu}{\sqrt{2}\sigma} \tag{B7}$$

$$E(f_1(x)) = \int_{-\infty}^{+\infty} f_1(x)g(x)dx = \int_0^{d*} k_c nxg(x)dx + \int_{d*}^{+\infty} R_b\sigma nlg(x)dx \tag{B8}$$

$$\begin{aligned}\int_0^{d*} k_c nxg(x)dx &= \int_{y_1}^{y_2} \frac{k_c n}{\sqrt{\pi}}(\sqrt{2}\sigma y + \mu)e^{-y^2}dy \\ &= \frac{\sqrt{2}k_c n\sigma}{\sqrt{\pi}}\int_{y_1}^{y_2} ye^{-y^2}dy + \frac{\mu k_c n}{\sqrt{\pi}}\int_{y_1}^{y_2} e^{-y^2}dy \\ &= \frac{k_c n\sigma}{\sqrt{2\pi}}(e^{-y_1^2} - e^{-y_2^2}) + \frac{\mu k_c n}{2}(erf(y_2) - erf(y_1))\end{aligned} \tag{B9}$$

$$\int_{d*}^{+\infty} R_b\sigma nlg(x)dx = \int_{y_2}^{+\infty} \frac{R_b\sigma nl}{\sqrt{\pi}}e^{-y^2}dy = \frac{R_b\sigma nl}{2}(1 - erf(y_2)) \tag{B10}$$

$$f_1^0 = E(f_1(x)) - k_1^e E(x) = \frac{k_c n\sigma}{\sqrt{2\pi}}(e^{-y_1^2} - e^{-y_2^2}) + \frac{R_b\sigma nl}{2}(1 - erf(y_2)) \tag{B11}$$

$$f_3(x) = W_c = \begin{cases} 0 & \text{if} \quad x \le 0 \\ \zeta\varepsilon R_b nx & \text{if} \quad x > 0 \end{cases} \tag{B12}$$

$$\begin{aligned}k_3^e = E(\frac{df_3(x)}{dx}) &= \int_0^{+\infty} \frac{df_3(x)}{dx}\frac{1}{\sqrt{2\pi}\sigma}e^{\frac{-(x-\mu)^2}{2\sigma^2}}dx \\ &= \int_{y_1}^{+\infty} \frac{\xi\varepsilon R_b n}{\sqrt{\pi}}e^{-y^2}dy = \frac{\xi\varepsilon R_b n}{2}(1 - erf(y_1))\end{aligned} \tag{B13}$$

$$\begin{aligned}f_3^0 &= \int_0^{+\infty} \xi\varepsilon R_b nx\frac{1}{\sqrt{2\pi}\sigma}e^{\frac{-(x-\mu)^2}{2\sigma^2}}dx - k_3^e E(x) \\ &= \frac{1}{\sqrt{\pi}} * \int_{y_1}^{+\infty} \xi\varepsilon R_b n(\sqrt{2}\sigma y + \mu)e^{-y^2}dy - k_3^e\mu \\ &= \frac{\xi\varepsilon R_b n\sigma}{\sqrt{2\pi}}e^{-y_1^2} + \frac{\mu\xi\varepsilon R_b n}{2}(1 - erf(y_1)) - k_3^e\mu \\ &= \frac{\xi\varepsilon R_b n\sigma}{\sqrt{2\pi}}e^{-y_1^2}\end{aligned} \tag{B14}$$

Following the same mathematical manipulation, we have W_f^e, T_f^e, W_c^e and T_c^e as below:

$$W_f^e = \frac{k_c n}{2}(erf(y_2) - erf(y_1))x + \frac{k_c n\sigma}{\sqrt{2\pi}}(e^{-y_1^2} - e^{-y_2^2}) + \frac{R\sigma nl}{2}(1 - erf(y_2)) \quad \text{(B15)}$$

$$T_f^e = rW_f^e \frac{R_b}{2}u \quad \text{(B16)}$$

$$W_c^e = \frac{\xi\varepsilon R_b n}{2}(1 - erf(y_1))x + \frac{\xi\varepsilon R_b n\sigma}{\sqrt{2\pi}}e^{-y_1^2} \quad \text{(B17)}$$

$$T_c^e = \frac{\varepsilon R_b^2 n}{4}(1 - erf(y_1))x + \frac{\varepsilon R_b^2 n\sigma}{2\sqrt{2\pi}}e^{-y_1^2} \quad \text{(B18)}$$

Appendix C

$$\mathbf{Y}_{n+1} = \mathbf{A}_1\mathbf{Y}_n + \mathbf{A}_2\mathbf{H}_n + \mathbf{A}_3\mathbf{W}_n \tag{C1}$$

$$\begin{aligned}\mathbf{R}_{n+1} = E(\mathbf{Y}_{n+1}\mathbf{Y}_{n+1}^T) &= \mathbf{A}_1\mathbf{R}_n\mathbf{A}_1^T + \mathbf{A}_2\mathbf{H}_n\mathbf{H}_n^T\mathbf{A}_2^T + \mathbf{A}_3\mathbf{I}\mathbf{A}_3^T \\ &+\mathbf{A}_1E(\mathbf{Y}_n)\mathbf{H}_n^T\mathbf{A}_2^T + \mathbf{A}_2\mathbf{H}_nE(\mathbf{Y}_n^T)\mathbf{A}_1^T + \mathbf{A}_1E(\mathbf{Y}_n\mathbf{W}_n^T)\mathbf{A}_3^T \\ &+\mathbf{A}_3E(\mathbf{W}_n\mathbf{Y}_n^T)\mathbf{A}_1^T + \mathbf{A}_2\mathbf{H}_nE(\mathbf{W}_n^T)\mathbf{A}_3^T + \mathbf{A}_3E(\mathbf{W}_n)\mathbf{H}_n^T\mathbf{A}_2^T\end{aligned} \tag{C2}$$

Firstly, $\mathbf{A}_2\mathbf{H}_nE(\mathbf{W}_n^T)\mathbf{A}_3^T$ and $\mathbf{A}_3E(\mathbf{W}_n)\mathbf{H}_n^T\mathbf{A}_2^T$ are zero because of the zero mean of $\mathbf{W}_n$. Then:

$$\begin{aligned}E(\mathbf{Y}_n\mathbf{W}_n^T) &= E([\mathbf{A}_1\mathbf{Y}_{n-1} + \mathbf{A}_2\mathbf{H}_{n-1} + \mathbf{A}_3\mathbf{W}_{n-1}]\mathbf{W}_n^T) \\ &= \mathbf{A}_1E(\mathbf{Y}_{n-1}\mathbf{W}_n^T) + \mathbf{A}_3E(\mathbf{W}_{n-1}\mathbf{W}_n) \\ &= \mathbf{A}_1E(\begin{bmatrix}\mathbf{Q}_{n-1} \\ \dot{\mathbf{Q}}_{n-1}\end{bmatrix}\begin{bmatrix}\mathbf{N}_{n+1} \\ \mathbf{P}_{n+1}\end{bmatrix}^T) + \mathbf{A}_3E(\begin{bmatrix}\mathbf{N}_n \\ \mathbf{P}_n\end{bmatrix}\begin{bmatrix}\mathbf{N}_{n+1} \\ \mathbf{P}_{n+1}\end{bmatrix}^T)\end{aligned} \tag{C3}$$

Expressing $[\mathbf{Q}_{n-1}\ \dot{\mathbf{Q}}_{n-1}]^T$ by using Eq. (C1) continuously until the state vector becomes $[\mathbf{q}_0\ \dot{\mathbf{q}}_0]^T$ and taking into account that $E(\mathbf{N}_n\mathbf{N}_m^T) = 0$ $(m \neq n)$ and $E(\mathbf{P}_n\mathbf{P}_m^T) = 0$ $(m \neq n)$, Eq. (C3) is changed to the following:

$$E(\mathbf{Y}_n\mathbf{W}_n^T) = \mathbf{A}_1^nE(\begin{bmatrix}\mathbf{q}_0 \\ \dot{\mathbf{q}}_0\end{bmatrix}\begin{bmatrix}\mathbf{N}_{n+1} \\ \mathbf{P}_{n+1}\end{bmatrix}^T) \tag{C4}$$

By applying the initial condition, which is constant, the value of Eq. (C4) becomes zero. Following the same process, $E(\mathbf{W}_n \mathbf{Y}_n^T)$ is also zero. Therefore, Eq. (C2) is simplified to:

$$\mathbf{R}_{n+1} = \mathbf{A}_1 \mathbf{R}_n \mathbf{A}_1^T + \mathbf{A}_2 \mathbf{H}_n \mathbf{H}_n^T \mathbf{A}_2^T + \mathbf{A}_3 \mathbf{I} \mathbf{A}_3^T + \mathbf{A}_1 E(\mathbf{Y}_n) \mathbf{H}_n^T \mathbf{A}_2^T + \mathbf{A}_2 \mathbf{H}_n E(\mathbf{Y}_n^T) \mathbf{A}_1^T \tag{C5}$$